Eur. Phys. J. C 50, 729–768 (2007)
DOI 10.1140/epjc/s10052-007-0271-1

THE EUROPEAN PHYSICAL JOURNAL C

Review

Prospects for e^+e^- physics at Frascati between the ϕ and the ψ

F. Ambrosino[5], F. Anulli[3], D. Babusci[3], S. Bianco[3], C. Bini[9,a], N. Brambilla[4], R. De Sangro[3], P. Gauzzi[9], P.M. Gensini[8], S. Giovannella[3], V. Muccifora[3], M. Negrini[2], F. Nguyen[10], S. Pacetti[3], G. Pancheri[3], M. Passera[6], A. Passeri[10], A.D. Polosa[9], M. Radici[7], Y.N. Srivastava[8], A. Vairo[4], G. Venanzoni[3], G. Violini[1]

[1] Universitá della Calabria, Cosenza and INFN Gruppo collegato di Cosenza, Italy
[2] Universitá di Ferrara and INFN Sezione di Ferrara, Italy
[3] Laboratori Nazionali di Frascati, INFN, Italy
[4] Universitá di Milano and INFN Sezione di Milano, Italy
[5] Universitá "Federico II" di Napoli and INFN Sezione di Napoli, Italy
[6] Universitá di Padova and INFN Sezione di Padova, Italy
[7] Dip. di Fisica Nucleare e Teorica, Universitá di Pavia and INFN Sezione di Pavia, Italy
[8] Dip. di Fisica dell'Universitá di Perugia and INFN, Sezione di Perugia, Italy
[9] Dipartimento di Fisica Universitá "La Sapienza", P. le A. Moro 5, 00185 Roma, Italy
[10] Universitá Roma3 and INFN Sezione di Roma3, Italy

Received: 25 July 2006 / Revised version: 16 February 2007 /
Published online: 4 April 2007 –

Abstract. We present a detailed study, done in the framework of the INFN 2006 Roadmap, of the prospects for e^+e^- physics at the Frascati National Laboratories. The physics case for an e^+e^- collider running at high luminosity at the ϕ resonance energy and also reaching a maximum center of mass energy of 2.5 GeV is discussed, together with the specific aspects of a very high luminosity τ-charm factory. Subjects connected to kaon decay physics are not discussed here, being part of another INFN Roadmap working group. The significance of the project and the impact on INFN are also discussed. All the documentation related to the activities of the working group can be found in http://www.roma1.infn.it/people/bini/roadmap.html.

1 Introduction

The Frascati National Laboratories (LNF) of INFN have a long and successful tradition in e^+e^- accelerators and in e^+e^- physics. The concept of e^+e^- colliders with the two beams circulating in the same vacuum chamber in opposite directions was developed at Frascati by Bruno Touscheck and his collaborators in the early sixties with the project AdA.

In the seventies, the new accelerator Adone worked in the center of mass energy region between 1.5 and 3.1 GeV. The Adone experiments contributed to the discovery of the unexpectedly rich multihadronic production and in 1974 confirmed the discovery of the J/ψ. Some of the hadronic cross section measurements done at Adone are still today the best results in that energy region, and are used in precision tests of the standard model.

The tradition continued with DAFNE that provided the first beam collisions in 1999 and that is still working at present. DAFNE is a ϕ-factory, that is an e^+e^- machine centred at the ϕ resonance energy $\sqrt{s} = 1019.4\,\mathrm{MeV}$. It has recently reached a peak luminosity of $1.5 \times 10^{32}\,\mathrm{cm}^{-2}\,\mathrm{s}^{-1}$ that is the highest luminosity ever reached by an e^+e^- collider in this energy region. Many features of this machine are unique. First of all the production of $K^0\overline{K^0}$ final states in a pure quantum state with the consequent possibility to study quantum interference effects, and to have pure monochromatic tagged K_S and K_L beams. In addition a ϕ-factory is also a source of high statistic samples of pseudoscalar and scalar mesons obtained through the ϕ radiative decays, and of monochromatic charged kaons directly from the ϕ. These samples allow one to obtain relevant results in hadronic physics, and also in atomic and nuclear physics (the study of hypernuclei and exotic atoms). For a comprehensive review of the aspects of physics that concern DAFNE, we refer to the DAFNE physics handbook that was written in 1995 [1] before the start-up of the experiments. For the status and the physics results of the experiments, we refer the reader to the Web sites of each experiment, namely KLOE [2], Finuda [3] and Dear [4].

The DAFNE schedule is defined up to the end of year 2008. In the last few years a discussion has started at LNF about the e^+e^- future program for the laboratory. Two main options have been considered up to now, not necessarily mutually exclusive.

The first option, that we call DAFNE-2 in the following, corresponds to continue a low energy e^+e^- program with a new version of DAFNE of higher luminosity, and also by

[a] e-mail: cesare.bini@roma1.infn.it

allowing the center of mass energy to span from the ϕ resonance energy up to $\sqrt{s} = 2.5\,\mathrm{GeV}$. The new machine can be built within the same DAFNE/Adone building and the Frascati Accelerator Division is studying now which are the possible machine schemes to obtain the required performance. A first project has been already developed [5].

The second option, that we call the flavour-factory, is more ambitious [6]. The idea is to profit from the experience developed by accelerator physicists with the linear collider studies, to build an e^+e^- machine of completely new concept, able to run around 10 GeV center of mass energy (super-B-factory) but also in the 3–4 GeV region (as a τ-charm factory). This project doesn't fit the present laboratories size, so that it requires a new site, and a very big financial and technical effort.

In this document, that is part of "Gruppo-1" section of the INFN roadmap, we consider in full detail the physics case for DAFNE-2 (in Sect. 2 below), describing the main particle physics issues and showing the possible reach of the project. We do not discuss the physics of kaon decays and kaon interferometry, since it will be extensively discussed in the document of the kaon physics working group [7]. Moreover we don't discuss the super-B-factory program, that also belongs to another working group. Nevertheless Sect. 3 will be devoted to the presentation of the main physics topics of the τ-charm factory that could be part of the flavour-factory program. Considerations about detector issues for the case of DAFNE-2, are presented in Sect. 4. Finally in Sect. 5 we summarise the relevance of the programs here outlined.

2 The physics case for DAFNE-2

2.1 Overview

DAFNE-2 is planned to be optimised in luminosity at the ϕ peak, reaching a luminosity of $\sim 8 \times 10^{32}\,\mathrm{cm^{-2}\,s^{-1}}$. In the higher energy region between 1 and 2.5 GeV is expected to reach a luminosity of $\sim 10^{32}\,\mathrm{cm^{-2}\,s^{-1}}$, much larger than any previous machine in the same energy region. With such a machine one can think to collect an integrated luminosity of $\sim 50\,\mathrm{fb^{-1}}$ in few years of data taking at the ϕ and $\sim 5\,\mathrm{fb^{-1}}$ in the same running time between 1 and 2.5 GeV. With respect to DAFNE, it corresponds to increase by a factor 20 the statistics at the ϕ and to open a new window on high statistics e^+e^- physics in the 1–2.5 GeV energy region. The only direct competitor project is VEPP-2000 at Novosibirsk [8–10] that will cover the center of mass energy between 1 and 2 GeV with two experiments. This project is expected to start by year 2007 with a luminosity ranging between $10^{31}\,\mathrm{cm^{-2}\,s^{-1}}$ at 1 GeV and $10^{32}\,\mathrm{cm^{-2}\,s^{-1}}$ at 2 GeV. Other "indirect" competitors are the higher energy e^+e^- colliders (τ-charm and B-factories) that in principle cover the DAFNE-2 energy range by means of radiative return. Moreover for some specific issues experiments at hadron machines are also competitive. A list of the competitors is reported in Sect. 5.

In the following sections we present the main physics issues of the DAFNE-2 project. We start with the possibility to improve the knowledge of the e^+e^- to hadrons cross sections in a very wide center of mass energy region, from the $\pi\pi$ threshold up to 2.5 GeV, and its implications on the precision tests of the standard model (Sect. 2.2), and on the vector meson spectroscopy (Sect. 2.3). Then we describe the physics potential of studying radiative decays (Sect. 2.4) and $\gamma\gamma$ collisions (Sect. 2.5). Finally we discuss also the subjects of the hadron form factors (Sect. 2.6) and of the kaon–nucleus interactions (Sect. 2.7).

2.2 Hadronic cross section

2.2.1 Precision tests of the standard model: Overview

The systematic comparison of the standard model (SM) predictions with very precise experimental data served in the last few decades as an invaluable tool to test the theory at the quantum level. It has also provided stringent constraints on many "new physics" scenarios. The (so far) remarkable agreement between the precise measurements of the electroweak observables and their SM predictions is a striking experimental confirmation of the theory, even if there are a few observables where the agreement is not so satisfactory. On the other hand, the Higgs boson has not yet been observed, and there are strong theoretical arguments hinting at the presence of physics beyond the SM. Future colliders, like the upcoming LHC or an e^+e^- international linear collider (ILC), will hopefully answer many such questions, offering at the same time great physics potential and a new challenge to provide even more precise theoretical predictions.

Precise SM predictions require precise input parameters. Among the three basic input parameters of the electroweak (EW) sector of the SM – the fine-structure constant α, the Fermi coupling constant G_F and the mass of the Z boson – α is by far the most precisely known, determined mainly from the anomalous magnetic moment of the electron with an amazing relative precision of 3.3 parts per billion (ppb) [11]. However, physics at nonzero squared momentum transfer q^2 is actually described by an effective electromagnetic coupling $\alpha(q^2)$ rather than by the low-energy constant α itself. The shift of the fine-structure constant from the Thomson limit to high energy involves non-perturbative hadronic effects which spoil this fabulous precision. Indeed, the present accuracies of these basic parameters are [11–13]

$$\delta\alpha/\alpha \sim 3 \times 10^{-9}\,, \quad \delta G_\mathrm{F}/G_\mathrm{F} \sim 9 \times 10^{-6}\,, \tag{1}$$

$$\delta M_Z/M_Z \sim 2 \times 10^{-5}\,, \quad \delta\alpha(M_Z^2)/\alpha(M_Z^2) \sim O(10^{-4})\,. \tag{2}$$

The relative uncertainty of $\alpha(M_Z^2)$ is roughly one order of magnitude worse than that of M_Z, making it one of the limiting factors in the calculation of precise SM predictions.

The effective fine-structure constant at the scale M_Z, $\alpha(M_Z^2) = \alpha/[1 - \Delta\alpha(M_Z^2)]$, plays a crucial role in basic EW radiative corrections of the SM. An important example is the EW mixing parameter $\sin^2\theta$, related to α, G_F and M_Z via the Sirlin relation [14–19]

$$\sin^2\theta_\mathrm{S}\cos^2\theta_\mathrm{S} = \frac{\pi\alpha}{\sqrt{2}G_\mathrm{F}M_Z^2(1-\Delta r_\mathrm{S})}\,, \tag{3}$$

where the subscript S identifies the renormalization scheme. $\Delta r_{\rm S}$ incorporates the universal correction $\Delta\alpha(M_Z^2)$, large contributions that depend quadratically on the top quark mass [20] (which led to its indirect determination before the discovery of this quark at the Tevatron [21, 22]), plus all remaining quantum effects. In the SM, $\Delta r_{\rm S}$ depends on various physical parameters such as α, $G_{\rm F}$, M_Z, M_W, $M_{\rm H}$, m_f, etc., where m_f stands for a generic fermion mass. As $M_{\rm H}$, the mass of the Higgs boson, is the only relevant unknown parameter in the SM, important indirect bounds on this missing ingredient can be set by comparing the calculated quantity in (3) with the experimental value of $\sin^2\theta_{\rm S}$. These constraints can be easily derived using the simple formulae of [23–27], which relate the effective EW mixing angle $\sin^2\theta_{\rm eff}^{\rm lept}$ (measured at LEP and SLC from the on-resonance asymmetries) with $\Delta\alpha(M_Z^2)$ and other experimental inputs like the mass of the top quark. It is important to note that the present error in the effective electromagnetic coupling constant, $\delta\Delta\alpha(M_Z^2) = 35\times10^{-5}$ [28], dominates the uncertainty of the theoretical prediction of $\sin^2\theta_{\rm eff}^{\rm lept}$, inducing an error $\delta(\sin^2\theta_{\rm eff}^{\rm lept}) \sim 12\times10^{-5}$ which is not much smaller than the experimental value $\delta(\sin^2\theta_{\rm eff}^{\rm lept})^{\rm EXP} = 16\times10^{-5}$ determined by LEP-I and SLD [29, 30]. Moreover, as measurements of the effective EW mixing angle at a future linear collider may improve its precision by one order of magnitude [31], a much smaller value of $\delta\Delta\alpha(M_Z^2)$ will be required (see next section). It is therefore crucial to assess all viable options to further reduce this uncertainty. The latest global fit of the LEP Electroweak Working Group, which employs the complete set of EW observables, leads to the value $M_{\rm H} = 91^{+45}_{-32}$ GeV, with a 95% confidence level upper limit of 186 GeV (see Fig. 1) [29, 30]. This limit increases to 219 GeV when including the LEP-II direct search lower limit of 114 GeV.

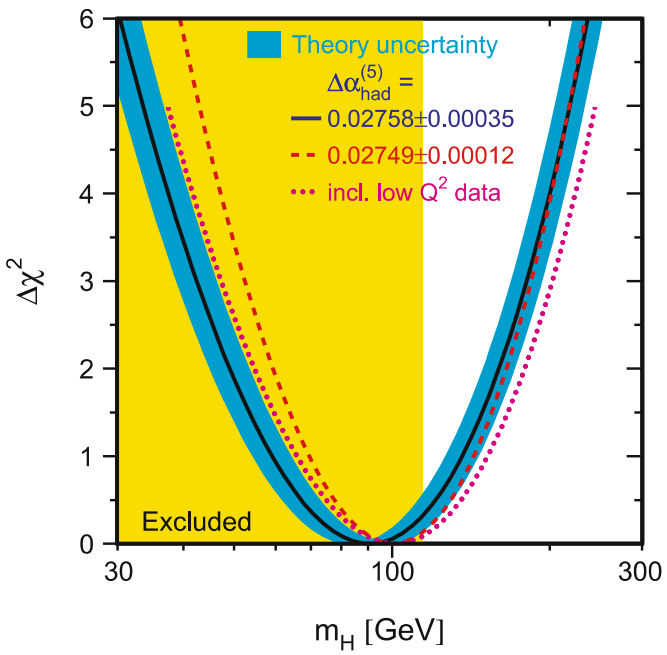

Fig. 1. The line is the result of the Electroweak Working Group fit using all data [29, 30]; the band represents an estimate of the theoretical error due to missing higher order corrections. The *vertical band* shows the 95% CL exclusion limit on $M_{\rm H}$ from the direct search

In the next few years the LHC may delight us with many discoveries, and the Higgs boson may be close at hand. Once its mass will be known, precision EW tests will provide excellent possibilities to establish new physics contributions beyond the SM. A high-precision EW program will be the natural complement to direct searches of new particles and will help indicate the directions that future studies must take. Eventually, if "new physics" will be directly uncovered at collider facilities, precision measurements of its properties will guide our search for even higher scale phenomena.

2.2.2 The effective fine-structure constant at the scale M_Z

Let us examine the determination of the running of the effective fine-structure constant to the scale M_Z, that can be defined by $\Delta\alpha(M_Z^2) = 4\pi\alpha\,{\rm Re}[\Pi^{(f)}_{\gamma\gamma}(0) - \Pi^{(f)}_{\gamma\gamma}(M_Z^2)]$, where $\Pi^{(f)}_{\gamma\gamma}(q^2)$ is the fermionic part of the photon vacuum polarisation function (with the top quark decoupled). Its evaluation includes hadronic contributions where long-distance QCD dynamics cannot be calculated analytically. These contributions cause the aforementioned dramatic loss of accuracy, by several orders of magnitude, which occurs moving from the value of α at vanishing momentum transfer to that at $q^2 = M_Z^2$. The shift $\Delta\alpha(M_Z^2)$ can be split in two parts: $\Delta\alpha(M_Z^2) = \Delta\alpha_{\rm lep}(M_Z^2) + \Delta\alpha^{(5)}_{\rm had}(M_Z^2)$. The leptonic contribution is calculable in perturbation theory and known up to three-loops: $\Delta\alpha_{\rm lep}(M_Z^2) = 3149.7686\times10^{-5}$ [32]. The hadronic contribution $\Delta\alpha^{(5)}_{\rm had}(M_Z^2)$ of the five light quarks (u, d, s, c, and b) can be computed from hadronic e^+e^- annihilation data via the dispersion relation [33]

$$\Delta\alpha^{(5)}_{\rm had}(M_Z^2) = -\left(\frac{\alpha M_Z^2}{3\pi}\right){\rm Re}\int_{4m_\pi^2}^{\infty}{\rm d}s\frac{R(s)}{s(s-M_Z^2-{\rm i}\epsilon)}\,, \tag{4}$$

where $R(s) = \sigma^{(0)}(s)/(4\pi\alpha^2/3s)$ and $\sigma^{(0)}(s)$ is the total cross section for e^+e^- annihilation into any hadronic state, with extraneous QED corrections subtracted off. In the 1990s, detailed evaluations of this dispersive integral have been carried out by several authors [34–44]. More recently, some of these analyses were updated to include new e^+e^- data – mostly from CMD-2 [45] and BES [46] – obtaining: $\Delta\alpha^{(5)}_{\rm had} = 2761\,(36)\times10^{-5}$ [47], $\Delta\alpha^{(5)}_{\rm had} = 2757\,(36)\times10^{-5}$ [48], $\Delta\alpha^{(5)}_{\rm had} = 2755\,(23)\times10^{-5}$ [49], and $\Delta\alpha^{(5)}_{\rm had} = 2749\,(12)\times10^{-5}$ [50]. The reduced uncertainty of the latter result has been obtained making stronger use of theoretical inputs. The reduction, by a factor of two, of the uncertainty quoted in the first article of [34–43] (70×10^{-5}), with respect to that in [48] (36×10^{-5}), is mainly due to the data of BES. The latest update, $\Delta\alpha^{(5)}_{\rm had} = 2758\,(35)\times10^{-5}$ [28], includes also the measurements of KLOE [51]. Table 1 (from [48]) shows that an uncertainty $\delta\Delta\alpha^{(5)}_{\rm had} \sim 5\times10^{-5}$, needed for precision physics at a future linear collider, requires the measurement of the hadronic cross section with a precision of $O(1\%)$ from threshold up to the Υ peak.

Table 1. Values of the uncertainties $\delta\Delta\alpha^{(5)}_{\rm had}$ (first column) and the errors induced by these uncertainties on the theoretical SM prediction for $\sin^2\theta^{\rm lept}_{\rm eff}$ (second column). The third column indicates the corresponding requirements on the R measurement

$\delta\Delta\alpha^{(5)}_{\rm had}\times 10^5$	$\delta(\sin^2\theta^{\rm lept}_{\rm eff})\times 10^5$	Request on R
35	12.5	present
7	2.5	$\delta R/R\sim 1\%$ for $\sqrt{s}\le M_{J/\psi}$
5	1.8	$\delta R/R\sim 1\%$ for $\sqrt{s}\le M_\Upsilon$

2.2.3 The muon $g-2$

During the last few years, in a sequence of increasingly precise measurements, the E821 Collaboration at Brookhaven has determined $a_\mu=(g_\mu-2)/2$ with a fabulous relative precision of 0.5 parts per million (ppm) [52–57], allowing us to test all sectors of the SM and to scrutinise viable alternatives to this theory [58]. The present world average experimental value is $a_\mu^{\rm EXP}=116\,592\,080\,(63)\times 10^{-11}\,(0.5\,{\rm ppm})$ [56, 57]. This impressive result is still limited by statistical errors. A new experiment, E969, has been approved (but not yet funded) at Brookhaven in 2004 [59, 60]. Its goal is to reduce the present experimental uncertainty by a factor of 2.5 to about 0.2 ppm. A letter of intent for an even more precise $g-2$ experiment was submitted to J-PARC with the proposal to reach a precision below 0.1 ppm [61]. But how precise is the theoretical prediction?

The SM prediction $a_\mu^{\rm SM}$ is usually split into three parts: QED, electroweak and hadronic (see [62–67] for recent reviews). The QED contribution to a_μ arises from the subset of SM diagrams containing only leptons (e,μ,τ) and photons. First computed by Schwinger more than fifty years ago [68], it is now known up to terms of order $(\alpha/\pi)^4$, and leading five-loop contributions have been evaluated. The prediction currently stands at $a_\mu^{\rm QED}=116\,584\,719.4\,(1.4)\times 10^{-11}$ [69], where the error is due to the uncertainty of the $O(\alpha^4)$ and $O(\alpha^5)$ terms, and to the uncertainty of α. The EW contribution to a_μ is suppressed by a factor $(m_\mu/M_W)^2$ with respect to the QED effects. Complete one- and two-loop calculations have been carried out leading, for $M_{\rm H}=150\,{\rm GeV}$, to $a_\mu^{\rm EW}=154(1)(2)\times 10^{-11}$ [70]. The first error is due to hadronic loop uncertainties, while the second one corresponds to an allowed range of $M_{\rm H}\in[114,250]\,{\rm GeV}$, to the current top mass uncertainty, and to unknown three-loop effects. The leading-logarithm three-loop contribution to $a_\mu^{\rm EW}$ is extremely small [70, 71].

Like the effective fine-structure constant at the scale M_Z, the SM determination of the anomalous magnetic moment of the muon is presently limited by the evaluation of the hadronic vacuum polarisation and, in turn, by our knowledge of the low-energy total cross-section for e^+e^- annihilations into hadrons. Indeed, the hadronic leading-order contribution $a_\mu^{\rm HLO}$, due to the hadronic vacuum polarisation correction to the one-loop diagram, involves long-distance QCD effects which cannot be computed perturbatively. However, using analyticity and unitarity, it was shown long ago that this term can be computed from hadronic e^+e^- annihilation data via the dispersion integral [72, 73]

$$a_\mu^{\rm HLO}=(1/4\pi^3)\int_{4m_\pi^2}^{\infty}{\rm d}sK(s)\sigma^{(0)}(s)$$
$$=(\alpha^2/3\pi^2)\int_{4m_\pi^2}^{\infty}{\rm d}sK(s)R(s)/s\,. \qquad (5)$$

The kernel function $K(s)$ decreases monotonically for increasing s. This integral is similar to the one entering the evaluation of the hadronic contribution $\Delta\alpha^{(5)}_{\rm had}(M_Z^2)$ in (4). Here, however, the weight function in the integrand gives a stronger weight to low-energy data. Figure 2 (from [49]) shows the fractions of the total contributions and the squared errors from various energy intervals in the dispersion integrals for $a_\mu^{\rm HLO}$ and $\Delta\alpha^{(5)}_{\rm had}(M_Z^2)$.

An important role among all e^+e^- annihilation measurements is played by the precise data collected in 1994–95 by the CMD-2 detector at the VEPP-2M collider in Novosibirsk for the $e^+e^-\to\pi^+\pi^-$ cross section at values of $\sqrt{s}$ between 0.61 and 0.96 GeV [45] (quoted systematic error 0.6%, dominated by the uncertainties in the radiative corrections). Recently [74, 75] the CMD-2 Collaboration released its 1996–98 measurements for the same cross section in the full energy range $\sqrt{s}\in[0.37,1.39]\,{\rm GeV}$. The part of these data for $\sqrt{s}\in[0.61,0.96]\,{\rm GeV}$ (quoted systematic error 0.8%) agrees with their earlier result published in [45]. In 2005, also the SND Collaboration (at the VEPP-2M collider as well)

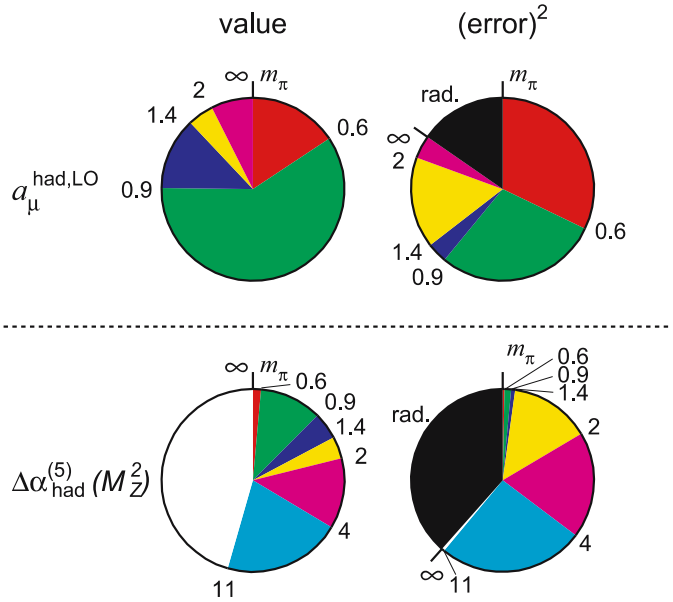

Fig. 2. The pie diagrams show the fractions of the total contributions and the squared errors from various energy intervals in the dispersion integrals in (4) and (5). The diagrams for the leading-order hadronic contribution to the muon $g-2$, shown in the *first row*, correspond to sub-contributions with energy boundaries at 0.6, 0.9, 1.4, 2 GeV and ∞, whereas for the hadronic contribution to the effective fine-structure constant, shown in the *second row*, the boundaries are at 0.6, 0.9, 1.4, 2, 4, 11.09 GeV and ∞. In the squared error diagrams, the contributions arising from the treatment of the radiative corrections to the data are also included [49]

released its analysis of the $e^+e^- \to \pi^+\pi^-$ process for $\sqrt{s}$ between 0.39 and 0.98 GeV, with a systematic uncertainty of 1.3% (3.2%) for $\sqrt{s}$ larger (smaller) than 0.42 GeV [76]. However, a recent preliminary reanalysis of these data [77] uncovered an error in the treatment of the radiative corrections, reducing the value of the measured cross-section. The new preliminary result appears to be in good agreement with the corresponding one from CMD-2. Further significant progress is expected from the e^+e^- collider VEPP-2000 [8–10] under construction in Novosibirsk. In 2004 the KLOE experiment at the DAFNE collider in Frascati presented a precise measurement of $\sigma(e^+e^- \to \pi^+\pi^-)$ via the initial-state radiation (ISR) method at the ϕ resonance [51] (see later). This cross section was extracted for $\sqrt{s}$ between 0.59 and 0.97 GeV with a systematic error of 1.3% and a negligible statistical one. There are some discrepancies between the KLOE and CMD-2 results, although their integrated contributions to $a_\mu^{\rm HLO}$ are similar. The data of KLOE and SND [76] disagree above the ρ peak, where the latter are significantly higher. However, the values of the latter appears to be lower after the new preliminary reanalysis presented in [77]. The study of the $e^+e^- \to \pi^+\pi^-$ process via the ISR method is also in progress at BABAR [78] and Belle [79]. On the theoretical side, analyticity, unitarity and chiral symmetry provide strong constraints for the pion form factor in the low-energy region [80]. Recent evaluations of the dispersive integral based on the CMD-2 analysis of [45] are in good agreement: $a_\mu^{\rm HLO} = 6934\,(53)_{\rm exp}(35)_{\rm rad} \times 10^{-11}$ [81], $a_\mu^{\rm HLO} = 6948\,(86) \times 10^{-11}$ [13,48], $a_\mu^{\rm HLO} = 6924\,(59)_{\rm exp}(24)_{\rm rad} \times 10^{-11}$ [49], $a_\mu^{\rm HLO} = 6944\,(48)_{\rm exp}(10)_{\rm rad} \times 10^{-11}$ [50]. Reference [81] already includes KLOE's results. The recent data of CMD-2 [74,75] and SND [76,77] are not yet included.

The authors of [44] pioneered the idea of using vector spectral functions derived from the study of hadronic τ decays [82] to improve the evaluation of the dispersive integral. However, the latest analysis with ALEPH, CLEO, and OPAL data yields $a_\mu^{\rm HLO} = 7110\,(50)_{\rm exp}(8)_{\rm rad}(28)_{\rm SU(2)} \times 10^{-11}$ [83], a value significantly higher than those obtained with e^+e^- data (see [84,85] for recent preliminary results from Belle). Isospin-breaking corrections were applied [86–88]. Indeed, although the precise CMD-2 $e^+e^- \to \pi^+\pi^-$ data [45] are consistent with the corresponding τ ones for energies below ~ 0.85 GeV, they are significantly lower for larger energies. KLOE's $\pi^+\pi^-$ spectral function confirms this discrepancy with the τ data. SND's 2005 results [76] were compatible with the τ ones, but the very recent preliminary reanalysis presented in [77] seems to indicate that this is no longer the case. This puzzling discrepancy between the $\pi^+\pi^-$ spectral functions from e^+e^- and isospin-breaking-corrected τ data could be caused by inconsistencies in the e^+e^- or τ data, or in the isospin-breaking corrections which must be applied to the latter [89–92].

The hadronic higher-order (α^3) contribution $a_\mu^{\rm HHO}$ can be divided into two parts: $a_\mu^{\rm HHO} = a_\mu^{\rm HHO}({\rm vp}) + a_\mu^{\rm HHO}({\rm lbl})$. The first one is the $O(\alpha^3)$ contribution of diagrams containing hadronic vacuum polarisation insertions [93]. Its latest value is $a_\mu^{\rm HHO}({\rm vp}) = -97.9\,(0.9)_{\rm exp}(0.3)_{\rm rad} \times 10^{-11}$ [49]. The second term, also of $O(\alpha^3)$, is the hadronic light-by-light contribution. As it cannot be directly determined via a dispersion relation approach using data (unlike the hadronic vacuum polarisation contribution), its evaluation relies on specific models of low-energy hadronic interactions with electromagnetic currents. Three major components of $a_\mu^{\rm HHO}({\rm lbl})$ can be identified: charged-pion loops, quark loops, and pseudoscalar (π^0, η, and η') pole diagrams. The latter ones dominate the final result and require information on the electromagnetic form factors of the pseudoscalars (see Sects. 2.4.1 and 2.5.5). In 2001 the authors of [94–96] uncovered a sign error in earlier evaluations of the dominating pion–pole part. Their estimate of $a_\mu^{\rm HHO}({\rm lbl})$, based also on previous results for the quark and charged-pions loop parts [97–100], is $a_\mu^{\rm HHO}({\rm lbl}) = 80\,(40) \times 10^{-11}$. A higher value was obtained in 2003 including short-distance QCD constraints: $a_\mu^{\rm HHO}({\rm lbl}) = 136\,(25) \times 10^{-11}$ [101]. Further independent calculations would provide an important check of this contribution.

The SM prediction of the muon $g-2$ is given by the sum $a_\mu^{\rm SM} = a_\mu^{\rm QED} + a_\mu^{\rm EW} + a_\mu^{\rm HLO} + a_\mu^{\rm HHO}$. The discrepancies between recent SM predictions and the current experimental value vary in a very wide range, from roughly 1 to 3σ, according to the values chosen for the hadronic contributions. If only e^+e^- data are employed, $a_\mu^{\rm SM}$ deviates from $a_\mu^{\rm EXP}$ by $2-3\sigma$. The analysis of this section shows that while the QED and EW contributions appear to be ready to rival the forecasted precisions of future experiments (like E969), much effort will be needed to reduce the hadronic uncertainty. This effort is challenging but possible, an d certainly well motivated by the excellent opportunity the muon $g-2$ is providing us to unveil (or constrain) "new physics" effects. Once again, a long-term program of hadronic cross-section measurements is clearly warranted.

2.2.4 Status of R at low energy

During the last thirty years the ratio R has been measured by several experiments. Usually, for energies below 2 GeV the cross section is measured for individual channels, while above that value the hadronic final states are treated inclusively. Figure 3 shows an up-to-date compilation of these data by Burkhardt and Pietrzyk [28]. The main improvements are in the region below 5 GeV (where the data are now closer to the prediction of perturbative QCD): between 2 and 5 GeV, the BESII collaboration reduced the error to $\sim 7\%$ [46] (before it was $\sim 15\%$); below 1 GeV, the CMD-2 and SND collaborations at Novosibirsk, and KLOE at Frascati, measured the pion form factor in the energy range around the ρ peak with a systematic error of 0.6%, 1.3%, and 1.3% respectively. In Fig. 3, the recent published results from the BABAR collaboration [109,110] on the cross sections e^+e^- to 3 and 4 hadrons are not yet included. The uncertainty in the 1–2 GeV region is still 15% [28].

The measurement of the hadronic cross section has been usually performed by varying the e^+e^- beam energies. An alternative approach, recently [102] proposed, consists of extracting $\sigma_{\rm had}$ from initial state radiation (ISR) events at flavour factories, where the high luminosity of the machine compensates for the reduced cross-section. This method, successfully applied by KLOE and BABAR, has the advantage of the same normalisation for each energy point, even if it requires a very solid theoretical understanding of radiative corrections, a pre-

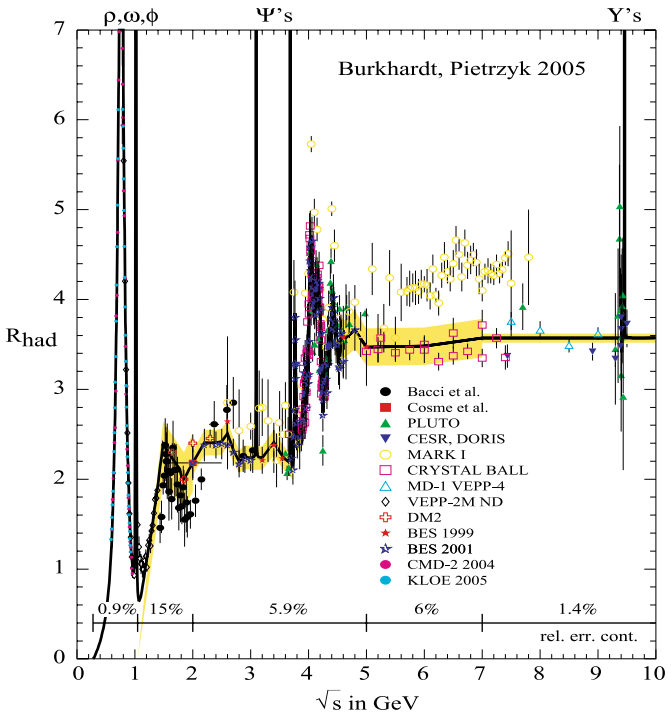

Fig. 3. An updated compilation of R measurements from [28]. In the *bottom line* the overall uncertainties of the different regions are reported

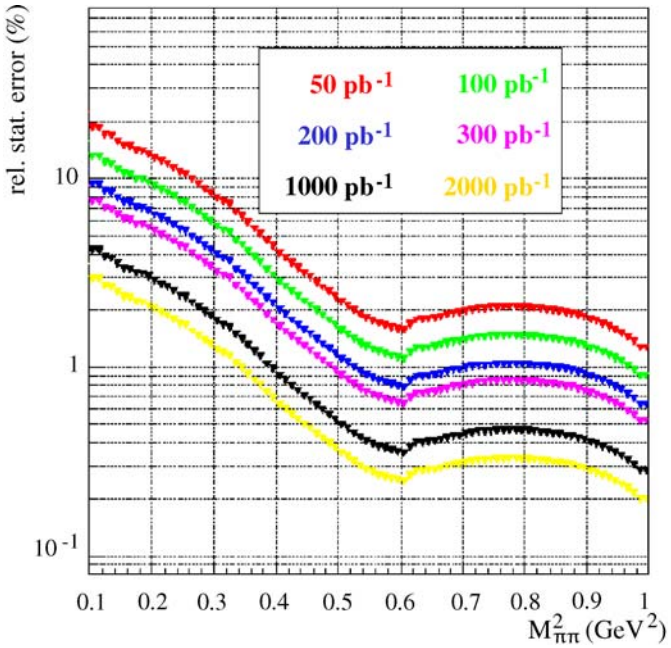

Fig. 4. The relative statistical error on the cross section $\mathrm{d}\sigma/\mathrm{d}M^2_{\pi\pi}$ as a function of the $\pi\pi$ invariant mass squared, $M^2_{\pi\pi}$, (bin width $=$ $0.01\,\mathrm{GeV}^2$), according to different integrated luminosities

cise determination of the angle and energy of the emitted photon, and the full control of background events, especially for events with the photon emitted in the final state (FSR). The Karlsruhe–Katowice group computed the radiative corrections up to NLO for different exclusive channels, implementing them in the event generator PHOKHARA [103–107]. The current precision for the $\pi^+\pi^-\gamma$ final state is 0.5%.

In the following we will consider the impact of DAFNE-2 on the hadronic cross-section measurements in the full accessible region [$2m_\pi$–2.5 GeV], by considering three main energy regions.

$\pi^+\pi^-$ threshold region. The threshold region, $[2m_\pi - 0.5\,\mathrm{GeV}]$, provides 13% of the total $\pi^+\pi^-$ contribution to the muon anomaly: $a_\mu^{\mathrm{HLO}}\ [2m_\pi - 0.5\,\mathrm{GeV}] = (58.0 \pm 2.1) \times 10^{-10}$ [81] To overcome the lack of precise data at threshold energies, the pion form factor is extracted from a parametrisation based on Chiral Perturbation Theory, constrained from space-like data [108]. The most effective way to measure the threshold in the time-like region is provided by ISR events, where the emission of an energetic photon allows to study the two pions at rest. However, at DAFNE, the process $\phi \to \pi^+\pi^-\pi^0$, where one photon gets lost, is hundreds of times more frequent than the signal, and therefore a precise measurement requires an accurate evaluation of the background. Furthermore, irreducible backgrounds due to $\phi \to \pi^+\pi^-\gamma$ are also present when running at the ϕ resonance peak. The background issue can be largely overcome by running at $\sqrt{s} < M_\phi$: such a possibility has been already explored by the KLOE experiment, which is taking more than $200\,\mathrm{pb}^{-1}$ of data at 1 GeV. Figure 4 shows the statistical precision that can be reached in the region below 1 GeV for different integrated luminosities, with a bin width of $0.01\,\mathrm{GeV}^2$. A statistics of $2\,\mathrm{fb}^{-1}$ at 1 GeV will allow to achieve a statistical error on a_μ^{HLO} at threshold below 1%. Notice that in order to maintain the systematic uncertainty at the same level, it is important to take data below the ϕ peak, to reduce the backgrounds.

The ρ peak region. The $\pi^+\pi^-$ region between 0.5 and 1 GeV has been studied by different experiments. CMD-2 [45] and SND [76] performed an energy scan at the e^+e^- collider VEPP–2M ($\sqrt{s} \in [0.4 - 1.4]$ GeV) with $\sim 10^6$ and $\sim 4.5 \times 10^6$ events respectively, with systematic errors ranging from 0.6% to 4% in the relative cross-section, depending on the 2π energy region. The pion form factor has also been measured by KLOE using ISR, and results are also expected soon by BABAR. KLOE published a result [51] based on an integrated luminosity of $140\,\mathrm{pb}^{-1}$, that led to a relative error of 1.3% in the energy region $[0.6 - 0.97]$ GeV, dominated by systematics. At the moment it has already collected more than $2\,\mathrm{fb}^{-1}$ at the ϕ meson peak, which represents, around the ρ peak, a statistics of $\sim 2 \times 10^7\ \pi^+\pi^-\gamma$ events. BABAR [109, 110] has already collected more than $300\,\mathrm{fb}^{-1}$ at the Υ peak, and is going to collect about $1\,\mathrm{ab}^{-1}$ by the end of data taking. The results of these four experiments in the next few years will probably allow to know the $\pi^+\pi^-$ cross-section for most of the ρ shape with a relative accuracy better than 1% (even considering both statistical and systematic errors). The discrepancies now present in the shape could be then washed out. In this case, a significant improvement from DAFNE-2 is not envisaged on this region.

The $1 - 2.5\,GeV$ energy region. The region [1–2.5 GeV], with an uncertainty of roughly 15%, is the most poorly known, and contributes about 40% to the uncertainty of the total disper-

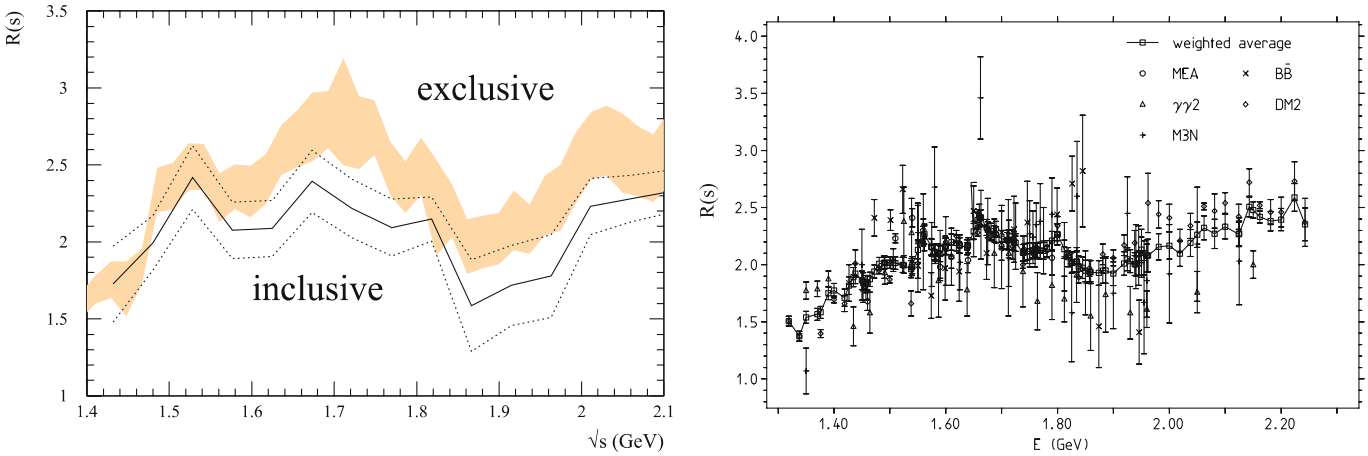

Fig. 5. *Left*: comparison between the inclusive R measurements and the sum of exclusive channels [49]. *Right*: a compilation [13] of the most recent R inclusive measurements in the same energy range. Notice that three out of the five experiments whose data are presented in this figure, come from Adone at Frascati in the seventies (namely MEA, $\gamma\gamma 2$ and $B\overline{B}$)

sion integral for $\Delta^{(5)}_{\rm had}(m_Z^2)$ [28]. It also provides most of the contribution to $a_\mu^{\rm HLO}$ above 1 GeV.

We will now consider the impact of DAFNE-2 for inclusive and exclusive measurements separately:

– **Inclusive measurements:** There is a systematic difference between the sum of exclusive channels and the inclusive measurements [49], where most of the recent inclusive data are from the early 80's (obtained with a total integrated luminosity of 200 $\rm nb^{-1}$).
Figure 5 (left) shows the comparison between the inclusive and the sum of exclusive R measurements in the energy range [1.4–2.1] GeV, while the plot on the right collects the most recent inclusive data in the same range [13].
With a specific luminosity of $10^{32}\,\rm cm^{-2}\,s^{-1}$, DAFNE-2 can perform a scan in the region from 1 to 2.5 GeV, collecting an integrated luminosity of 20 $\rm pb^{-1}$ per point (corresponding to few days of data taking). By assuming an energy step of 25 MeV, the whole region would be scanned in one year of data taking. A detector à la KLOE, plus some minor improvements such as a finer calorimeter readout and an inner tracker (see Sect. 4), will be capable to perform an inclusive R measurement at the percent level. This would represent a major improvement on this issue.

– **Exclusive channels:** A different issue concerns the exclusive measurements. In this case, BABAR has published results on e^+e^- into 3 and 4 hadrons, obtained with an integrated luminosity of 89 $\rm fb^{-1}$ [109, 110], and it is expected to reach 1 $\rm ab^{-1}$ by the end of the data taking. However, due to the ISR photon emission at the $\Upsilon(4s)$ resonance, the effective luminosity for tagged photon ($\theta_\gamma > 20^\circ$) in the energies below 2.5 GeV, will be of the order of few $\rm pb^{-1}$ at full statistics. This is shown in Fig. 6, where a bin width of 25 MeV and an overall efficiency of 10% are assumed [109, 110].
Figure 7 shows the statistical error for the channels $\pi^+\pi^-\pi^0$, $2\pi^+2\pi^-$ and $\pi^+\pi^-K^+K^-$, which can be achieved by an energy scan at DAFNE-2 with 20 $\rm pb^{-1}$ per point, compared with BABAR with published (89 $\rm fb^{-1}$), and full (890 $\rm fb^{-1}$) statistics. As it can be seen, an energy scan allows to reach a statistical accuracy of the order of 1% for most of the energy points.
We finally estimate the statistical accuracy which can be reached by DAFNE-2 using ISR at $\sqrt{s} = 2.5$ GeV.
Figure 8 shows the statistical accuracy for the same exclusive channels achieved by DAFNE-2 with 2 $\rm fb^{-1}$ at 2.5 GeV, compared with BABAR with published (89 $\rm fb^{-1}$), and full (890 $\rm fb^{-1}$) statistics. In this case improvements from DAFNE-2 are not so significant.

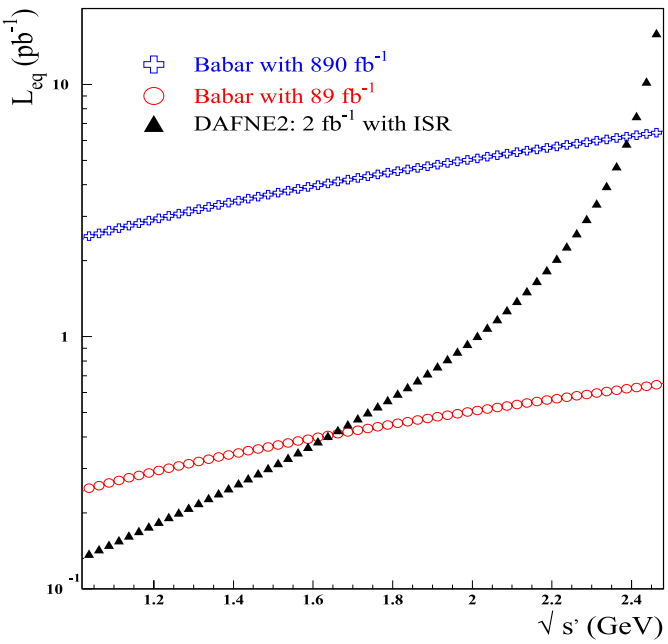

Fig. 6. Equivalent luminosity for: BABAR with 890 $\rm fb^{-1}$ (*cross*); BABAR with 89 $\rm fb^{-1}$ (*circle*); DAFNE-2 with 2 $\rm fb^{-1}$, using ISR at 2.5 GeV (*triangle*). A bin width of 25 MeV is assumed. A polar angle of the photon larger than 20° and an overall efficiency of 10% are assumed [109, 110]

Finally we notice that an issue for this kind of measurement is the accuracy in the determination of the center of mass energy.

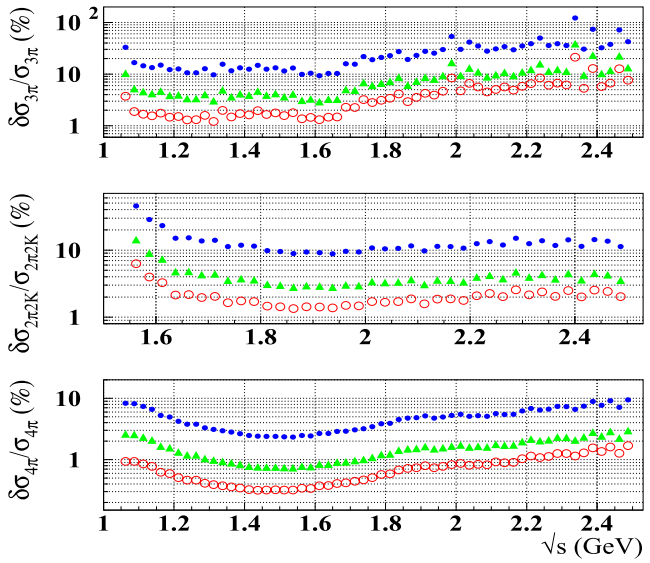

Fig. 7. Comparison of the statistical accuracy in the cross-section among DAFNE-2 with an energy scan with 20 pb^{-1} per point (○); published BABAR results (●), BABAR with full statistics (▲) for $\pi^+\pi^-\pi^0$ (*top*), $\pi^+\pi^-K^+K^-$ (*middle*) and $2\pi^+2\pi^-$ (*down*) channels. An energy step of 25 MeV is assumed

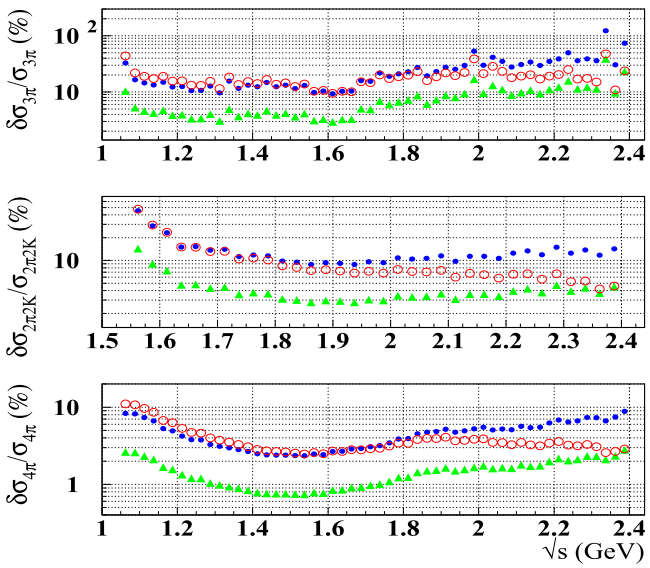

Fig. 8. Comparison of the statistical accuracy in the cross-section among DAFNE-2 with ISR at 2.5 GeV, 2 fb^{-1} (○); published BABAR results (●), BABAR with full statistics (▲) for $\pi^+\pi^-\pi^0$ (*top*), $\pi^+\pi^-K^+K^-$ (*middle*) and $2\pi^+2\pi^-$ (*down*) channels. A bin width of 25 MeV is assumed

Based on the KLOE experience, without resonant depolarization it's reasonable to obtain an accuracy on the c.m. energy of $O(10^{-4})$, i.e. 100–200 keV. For a better precision other methods, like resonant depolarization, are needed.

2.2.5 Conclusions

In summary, the possibility to make precision tests of the standard model in future experiments, requires a more accurate knowledge of the hadronic cross-section in all the energy range between the $2m_\pi$ threshold and 2.5 GeV. The region between 1 and 2.5 GeV is at present the most poorly known and is crucial for the computation of the hadronic corrections to the effective fine structure constant at the scale m_Z. In order to improve the theoretical accuracy on a_μ, a very accurate measurement at lower energy would also be required. In both regions, DAFNE-2 can give important contributions.

2.3 Vector mesons spectroscopy

Apart from allowing precision tests of the standard model, the measurement of the $\sqrt{s}$ dependence of the cross sections of exclusive channels, represents the primary source of information for the vector meson spectroscopy in the low energy region. This study of the vector meson spectroscopy is interesting to test and to provide experimental inputs to the models of the strong interactions at low energies. Moreover the existence of glueballs and hybrid mesons, predicted by QCD in this energy range and never observed in a clean way, can be investigated.

2.3.1 Vector mesons below 2.5 GeV

An e^+e^- machine with $1.0 \leq \sqrt{s} \leq 2.5$ GeV can give an important contribution to the study of the vector mesons. A high statistics scan of the energy region quoted above can: (i) improve the knowledge on the established vector mesons, (ii) well measure the parameters of other vector states, whose interpretation is still not clear, (iii) search for possible new vector states. Moreover, since there are discrepancies between some recent measurement of exclusive cross sections of the BABAR Collaboration [109–111] with the ISR method and the older energy scan measurements [112], a test of the ISR method versus the energy scan one can be performed, by running at the maximum $\sqrt{s}$ and comparing the results with the energy scan with the same detector.

Established mesons. In Table 2 the generally accepted vector mesons below 2.5 GeV are reported. The agreement of the observed masses with the prediction of the quark model [113] suggests the interpretation of these mesons as the fundamental states and the first radial and orbital excitations of the $q\bar{q}$ system.

However this interpretation is not universally accepted [114, 115], since there are some inconsistencies with the predictions of the quark model (in its $^3P_0$ version [116–118]). In Fig. 9 are reported the cross sections of $e^+e^- \to 4\pi$; according to the $^3P_0$ model, the ρ_{2S} contribution to this final state is negligible, while the ρ_{1D} one is large and is dominated by the $a_1(1260)\pi$ and $h_1(1170)\pi$ intermediate states, with simi-

Table 2. Classification of vector mesons

	$(u\bar{u}-d\bar{d})/\sqrt{2}$	$(u\bar{u}+d\bar{d})/\sqrt{2}$	$s\bar{s}$
$1\,^3S_1$	$\rho(770)$	$\omega(782)$	$\phi(1020)$
$2\,^3S_1$	$\rho(1450)$	$\omega(1420)$	$\phi(1680)$
$1\,^3D_1$	$\rho(1700)$	$\omega(1650)$	–

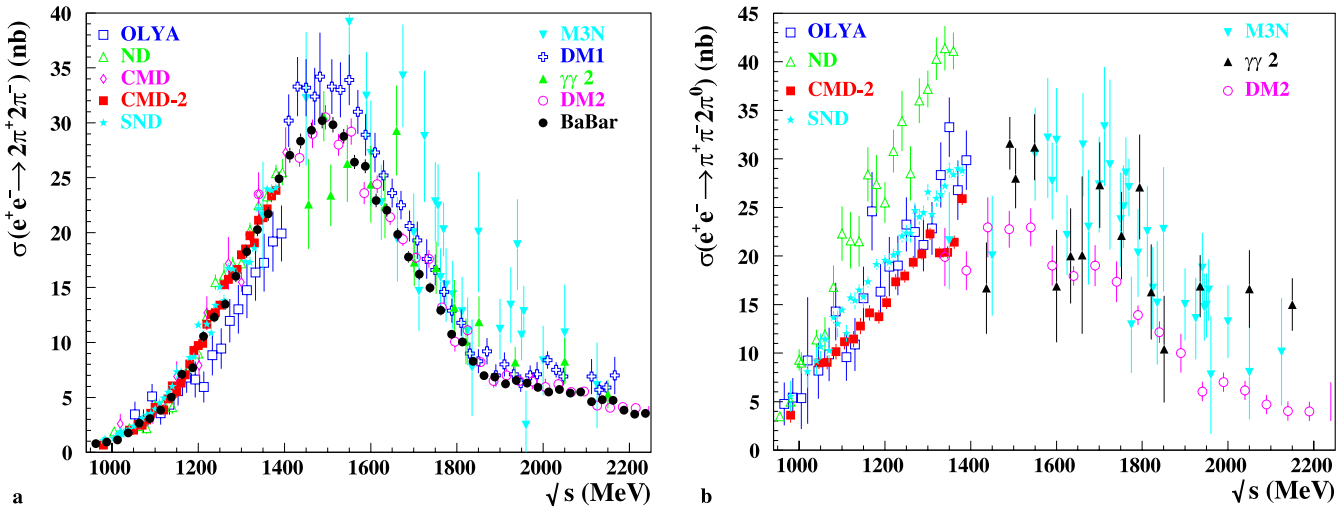

Fig. 9. $e^+e^- \to 4\pi$ cross sections [141, 142, 148]

lar partial widths. As $h_1\pi$ only contributes to the $\pi^+\pi^-\pi^0\pi^0$ final state, while $a_1\pi$ contributes to both $\pi^+\pi^-\pi^0\pi^0$ and $\pi^+\pi^-\pi^+\pi^-$, one would expect $\sigma(e^+e^- \to \pi^+\pi^-\pi^0\pi^0) > \sigma(e^+e^- \to \pi^+\pi^-\pi^+\pi^-)$ after the subtraction of the $\omega\pi^0$ cross section from $\sigma(e^+e^- \to \pi^+\pi^-\pi^0\pi^0)$. But experimentally one finds $\sigma(e^+e^- \to \pi^+\pi^-\pi^+\pi^-) \simeq 2\sigma(e^+e^- \to \pi^+\pi^-\pi^0\pi^0)$. A possible explanation is a mixing of a vector hybrid $\rho_{\rm H}$ with the ρ_{2S} and a small contribution of ρ_{1D}. The observed 4π cross sections will be explained by the fact that the dominant $\rho_{\rm H}$ decay channel is $a_1(1260)\pi$[119].

A similar pattern can be envisaged for the isoscalar sector, i.e. possible mixing of $\omega(1420)$ and $\omega(1650)$ with a hybrid $\omega_{\rm H}$.

Concerning the $s\bar{s}$ mesons, if the $\phi(1680)$ is the $2\,^3S_1$ state, the ϕ_{1D} is still missing.

Also the study of the radiative decays [120, 121] could help in testing the possible mixing of these mesons with hybrids (see next section).

Gluonic mesons. Hybrid mesons, i.e. mesons with excited gluonic degrees of freedom are predicted by QCD, with different, also exotic, quantum numbers. In the cases of u and d constituent quarks, the masses are predicted to be in the region 1.3–1.9 GeV. There is general agreement on the mass ordering of such mesons: $0^{-+} < 1^{-+} < 1^{--} < 2^{-+}$. There is also experimental evidence of exotic resonances, $\pi_1(1400)$ [122, 123] and $\pi_1(1600)$ [124], both with $J^{PC} = 1^{-+}$. If $\pi_1(1400)$ is the lowest hybrid, the lightest vector hybrid could be around 1.65 GeV, allowing the mixing pattern described above. If, on the other hand, the lowest hybrid is $\pi_1(1600)$, one could expect the lightest vector state at 1.9–2.0 GeV, excluding the mixing with the other vector mesons, but well inside the energy region covered by the machine under consideration. The $I = 1$ vector hybrid should decay essentially into $a_1(1260)\pi$ or $\rho\pi\pi$, then should be observable in the 4π final state. The $I = 0$ vector hybrid should decay into $\rho\pi$ and $\rho(1450)\pi$, allowing 3 and 5π final states. Models predicts also strange hybrids ($s\bar{s}g$) around 2.0 GeV, that should be observable in $K\overline{K}\pi$ and $K\overline{K}\pi\pi$ final states.

Concerning glueballs, according to the lattice calculations [125, 126], only the scalar $J^{PC} = 0^{++}$ is accessible at these energies via the radiative decays of the vector mesons (see next section).

Other vector mesons. Other vector mesons are present in the mass region under consideration.

The $\rho(1900)$ ($J^{PC} = 1^{--}$ and $I = 1$) is well established, measured by various experiments, but with different values of mass and width as reported in Table 3.

The open questions than can be answered by a high statistics measurement are: (i) is the mass above or below the nucleon-antinucleon threshold?, and (ii) the $\rho(1900)$ is large or narrow?

These questions are connected to the interpretation of this particle, two seem to be favoured: (a) baryonium state, (b) hy-

Table 3. $\rho(1900)$ parameters. BABAR results are obtained using the radiative return method

Experiment	Process	Mass (GeV)	Width (MeV)
DM2	$e^+e^- \to 6\pi$	~ 1.93	~ 35
FENICE [130]	$e^+e^- \to$ hadrons	~ 1.87	~ 10
E687 [149, 150]	$3\pi^+3\pi^-$ photoproduction	1.91 ± 0.01	33 ± 13
BABAR [111]	$e^+e^- \to 3\pi^+3\pi^-$	1.88 ± 0.03	130 ± 30
BABAR	$e^+e^- \to 2\pi^+2\pi^-2\pi^0$	1.86 ± 0.02	160 ± 20
BABAR [151]	$e^+e^- \to 2\pi^+2\pi^-$	1.88 ± 0.01	180 ± 20
BABAR	$e^+e^- \to \pi^+\pi^-2\pi^0$	1.89 ± 0.02	190 ± 20

brid meson. Baryonium can be either a diquark–antidiquark state with angular momentum $L = 1$ [127], or a $N\overline{N}$ quasi-nuclear bound state [128, 129]. In both cases it should be strongly coupled to $N\overline{N}$ and produce some visible signal, like threshold enhancements in the $e^+e^- \to N\overline{N}$ cross section. A threshold enhancement, compatible with a resonance below $p\overline{p}$ threshold [130], has been observed in the proton time-like form factor by PS170 [131] experiment at LEAR, and recently confirmed by BABAR [132]. Moreover BES-II Collaboration [133] has observed an enhancement at the $p\overline{p}$ threshold in $J/\psi \to p\overline{p}\gamma$, interpreted as the effect of a resonance of mass 1859 MeV and total width smaller than 30 MeV, but with different quantum numbers: $J^{PC} = 0^{-+}$ and $I = 0$. More recently it has been identified with the $X(1835)$ observed in $J/\psi \to \eta'\pi^+\pi^-\gamma$ [134]. Other threshold enhancements have been reported by BES-II Collaboration at the $p\overline{\Lambda}$ threshold, observed both in $J/\psi \to p\overline{\Lambda}K^-$ and $\psi' \to p\overline{\Lambda}K^-$, and by BELLE Collaboration [135, 136] at the $p\overline{p}$, $p\overline{\Lambda}$ and $\Lambda\overline{\Lambda}$ thresholds.

The hypothesis (b) is supported by the fact that in some model, as stated in the previous subsection, vector hybrids with 1.9–2.0 GeV mass and ~ 100 MeV decay width are predicted, and by the fact that OBELIX experiment did not observe evidence of baryonium type signal in $\overline{n}p \to 3\pi^+2\pi^-\pi^0$ [137].

The $\rho(2150)$ has been observed by GAMS Collaboration [138] in $\pi^-p \to \omega\pi^0 n$ and recently by BESII in $\psi' \to \pi^+\pi^-\pi^0$.

Two other vector states, $\omega(1250)$ and $\rho(1250)$ have been reported in a recent reanalysis of the SND and CMD2 data on $e^+e^- \to \pi^+\pi^-\pi^0$ and $e^+e^- \to \omega\pi^0$ respectively [139].

Finally the a vector $X(1750)$, with 1753 MeV mass and 122 MeV total width, observed by FOCUS [140] in diffractive photoproduction of K^+K^- deserves a clear interpretation.

2.3.2 Exclusive channels

We give here a list of some interesting multihadronic channels, that can be measured at DAFNE-2.

$e^+e^- \to \pi^+\pi^-\pi^0$. The recent cross section measurement done by BABAR is in disagreement with the previous result of the DM2 experiment at $\sqrt{s} \geq 1.3$ GeV as shown in Fig. 10, and this reflects in the parameters of the two ω excitations, see Table 4.

A new measurement of this final state is needed, also to test the ISR method versus the energy scan one.

Furthermore, the interest of this final state is increased by the fact that $\rho\pi$ is one of the preferred decay channels for an isoscalar vector hybrid.

$e^+e^- \to 4\pi$. The $e^+e^- \to \pi^+\pi^-\pi^+\pi^-$ has been recently measured by BABAR with the ISR method and is in good agreement with the previous measurements, while the most recent high statistics results on $e^+e^- \to \pi^+\pi^-\pi^0\pi^0$ are those of SND and CMD2 Collaboration, but limited to the region $\sqrt{s} \leq 1.4$ GeV. Both cross section are described as dominated by the $a_1(1260)\gamma$ intermediate state, however a new measurement with higher statistics, also of the angular distributions of the decay products [141, 142], could be interesting.

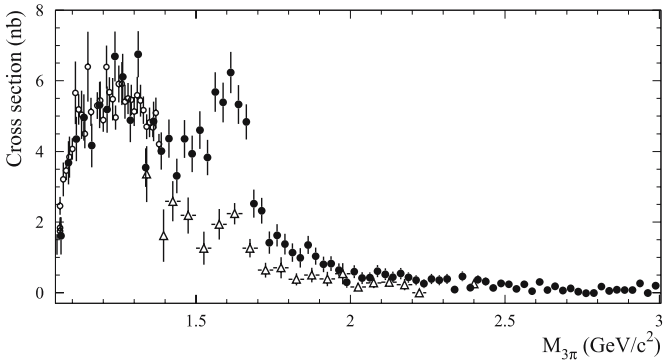

Fig. 10. Invariant mass spectrum of $\pi^+\pi^-\pi^0$ from BABAR radiative return (*full circles*) compared with e^+e^- scan data from DM2 (*triangles*) and CMD-2 (*open circles*)

Table 4. $\omega(1420)$ and $\omega(1650)$ parameters from the recent measurements of $e^+e^- \to \pi^+\pi^-\pi^0$

	SND + DM2		BABAR	
	Mass (MeV)	Width (MeV)	Mass (MeV)	Width (MeV)
$\omega(1420)$	1400 ± 140	870 ± 670	1350 ± 30	450 ± 100
$\omega(1650)$	1770 ± 80	490 ± 240	1660 ± 10	230 ± 35

Being $a_1(1260)\gamma$, together with $\rho\pi\pi$ the main decay channels expected for isovector vector hybrids, the 4π channel is the more promising for the search of such mesons.

$e^+e^- \to \pi^+\pi^-\pi^+\pi^-\pi^0$. Two processes mainly contribute to this final state: $e^+e^- \to \omega\pi^+\pi^-$, sensitive to the $\omega(1420)$ and $\omega(1650)$ parameters, and $e^+e^- \to \eta\pi^+\pi^-$, which instead is sensitive to $\rho(1450)$ and $\rho(1700)$.

Also this final state can be exploited to search for isoscalar vector hybrids that could decay into $\rho(1450)\pi$.

$e^+e^- \to 6\pi$. This cross sections has recently been measured by BABAR [111]; there is good agreement with the previous measurements in the $e^+e^- \to 3\pi^+3\pi^-$ channel, while in the $e^+e^- \to 2\pi^+2\pi^-2\pi^0$ there is some discrepancy with the DM2 data.

Furthermore these are the "golden" channels for the study of the properties of the $\rho(1900)$.

$e^+e^- \to K^+K^-$, $K_{\rm S}K_{\rm L}$. These final states can be exploited to extract the $\phi(1680)$ parameters. The charged one is the final state in which FOCUS has observed the vector state $X(1750)$ in diffractive photoproduction.

$e^+e^- \to K\overline{K}\pi$, $K\overline{K}\pi\pi$. These final states are interesting for the study of the $\phi(1680)$ and for the search of strange vector hybrids, through the decay chains $\phi_{\rm H} \to K^\star K \to K\overline{K}\pi$, and $\phi_{\rm H} \to K_1(1400)K \to K^\star\pi K \to K\overline{K}\pi\pi$.

$e^+e^- \to \phi f_0(980), \phi\eta, \phi\eta'$. A combined study of the processes $e^+e^- \to \phi f_0(980)$ and $e^+e^- \to \phi\eta(\eta')$ with center of mass energies up to ~ 3 GeV, should help to shed light on the still controversial nature of the $f_0(980)$ scalar meson.

In fact as shown in [143] it is possible to construct an analytic parameterization defined in the whole q^2-complex plane for a generic ϕM transition form factor $F_{\phi M}(q^2)$ (where M is any pseudoscalar or scalar light meson).

The main ingredients of this procedure are:

a. the perturbative QCD counting and helicity rule [144, 145] to describe the asymptotic behaviour;
b. data on the annihilation cross section $\sigma(e^+e^- \to \phi M)$ and a Breit–Wigner parameterization in the resonance region that is from the theoretical threshold $(2M_\pi)^2$ up to $\sim (3\,\mathrm{GeV})^2$;
c. the dispersion relations for the logarithm [146] to perform the analytic continuation, below the threshold $(2M_\pi)^2$, down to $q^2 = 0$.

The steps a and b of the procedure outlined above are strongly dependent on the nature of the meson M under consideration. In fact the power law asymptotic behaviour counts the hadronic fields in the final state [144, 145] (step a) and, by invoking the quark-hadron duality [147], such a behaviour is restored also in the resonance region, which is covered by the data and by the Breit–Wigner parameterization (step b). Hence the value at $q^2 = 0$ of the transition form factor provided by step c, is unambiguously linked to the assumed quark structure of M.

It follows that the radiative decay rate $\Gamma(\phi \to M\gamma)$, which is proportional to $F_{\phi M}(0)^2$, may be predicted, under different hypotheses about the nature of the meson M, and then compared with data. On this respect, a comparison among the ϕM transition form factors, with $M = \eta$, η', and $f_0(980)$, is sensitive to the relative quark composition of these mesons.

2.3.3 Threshold enhancements

As stated above the experimental signatures of a baryonium are a structure in some multihadronic final state and a threshold enhancement in the baryon–antibaryon cross section. Several thresholds should be accessible to a machine running up to 2.5 GeV: $N\overline{N}$ and $\Lambda\overline{\Lambda}$ in which such enhancements have been already observed [130, 131, 133, 135, 136], plus $\overline{\Sigma}^0\Lambda$ and its charge conjugate, and also $\Sigma\overline{\Sigma}$.

2.3.4 Statistical considerations

An energy scan of the region between 1.0 and 2.5 GeV with 15 MeV step, corresponding to 100 energy points, can be envisaged. The less common among the exclusive processes listed above have cross sections of the order of 1 nb. Assuming a luminosity of $10^{32}\,\mathrm{cm}^{-2}\,\mathrm{s}^{-1}$, in one 10^7 year data taking, it will be possible, for those final states, to collect about 10 000 events per point reaching a statistical accuracy of about 1%.

An alternative method to measure the multihadronic cross sections is the ISR based one, by running the machine at the maximum $\sqrt{s} = 2.5$ GeV. The ratio of the statistical uncertainty achievable with the energy scan method (15 MeV step, one year at $L = 10^{32}\,\mathrm{cm}^{-2}\,\mathrm{s}^{-1}$), to the ISR one in similar conditions (15 MeV step and an integrated luminosity of $1\,\mathrm{fb}^{-1}$) is reported in Fig. 11. Notice that for most of the spectrum, the scan method is statistically more convenient.

The main competitors for these measurements are the B-factories that can cover all the relevant energy region, for many exclusive channels. In any case as clearly shown in Fig. 7 of Sect. 2.2, DAFNE-2 will collect larger statistics than the full BABAR data sample.

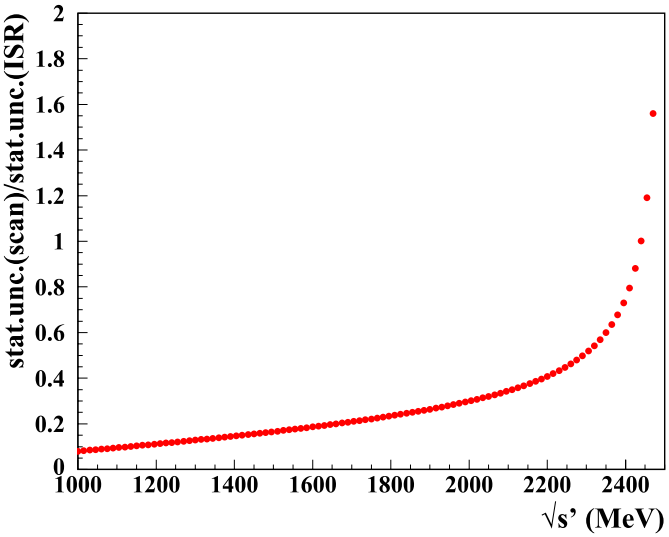

Fig. 11. Ratio of the statistical uncertainties of the energy scan method to the ISR one ($\sqrt{s'} = \sqrt{s} - E_\gamma$)

2.4 Radiative decays

Radiative decays represent another important tool for studying the structure of the hadrons. DAFNE-2 can contribute in two respects: first by continuing the ϕ radiative decays program started by KLOE but also profiting of the higher center of mass energy available by looking for radiative decays of excited vector mesons.

The high production rate of η and η' mesons from the ϕ expected at DAFNE-2 will allow the measurement of rare decays and the precise determination of kinematical distributions for processes with larger rates, thus providing an invaluable test-bed for QCD at low energies. We mention in particular the several tests of chiral perturbation theory (ChPT in the following) [154, 155] that will be discussed in the following. ϕ radiative decays are also an important source of light scalar mesons: the well established $f_0(980)$, $a_0(980)$ and the questioned $\sigma(600)$. An accurate measurement of the production branching ratio and of the mass spectra for the $\phi \to f_0(980)\gamma/a_0(980)\gamma$ decays can clarify the controversial exotic nature of the involved scalars. The high luminosity of DAFNE-2 will provide an unprecedent statistics of the $\pi\pi/\eta\pi$ decay channels, already studied at KLOE, and will open the possibility to search for the $K\overline{K}$ final state. The existence of the $\sigma(600)$ meson can also be clarified by fitting the low mass region for the $\pi\pi$ channel. The search for exotic states can be also performed in the high energy option, where the radiative decays of excited vector mesons could provide an evidence for the existence of hybrids or glueballs.

2.4.1 ϕ radiative decays

In the high luminosity option DAFNE-2 can fulfil the physics program involving ϕ radiative decays already performed at

DAFNE with the KLOE detector. Table 5 shows the rates of the main ϕ radiative decays. The larger sample of $f_0(980)$ and $a_0(980)$ will allow to access the $K\overline{K}$ decay channels while the high intensity beams of tagged η and η' mesons can be used to improve the search of rare η decays and to provide a real η' factory.

Light scalar mesons: $f_0(980)$ and $a_0(980)$. The $f_0(980)$ and $a_0(980)$ mesons are, respectively, the isospin singlet and the neutral element of the isospin triplet of the lowest mass scalars. Although their experimental evidence dates the beginning of the seventies [156, 157] and a lot of effort was spent since then to understand their controversial nature, the situation is still unclear. Indeed, there are several theoretical models proposed to explain their composition, as ordinary $q\overline{q}$ mesons, 4-quark states or $K\overline{K}$ molecules [158–160].

In this context, one of the open questions is the s quark content of $f_0(980)$ and $a_0(980)$. Indeed, due to their quantum numbers and mass degeneracy, a common large $s\overline{s}$ contribution is an evidence for an exotic nature of these particles. This is revealed by an higher coupling of the scalar mesons (S) to the $K\overline{K}$ final state with respect to $\pi\pi/\eta\pi$. Using ϕ radiative decays, it is possible to extract the $K\overline{K}$ couplings also using the most copious decay chains $\phi \to S\gamma \to \pi\pi\gamma/\eta\pi\gamma$ as already made by the VEPP-2M experiments [161–164] and, with higher precision, by KLOE [165–167]. However, this requires a modelling of the process. With the higher luminosity expected at DAFNE-2, it is possible to directly detect the $\phi \to [f_0(980) + a_0(980)]\gamma \to K\overline{K}\gamma$ decay chain, thus allowing a direct measurement of the couplings. Having $50\,\mathrm{fb}^{-1}$, the number of expected $K^0\overline{K^0}\gamma$ final state is in the range $2 - 8 \times 10^3$ while two orders of magnitude more are expected for $K^+K^-\gamma$ [168]. Despite the higher statistics, the last decay channel is expected to be overwhelmed by an irreducible background due to $\phi \to K^+K^-$ events with final state radiation which is a factor 10 larger than the signal.

In the discussion of the $\gamma\gamma$ physics program (see Sect. 2.5) we will show other complementary measurements on scalar meson physics at DAFNE-2.

η physics. DAFNE has shown that a ϕ factory is actually one of the best places to study η physics. Indeed precision results for the dynamics of $\eta \to 3\pi$ decays as well as upper limits on rare C and CP violating decays have been published by KLOE [169–171], taking benefit from the high statistics available and the clean experimental signature characterised by a highly energetic, monochromatic, recoil photon and the possibility to maintain background well below the percent level.

Table 5. Rates of the main ϕ radiative decays. $f_0(980)\gamma$ and $a_0(980)\gamma$ are the main contributions to the $\pi\pi\gamma$ and $\eta\pi\gamma$ final states

final state	branching ratio	rate (evts/fb^{-1})
$\eta\gamma$	1.3%	3.9×10^7
$\pi^0\gamma$	1.25×10^{-3}	3.7×10^6
$\eta'\gamma$	6.2×10^{-5}	1.9×10^5
$\pi\pi\gamma$	1.1×10^{-4}	3.0×10^5
$\eta\pi\gamma$	8.3×10^{-5}	2.5×10^5

DAFNE-2 will open the opportunity to study rare and medium rare η decays with great precision, as far as the integrated luminosity at the ϕ peak will reach the tens of fb^{-1} domain: $\sim 2 \times 10^9\eta$'s are produced with $50\,\mathrm{fb}^{-1}$. Let us briefly enumerate the channels of higher interest for DAFNE-2:

1. $\eta \to \pi^0\gamma\gamma$
   This decay's BR has been a puzzle for experimentalists over last 40 years or so, with its estimated value ranging from 25% down to the recent KLOE preliminary result of $(8.4 \pm 3.0) \times 10^{-5}$ obtained with a sample of 68 ± 23 candidate events in $450\,\mathrm{pb}^{-1}$. The theoretical interest in this decay resides in offering a unique window on pure p^6 terms of the chiral Lagrangian. The amount of events which can be collected at DAFNE-2, using a realistic efficiency extrapolated from the KLOE result, is about $200/\mathrm{fb}^{-1}$ allowing for both a precision measurement of the BR and for the first study of the $M_{\gamma\gamma}$ spectrum. Since it is essentially a measurement based on photon counting (the main background source being the $\eta \to \pi^0\pi^0\pi^0$ decay), it can profit from an improvement of the calorimeter granularity (see Sect. 4).
2. $\eta \to \pi\pi$
   As for $K_\mathrm{L} \to \pi\pi$ the two pion mode for the η is CP violating. In the standard model it is further dynamically suppressed to the $O(10^{-27})$ level; possible contributions from the θ term of the QCD Lagrangian may well increase it, but constraints from neutron EDM show that this contribution cannot exceed $O(10^{-17})$. In some extensions of the SM it can be slightly increased up to $O(10^{-15})$ [172]. KLOE has improved the limits on the $\pi^+\pi^-$ mode by an order of magnitude w.r.t. previous measurements, settling the upper limit at the 10^{-5} level. DAFNE-2 could explore the region down to $\approx 10^{-6}$ and could surely also improve the upper limit on the $\pi^0\pi^0$ final state, which is currently only 3.3×10^{-4}, although KLOE has already good handles to refine it.
3. $\eta \to \mu^+\mu^-(e^+e^-)$ and LF violating modes
   While the branching fraction of the $\eta \to \mu^+\mu^-$ decay has been measured, even if with large errors, the standard model expectations for the e^+e^- mode are only at the 10^{-9} level, preventing its observation even at DAFNE-2. It must be also stressed that QED background can be a relevant issue for both these modes. Anyhow, DAFNE-2 can improve the $\mu^+\mu^-$ BR determination, checking the unitarity bound ($= 4.3 \times 10^{-6}$). It is obvious that a natural byproduct of the $\mu^+\mu^-$ and e^+e^- searches will also result in a reduction on the upper limit on the lepton flavour violating modes $\eta \to \mu^\pm e^\mp$. Improvements of the detector particle ID capability w.r.t. KLOE will be a good handle for this kind of searches.
4. Dalitz and double Dalitz decays
   The electromagnetic form factor of pseudoscalar mesons is an important ingredient in the evaluation of the pseudoscalar pole part of the light-by-light contribution to the muon anomalous magnetic moment (see Sect. 2.2.3). Precise information can be extracted by studying Dalitz and, mainly, double Dalitz decays of the η, the latter being not yet observed so far. At DAFNE-2 a number as high as $3000/\mathrm{fb}^{-1}$ are expected to be produced, and even with a detection efficiency of few % one could accurately measure the BR and spectrum for these decays.

5. $\eta \to \pi^+\pi^- e^+e^-$
   The study of this final state is very interesting, because it provides a test for possible CP violating mechanisms beyond the standard model. This can be achieved by studying the asymmetry in the angle between the $\pi^+\pi^-$ and e^+e^- planes in the η rest frame, which arises from the interference between CP-conserving and CP-violating amplitudes. The measured BR for this final state implies that $17\,000\,\mathrm{events/fb^{-1}}$ of this kind would be produced at DAFNE-2.

η' physics. DAFNE-2 would provide a real η' factory via ϕ radiative decays, with a production rate of $2 \times 10^5\ \eta'/\mathrm{fb}^{-1}$. Notice that a similar production rate can be obtained via $\gamma\gamma \to \eta'$ at $\sqrt{s} = 2.5\,\mathrm{GeV}$. The possibility to use both methods to obtain samples of η' in completely different background and tagging configurations is to be considered as very important. Most of η' branching fractions can be well measured and brought to the same accuracy of the best measured one, namely $\eta' \to \eta\pi^+\pi^-$ which is currently known with an error of 3%. Since the error on the $\eta - \eta'$ mixing angle at KLOE is dominated by the knowledge of this BR, one could also try to improve it by measuring simultaneously *all* the main η' modes using the tagged recoil photon. Anyhow, it must be stressed that for some of the η' decays the background from η and/or kaon decays with same or similar final state could be a relevant issue. Apart from the mixing angle determination, many of the η' final states are of interest in themselves, and can provide inputs to the phenomenology of low energy QCD. We will now briefly review these final states and their importance.

1. $\eta' \to \pi\pi\eta$
   The $\pi^+\pi^-\eta/\pi^0\pi^0\eta$ modes account for about $44\%/21\%$ of all η' decays. Their main interest is in studying the dynamics of the three bodies via the Dalitz plot technique. Since there is no tree contribution from VMD, the scalar mesons $\sigma(600)$ and $a_0(980)$ are believed to be dominant in the imaginary and real part of the matrix element amplitude respectively [173]. A recent full p^4 ChPT calculation with higher order resummation via Bethe–Salpeter equations has been performed to precisely predict the dynamics of these decays [174]. The best experimental results currently available come from GAMS [175] for the $\pi^0\pi^0\eta$ mode (about 6000 events) and from the VES collaboration for the $\pi^+\pi^-\eta$ mode [176]. The latter have been obtained with about 20 000 events in hadronic production (diffractive + charge exchange). The very abundant and clean sample which can be collected at DAFNE-2 could bring the study of these Dalitz plots into a precision era, similarly to the precise measurement of the $\eta \to 3\pi$ Dalitz plot parameters done by KLOE.
2. $\eta' \to \pi^+\pi^-\gamma$ (including $\rho\gamma$)
   As for the corresponding η decay mode, this channel is sensitive to the box anomaly contribution of the chiral Lagrangian. This term should manifest itself as a deviation from simple ρ dominance in the observed dipion invariant mass spectrum. Since this final state accounts for about 30% of η' decays the production rate is quite high ($60\,000\,\mathrm{events/fb^{-1}}$), allowing for precise fit to the spectrum. The existing measurements [177–179] are based on few thousand events, and give sometimes opposite conclusions on the presence of the box anomaly term. As for the corresponding η decay chain, C-parity violation of this process is very interesting and can be tested by means of the charge asymmetry.
3. $\eta' \to \omega\gamma$
   This decay rate is quite small (about 3%) and poorly known (10% accuracy). However it is quite interesting since it can be related, together with the BR's of $\eta' \to \rho\gamma$, $\phi \to \eta'\gamma$ and with the η' two photon width, to the gluonic content of the η' [180]. The search in the chain $\phi \to \eta'\gamma$ with $\eta' \to \omega\gamma$ and $\omega \to \pi^+\pi^-\pi^0$ will provide a clean signature due to the two almost monochromatic photons and the sharp ω mass peak. A measurement at the level of $\leq 3\%$ can be reached, thus over constraining the determination of the η' gluonic content.
4. $\eta' \to \pi^+\pi^-\pi^0$
   This mode, as the corresponding η decay, is due to the isospin violating part of the strong Lagrangian and is in principle a source of precise information about quark mass differences. Moreover the ratio of this BR to the corresponding isospin conserving $\eta' \to \eta\pi\pi$ can be related to the $\pi^0 - \eta$ mixing [181]. From the experimental point of view only a very weak upper limit exists ($< 5\%$), while theoretical expectations range in the 10^{-3} domain.
5. Dalitz decays
   As already mentioned for the η, Dalitz and double Dalitz decays can give precious information about the pseudoscalar e.m. form factors, which are key ingredients in evaluating the light-by-light scattering part of the muon anomalous magnetic moment. While double Dalitz decays seem to be outside the capabilities of DAFNE-2, with only few events produced per $10\,\mathrm{fb}^{-1}$ of integrated luminosity, the single Dalitz modes, whose expected rates are two order of magnitudes larger and for which today only an upper limit exists, could be measured for the first time.

Competing facilities. In the panorama of the experimental programs foreseen in the next years, there are no strong competitors in the study of light scalar meson produced through ϕ radiative decays. The primary goal of the experiments at VEPP-2000 [8–10] is the coverage of the $1.4 - 2.0\,\mathrm{GeV}$ region in the hadronic cross section measurement.

The $f_0(980)$ and $a_0(980)$ scalar mesons are currently studied by many experiments and for this certainly will continue in the following years. Since the characteristics of the production mechanism is also sensitive to their nature, it will be still interesting in the future their study through ϕ radiative decay.

Concerning the η/η' physics, the strongest competitors are the experiments of the MAMI [182] and COSY [183] facilities. After the end of the running period at the BNL laboratory, the Crystal Ball [184] detector was moved to Mainz in order to study $\eta(\eta')$ mesons produced in the reaction at threshold $\gamma p \to p\eta(\eta')$. The just concluded MAMI-B run provided a sample of 3×10^7 ηs and the foreseen upgrade to MAMI-C will open up the possibility of producing η' mesons too. While the detector is well suited for the study of fully neutral decays, the simple tracking system and the absence of the magnetic field do not allow accurate measurements for decays involving charged particles. The start of the data taking for the WASA experiment at COSY [185] is foreseen in January 2007. Here the

η and η' mesons are produced in the $pp \to pp\eta(\eta')$ reactions and are precisely tagged by a forward spectrometer through the measurement of the pp missing mass ($4-8\,\mathrm{MeV/FWHM}$). The central detector, made by a CsI electromagnetic calorimeter and a straw tubes drift chamber in a magnetic field, is optimised for events involving electrons and photons, with small particle ID capabilities. Both Crystal Ball and WASA have a very high η/η' production flux and a precise meson tagging but they need a selective trigger and have a large – and not perfectly known – level of multihadronic background. Moreover, the running time which the experiments dedicates to these kind of measurements is limited and their reduced particle ID detector capabilities limit the number of possible measurements. As already demonstrated by DAFNE, a ϕ factory offers a much cleaner environment, allowing the usage of an unbiased trigger.

2.4.2 Radiative decays in the high energy option

Radiative decays of excited vector mesons can provide a tool to separate $q\overline{q}$ states from hybrids according to the model of [186–188]. In the framework of the quark model, large partial widths are predicted for some decay channels, that could be measured in an e^+e^- machine running at $1.0 \leq \sqrt{s} \leq 2.5\,\mathrm{GeV}$. In particular the decays of $\rho(1450) \to f_2(1270)\gamma$, $\rho(1700) \to f_1(1285)\gamma$, $\omega(1420) \to a_2(1320)\gamma$ and $\omega(1650) \to a_1(1260)\gamma$ can be exploited, since their decay widths are predicted of the order of 500–1000 keV in the hypothesis that the mesons are $q\overline{q}$, while the decay of the ρ_{H} and ω_{H} hybrids to the same particles are strongly suppressed. In a similar way the structure of the $\phi(1680)$ can be tested through the decay $\phi(1680) \to f_2'(1525)\gamma$ ($\Gamma \sim 200\,\mathrm{keV}$), while $\phi_{\mathrm{H}} \to f_2'(1525)\gamma$ is suppressed. Also the angular distributions of these decays are calculated in [186–188] and can be measured, thus providing a further test of the structure of the vector mesons. Furthermore the decays $\omega(1650) \to a_0(1450)\gamma$ and $\rho(1700) \to a_0(1450)\gamma$ can provide information on the properties of the $a_0(1450)$, whose existence is questioned.

Radiative decays of the $\rho(1700)$ can also shed some light in the sector of the $f_0(1370)$, $f_0(1500)$, and $f_0(1710)$. Two isoscalar scalar are expected in that mass region, so that the excess can be explained with the presence of a scalar glueball that mixes with a $(u\overline{u}+d\overline{d})$ and a $s\overline{s}$ scalar meson. In particular the ratio $\Gamma(\rho(1700) \to f_0(1370)\gamma)/\Gamma(\rho(1700) \to f_0(1500)\gamma)$ is very sensitive to the mixing scheme, i.e. the glueball is the lightest, the middle or the heaviest of the three states.

The final states in which the above decays can be studied are then $\pi^+\pi^-\gamma$, $4\pi\gamma$, and $\eta\pi\pi\gamma$ for the ρ mesons, $\pi^+\pi^-\pi^0\gamma$ for the ω recurrences, in addition to $\eta\pi^0\gamma$ and $K\overline{K}\gamma$ for $a_0(1450)\gamma$, and $K\overline{K}\gamma$ for the $\phi(1680)$ decays. The corresponding cross sections should range from ~ 10 to few hundreds pb, then in one year scan with 15 MeV energy step at $10^{32}\,\mathrm{cm}^{-2}\,\mathrm{s}^{-1}$ luminosity, from ~ 50 to 1000 events per energy point are expected.

2.5 $\gamma\gamma$ physics

2.5.1 Introduction

The term "$\gamma\gamma$ physics" (or "two-photon physics") stands for the study of the reaction (see Fig. 12)

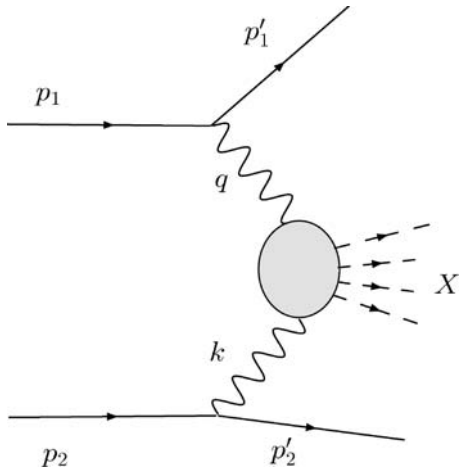

Fig. 12. Two-photon particle production in a e^+e^- collider

$$e^+e^- \to e^+e^-\gamma^*\gamma^* \to e^+e^- + X\,,$$

where X is some arbitrary final state allowed by conservations laws. These processes, even though of $\mathcal{O}(\alpha^4)$, show a logarithmic dependence from the energy E of the colliding beams that reflects in a not negligible cross section. It turns out that for E greater than a few GeV the $\gamma\gamma$ processes dominate with respect to the corresponding annihilation processes.

For quasi-real photons the number of produced events can be estimated from the expression:

$$N = L_{ee} \int \mathrm{d}W_{\gamma\gamma} \frac{\mathrm{d}L}{\mathrm{d}W_{\gamma\gamma}} \sigma(\gamma\gamma \to X)\,, \qquad (6)$$

where L_{ee} is the integrated luminosity, $W_{\gamma\gamma}$ is the photon–photon center of mass energy ($W_{\gamma\gamma} = M_X$), $\mathrm{d}L/\mathrm{d}W_{\gamma\gamma}$ the photon–photon flux (in MeV^{-1}) and σ is the cross section into a given final state. By knowing the fluxes of virtual photons emitted by the two colliding leptons, from the study of $e^+e^- \to e^+e^- + X$ one can really extract information on the process $\gamma\gamma \to X$.

From the point of view of hadronic physics, photon–photon scattering [189] complements the investigations of all the states which are directly coupled to one photon, i.e. states for which $J^{PC} = 1^{--}$ and which proceed through the usual annihilation process. Indeed since the two-photon state is a $C = +1$ state and the value $J = 1$ is excluded (Landau–Yang theorem), photon–photon scattering gives direct access to the study of states with $J^{PC} = 0^{\pm+}$, $2^{\pm+}$.

The cross section $\sigma(\gamma\gamma \to X)$ was studied over the past decades in e^+e^- colliders operated at c.m. energies of about 10 GeV or more. Concerning the low-energy region $m_\pi \leq W_{\gamma\gamma} \leq m_{f_0}$ the existing measurements are affected by two clear deficiencies:

- the large statistical and systematic uncertainties due to the relatively small data samples and relatively large background contributions;
- the very small detection efficiency and particle identification ambiguities for low-mass hadronic systems.

Due to the combination of high luminosity and favourable kinematical conditions, DAFNE, equipped with the large

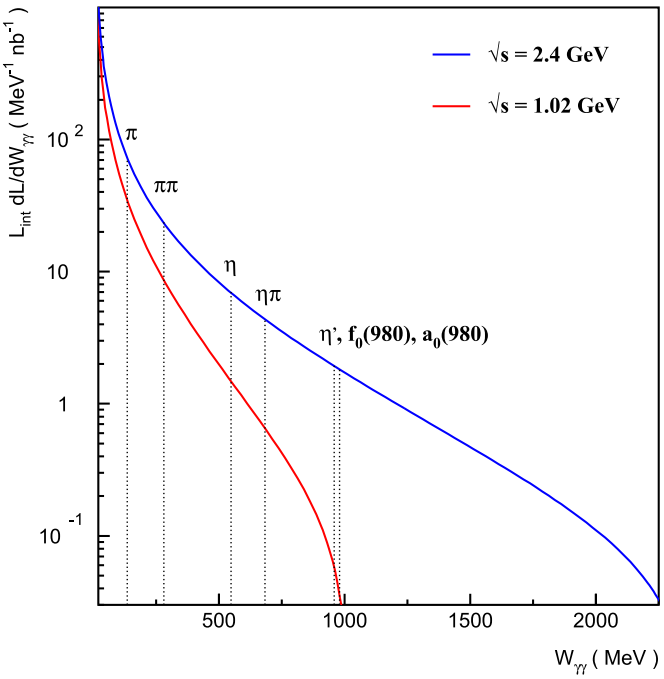

Fig. 13. Photon–photon flux at DAFNE as function of $W_{\gamma\gamma}$ for two values of $\sqrt{s}$ and an integrated luminosity machine $L_{\rm int} = 1\,{\rm fb}^{-1}$

multi-particle detector KLOE, offers the opportunity for new precision measurements of low-mass hadronic systems with high statistics and considerably smaller systematic errors.

This can be visualised by looking at the luminosity function given in Fig. 13, showing some of the processes that can be investigated at $\sqrt{s} = 1.02\,{\rm GeV}$ and the processes that will be available increasing the energy of the machine up to $\sqrt{s} = 2.5\,{\rm GeV}$.

In order to isolate experimentally these processes and suppress systematic errors arising from non $\gamma\gamma$-interactions, it is necessary to equip KLOE with (at least one) tagging systems to detect the scattered electrons.

A feasibility study for high-precision measurements of $\gamma\gamma$-reactions leading to hadrons at DAFNE was carried out more than ten years ago [190, 191]. The physics program and the characteristics of the tagging systems were investigated in detail. Although the results of this study are still valid, in the following we will re-consider some of the physics topics in light of the developments occurred since then.

2.5.2 The process $\gamma\gamma \to \pi^0\pi^0$: the σ case

One of the first attempts to describe nucleon–pion interactions within a spontaneously broken $\mathrm{SU}(2)_{\rm L} \otimes \mathrm{SU}(2)_R$ theory was the linear sigma model by Gell-Mann and Lévy [192, 193].

In this theory an "artificial" σ field with the quantum numbers of vacuum is required, by chiral invariance, to couple to pions and nucleons, suggesting the existence of a 0^{++} particle to be looked for. The natural process where a σ contribution is expected to be important is the $\pi\pi \to \pi\pi$ scattering. Experimental studies have never provided over the years a clear signal for it and the assessment of σ in this channel has become more and more controversial.

Extending the linear sigma model from $\mathrm{SU}(2)_{\rm L} \otimes \mathrm{SU}(2)_R$ to $\mathrm{SU}(3)_{\rm L} \otimes \mathrm{SU}(3)_R$, to include the strange sector, a generalized sigma model with 9 scalars and 9 pseudoscalars can be built, see e.g. [197]. Diverse solutions of this kind have been explored in the literature but none of them has proved to be really effective at explaining data.

The only successful approach to build a theory of pions at low energies is that proposed by Callan–Coleman–Wess–Zumino (CCWZ) where the chiral symmetry is realized non-linearly and the σ field is removed from the spectrum. This construction is at the basis of modern chiral perturbation theory (ChPT) [198], the standard effective approach to describe the interactions of the QCD pseudo-Goldstones at low energies.

Anyway there are persistent experimental indications of some structure in low energy $\pi\pi$ collisions. Many explanations of such isoscalar enhancement have been provided during the years. One of the most interesting results has been proposed recently in [194]. It has been shown that the $\pi\pi$ scattering amplitude contains indeed a pole with the quantum numbers of vacuum, which we will call the σ by analogy with the old linear σ field, with a mass of $M_\sigma = 441^{+16}_{-8}\,{\rm MeV}$ and a width $\Gamma_\sigma = 544^{+25}_{-18}\,{\rm MeV}$. This is also in reasonably good agreement, as for the mass predicted, with the observations made by the E791 Collaboration at Fermilab [195]: in the $D \to 3\pi$ Dalitz plot analysis, E791 finds that almost 46% of the decay width proceeds through $D \to \sigma\pi$ with a $M_\sigma = 478 \pm 23 \pm 17\,{\rm MeV}$ and $\Gamma_\sigma = 324 \pm 40 \pm 21\,{\rm MeV}$. BES [196] has looked for σ in $J/\psi \to \omega\pi^+\pi^-$ giving a mass value of $M_\sigma = 541 \pm 39\,{\rm MeV}$ and a width of $\Gamma_\sigma = 252 \pm 42\,{\rm MeV}$. For a summary of the experimental situation see [12].

The problem of assessing the existence and the nature of this state is not confined to low energy spectroscopy. Just to mention a possible relevant physical scenario in which σ could play a role, consider the contamination of $B \to \sigma\pi$ in $B \to \rho\pi$ decays (possible because of the large σ width). This could sensibly affect the isospin analysis for the CKM-α angle extraction [199–201], as it could be tested if the experimental precision on this measurement would grow. Recent studies of the γ angle through a Dalitz analysis of neutral D decays, need the presence of a σ resonance in the fits [202].

Here we want to highlight the possibility that a σ *resonance* could be found (or disproved) in e^+e^- collisions at DAFNE and DAFNE-2. We consider 2 experimental options: a run at a center of mass energy of 1 GeV, a region where the ϕ backgrounds are considerably diminished, and better, a run at a center of mass energy of 2.5 GeV in the high energy option of DAFNE-2. In the second option the photon-photon center of mass energy $W_{\gamma\gamma}$ range can be considerably extended as discussed in the following (see Sect. 2.5.6). We consider in particular the $e^+e^- \to e^+e^-\pi^0\pi^0$, γ-fusion channel. Consider that the $\gamma\gamma \to \pi^+\pi^-$ reaction in this energy region is dominated by the Born term, and is also characterized by a large background given by $\gamma\gamma \to \mu^+\mu^-$. From this point of view the $\pi^0\pi^0$ final state provides the cleanest environment where to look for a signal from the σ meson. Moreover if an isoscalar resonance is found in $\gamma\gamma \to \pi\pi$ data, this would further underscore the 4-quark hypothesis, since the sigma and the other sub-GeV scalar particles can hardly be explained as quark-antiquark states.

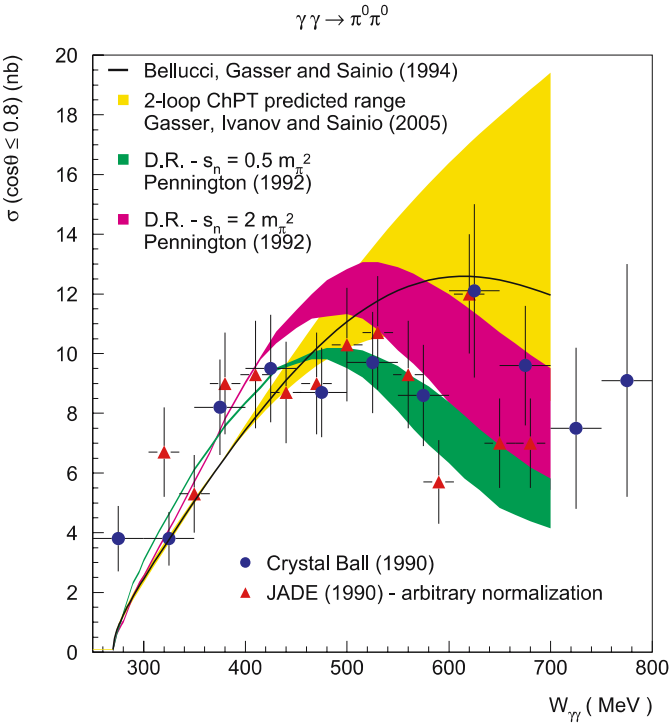

Fig. 14. Comparison of all the present data from Crystal Ball and JADE (arbitrarily normalized to the Crystal Ball data) to the predictions based ChPT [203–205] (*solid line* and *yellow band*) and on dispersion relation tecniques [211] (*green* and *magenta bands*)

On the theoretical side the process $e^+e^- \to e^+e^-\pi^0\pi^0$ has been considered in several papers. Some of these results are summarised in Fig. 14. This includes the results of a 2-loop ChPT calculation [203–205, 214] for the $\gamma\gamma \to \pi^0\pi^0$ channel in the region of photon–photon c.o.m. energy from about $2m_\pi$ up to 700 MeV, and the results of an approach based on dispersive techniques [211]. These calculations are compared to the only available data, from Crystal Ball [209] and from JADE [210], the latter having been rescaled to the normalization of the former. The large uncertainty in these data are such that no conclusion can be drawn on the agreement with either of the theoretical approaches, nor on the possible existence of a resonance-like structure in the region around 400–500 MeV as discussed in [206] where a Breit–Wigner parametrization was used to model the departure from ChPT of a resonant isospin = 0 contribution to the $\gamma\gamma \to \pi^0\pi^0$ amplitude. The possibility of a destructive interference between the isospin 0 and 2 amplitudes, with a suppression of the σ signal, was furhtermore discussed in [211, 212]. It is therefore clear that new data in the $\gamma\gamma \to \pi^0\pi^0$ channel are essential in order to see progress in this area. The size of the difference between the theoretical curves in Fig. 14 and the size of the respective uncertainty bands, provide ambitious but useful benchmarks for the accuracy of new experimental measurements of these processes.

On the experimental side we notice first that an integrated luminosity of 1 fb^{-1} at $\sqrt{s} = 2.5$ GeV allows in principle to reduce to about 2% the uncertainty on the experimental points in the 400–500 MeV region (50 MeV wide bins) shown in Fig. 14 if the selection efficiency is 1 and no background contributes to the uncertainty. A slightly worse uncertainty can be obtained running at 1 GeV. However we notice that the $W_{\gamma\gamma}$ region where the effect of the σ should be more evident is affected by several backgrounds, such as $e^+e^- \to \omega\pi^0 \to \pi^0\pi^0\gamma$ with one lost photon, that requires a crossed analysis of several distributions; the experimental resolution on $W_{\gamma\gamma}$ has to be considered also for the comparison between data and theoretical predictions. This certainly calls for a more selective analysis of data making use of forward detectors to tag electrons; the details can be found in [206] and are also discussed in Sect. 2.5.6.

We believe that DAFNE-2 has the concrete opportunity to discriminate between the curves shown in Fig. 14 and possibly find (or disprove) a resonant σ in the cleanest possible channel. This can be done both in a dedicated run at 1 GeV center of mass or, even better by running at the maximum energy of 2.5 GeV to explore a larger $W_{\gamma\gamma}$ range.

2.5.3 The two-photon widths of $f_0(980)$ and $a_0(980)$

Extending the measurement of $\gamma\gamma \to \pi\pi$ and $\gamma\gamma \to \eta\pi$ to the $W_{\gamma\gamma}$ region around 1 GeV, the $f_0(980)$ and $a_0(980)\gamma\gamma$ widths can also be measured. This measurement is possible by running at the maximum attainable centre of mass energy of 2.5 GeV, in order to maximise the effective $\gamma\gamma$ luminosity in the 1 GeV region (see Fig. 13). In both cases a peak in the $W_{\gamma\gamma}$ dependence of the $\gamma\gamma \to \pi\pi(\eta\pi)$ cross section around the meson mass allows to extract the $\gamma\gamma$ width.

The $\gamma\gamma$ widths of $f_0(980)$ and $a_0(980)$ are rather poorly known (relative uncertainties about 30% see [12]). On the other hand, due to the dependence on the fourth power of the constituent charges their values are strongly related to the inner quark structure. For a complete discussion of this issue see [215].

2.5.4 The two-photon widths of the pseudoscalar mesons

The topic of the mixing of the pseudoscalar (PS) mesons holds a central role in hadronic physics. In particular, η–η' mixing has been actively investigated both from the theoretical and phenomenological side (for a review on the subject see [216]).

Mixing can be described in two different basis: the octet-singlet basis with mixing angle θ, and the quark-flavour basis with mixing angle $\phi = \theta - \tan^{-1}(\sqrt{2})$.

In addition to the state mixing, the phenomenological analysis of decay or scattering processes involves also the weak decay constants defined by ($P \equiv \eta, \eta'$)

$$\left\langle 0 \left| A_\mu^k \right| P(q) \right\rangle = \mathrm{i} f_P^k q_\mu \quad (k = 8, 0; q, s)\,,$$

where A_μ^k are the neutral axial-vector currents. In the past it has frequently been assumed that the constants in the $\{\eta_8, \eta_0\}$ basis follow the same pattern of state mixing and depend on two parameters f_8 and f_0. Recently, a theoretical investigation in the framework of ChPT [217] and a phenomenological analysis [218] have clearly shown that a correct treatment of the η–η' system requires two mixing angles θ_8 and θ_0, which, as a consequence of flavour symmetry breaking, differ considerably. In principle, this more general mixing scheme should also apply to decay constants in the $\{\eta_q, \eta_s\}$ basis (where the constants f_q and f_s are introduced), but analysis [218] yields, practically, the same value for ϕ_q and ϕ_s. This result gives sup-

port to the assumption according to which one mixing angle ϕ only is required to describe the decay constants mixing in the quark-flavour basis.

The value of the angle ϕ can be inferred from the analysis of many processes involving the η and η' mesons. This analysis has been performed in [219] and yields a weighted average $\overline{\phi} = (39.3 \pm 1.0)^\circ$ to be compared with the theoretical value (to first order in flavour symmetry breaking) $\phi_{\rm th} = 42.4^\circ$. Another, more recent analysis [220] has derived values for the two angles: $\phi_q = (39.3 \pm 1.3)^\circ$ and $\phi_s = (41.4 \pm 1.4)^\circ$.

The decay constants can be separately extracted from the two-photon decays of the η and η'. By using a phenomenological estimate for ϕ and the experimental values [12]

$$\Gamma(\eta \to \gamma\gamma) = 0.510 \pm 0.026\,\text{keV}$$
$$\Gamma(\eta' \to \gamma\gamma) = 4.29 \pm 0.15\,\text{keV}$$

one obtains [218]:

$$\frac{f_q}{f_\pi} = 1.07 \pm 0.04\,, \quad \frac{f_s}{f_\pi} = 1.41 \pm 0.11\,, \tag{7}$$

where f_π is the pion decay constants ($f_\pi = 131\,\text{MeV}$). For these decay constants the theoretical estimates to first order in flavour symmetry breaking are:

$$f_q = f_\pi\,, \quad f_s = \sqrt{f_K^2 - f_\pi^2} = 1.41 f_\pi\,.$$

We see that f_q/f_π is more than one standard deviation away from its theoretical estimate, while, even if its central value agrees perfectly with the theoretical prediction, the constants f_s is not well determined. This situation is far from being satisfactory and calls for more precise measurements of the two-photon width of the η and η' mesons. Moreover notice that even the π^0 two-photon width is poorly known (relative uncertainty of $\sim 8\%$) and its determination can be improved at DAFNE-2. Given the small value of these widths, the only way to pursue this experimental program is the study of meson formation in $\gamma\gamma$ reactions. In Table 6 we report the estimates for the total production rate in the process $e^+e^- \to e^+e^-P$ with P a pseudoscalar meson.

2.5.5 Meson transition form factors

The study of the process $e^+e^- \to e^+e^- + \text{PS}$ when one of the final leptons is scattered at large angle gives access to the process $\gamma\gamma^* \to \text{PS}$, i.e. with one off-shell photon. The amplitude of this process is given by (see Fig. 12)

$$T_{\mu\nu} = \mathrm{i}\epsilon_{\mu\nu\rho\sigma} k^\rho q^\sigma F_{P\gamma\gamma^*}(Q^2)\,, \tag{8}$$

where $F_{P\gamma\gamma^*}$ is the photon–meson transition form factor.[1] Here we assumed $k^2 = 0$ and, by neglecting the electron mass, we defined

$$Q^2 = -q^2 = 2E_1E_1'(1 - \cos\theta_1) \neq 0\,,$$

[1] We remark that the same pion form factor, but in the time-like region, intervenes in the so called Dalitz decay $\pi^0 \to e^+e^-\gamma$ (see [221]).

Table 6. $e^+e^- \to e^+e^-P$ total rate for an integrated luminosity of $1\,\text{fb}^{-1}$ at two different center of mass energies. No tag efficiency is included in the rate calculation

$\sqrt{s}$ (GeV)	π^0	η	η'
1.02	4.1×10^5	1.2×10^5	1.9×10^4
2.4	7.3×10^5	3.7×10^5	3.6×10^5

where E_1, E_1' are the energies of the initial and final lepton, respectively, and θ_1 is the scattering angle. From (8) one obtains:

$$\Gamma(P \to \gamma\gamma^*) = \frac{\pi\alpha^2}{4} M_P^3 F_{P\gamma\gamma^*}^2(Q^2)\,. \tag{9}$$

There has been a considerable effort to predict and measure these form factors. In the framework of pQCD the leading order prediction for the asymptotic behaviour is:

$$\lim_{Q^2\to\infty} Q^2 F_{P\gamma\gamma^*}(Q^2) = \sqrt{2} f_P\,.$$

Instead, from the axial anomaly in the chiral limit of QCD it is possible to deduce the behaviour of these form factors in the limit $Q^2 \to 0$. For π^0 and η one has:

$$\lim_{Q^2\to 0} F_{P\gamma\gamma^*}(Q^2) = \frac{1}{2\sqrt{2}\pi^2}\frac{1}{f_P}\,,$$

to leading order in m_u^2/M_P^2 and m_d^2/M_P^2, where m_u and m_d are the masses of the u and d quarks. Due to the large mass of the quark s this result does not hold for the η'. Furthermore, the authors of [222] proposed a simple-pole formula connecting these two regimes:

$$F_{P\gamma\gamma^*}(Q^2) = \frac{1}{2\sqrt{2}\pi^2 f_P}\frac{1}{1 + Q^2/\Lambda_P^2}$$

with $\Lambda_P^2 = 4\pi^2 f_P^2$.

From the experimental side these functions can be obtained from the measurements of the differential rates $\mathrm{d}\sigma(e^+e^- \to e^+e^- + P)/\mathrm{d}Q^2$ when one of the virtual photons is emitted at small angle (i.e. is nearly real), while the other is tagged by detecting one of the final leptons emerging at a finite angle respect to its original flight direction. This kind of study has been performed in the past by CELLO [223] and CLEO [224], and the Q^2 evolution of the form factors turned out to be consistent with theoretical expectations (see Fig. 15). The Q^2 region covered by the whole dataset extends from 0.5 to $8\,\text{GeV}^2$. These data were also used to extract the slope a_π of the pion form factor $F_{P\gamma\gamma^*}(Q^2)$. For example, for the π^0 it turns out [221]

$$a_\pi = 0.0326 \pm 0.0037 \quad \text{(CELLO)} \tag{10}$$
$$a_\pi = 0.0303 \pm 0.0017 \quad \text{(CLEO)}\,. \tag{11}$$

However, these extrapolations are model dependent and a direct and accurate determination would be important also in light of the role played by this parameter in the determination of the hadronic light-by-light scattering contribution to the muon anomalous magnetic moment (see Sect. 2.2.3).

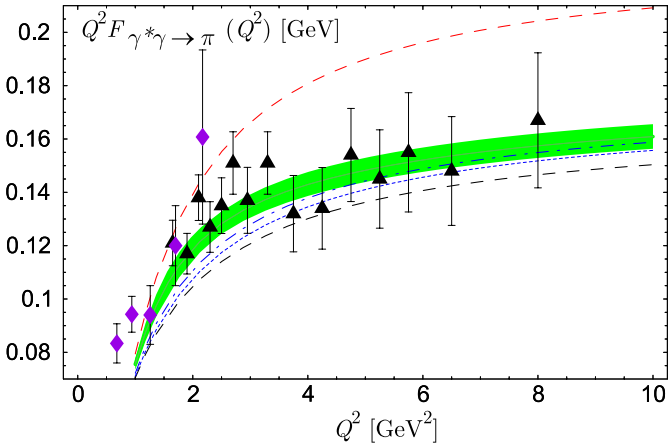

Fig. 15. Pion transition form factor in comparison with CELLO (*diamonds*) and CLEO data (*triangles*). The curves refer to different theoretical models (figure taken from [225])

In principle, the measurement of the slope parameter can be performed at DAFNE by implementing the KLOE detector with a somewhat large angle tagging system (see [190, 191]).

2.5.6 Experimental considerations

Measurements related to $\gamma\gamma$ physics have been performed in previous experiments with or without tagging the two-photon events by detection of the scattered electrons.

Tagging can be performed on one side or on both sides (single or double tag mode), allowing almost unambiguous identification of the events coming from the $\gamma\gamma$-interactions. Unfortunately, that comes at the price of a significant yield reduction. Moreover, the electrons are detected in specifics angular and energy ranges, producing a distortion of the invariant mass spectrum of the $\gamma\gamma$ system that can be effectively reconstructed. Thus, the actual needs for a tagging system have to be carefully evaluated.

Why tagging is needed? The measurement of the $\gamma\gamma \to \pi\pi$ cross sections and of the pseudoscalar mesons radiative widths have to be regarded as second generation experiments. Lower systematic errors are therefore required together with high statistics, calling for a strong background reduction.

The main source of background comes from annihilation processes, the worst situation represented by a machine working at a center of mass energy corresponding to the peak of the ϕ meson resonance. In this case, ϕ decays with one or more particles undetected can mimic the $\gamma\gamma$ final states, with production rates three or four order of magnitudes larger.

In order to suppress this background one can take advantage of the fact that the $\gamma\gamma$ system has essentially zero transverse momentum, as shown in Fig. 16, contrary to background coming from e^+e^- annihilation, where one or more particles are not detected.

A cut on this variable gives a rejection factor of the order of few tens, depending on the background type. It should be noted that at low energy colliders the typical two-photon selection criterion $E_{\rm vis}/E_{\rm cm}$ (i.e. the ratio of the visible over the center of mass energy) does not help, because of the low particle multiplicity. We can therefore conclude that two-photon reactions cannot be studied at the ϕ peak without a suitable tagging system.

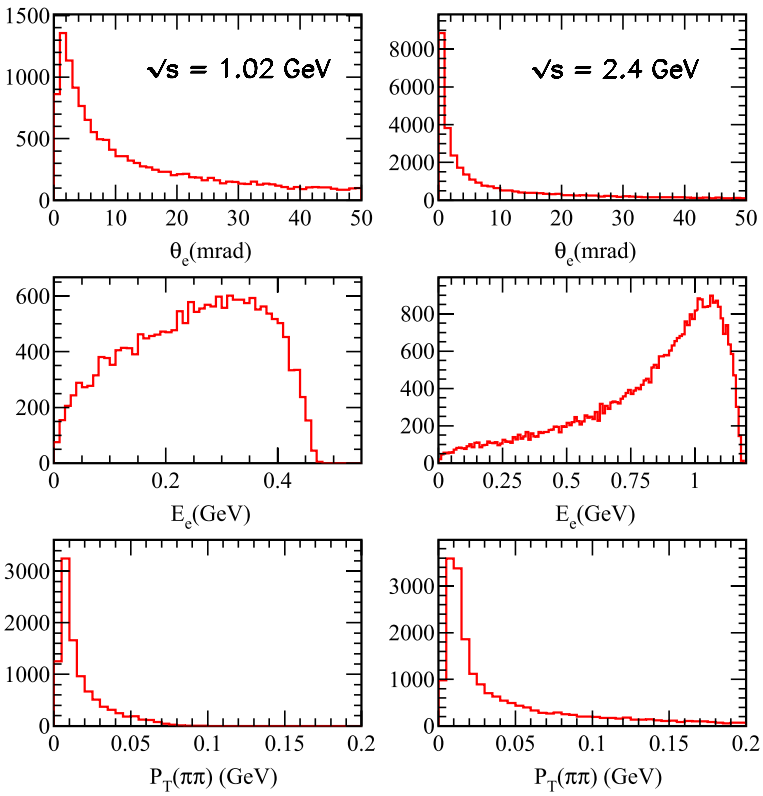

Fig. 16. Energy and angle distribution of scattered electrons for the two machine energy options. The distribution of the total transverse momentum of the $\gamma\gamma$ system is shown in the *bottom plots*

For a collider running at higher energies, the level of background due to hadronic events would be much lower, but not negligible and tagging would help to reach the necessary rejection factor.

It is worthwhile to mention that tagging the two-photon events would also be useful to reject a possible background for particular measurements of one-photon processes, like the measurement of the $e^+e^- \to \pi^+\pi^-$ cross section from initial state radiation events.

Requirements for a tagging system. In a low energy e^+e^- collider, as those considered here, tagging can be performed more easily than with machines that works at higher energies, like the old PEP and PETRA colliders and the new B-meson factories, as a consequence of the greater average scattering angle of the electrons, $\overline{\theta_e} \simeq m/E_{\rm beam} = 1\,{\rm mrad}$. This advantage can be exploited only partially owing to the limits imposed by the low-β insertion quadrupoles and by the minimum angle covered by the central detector, which is of the order of $200 - 300\,{\rm mrad}$ for a typical general purpose detector. Only a minor fraction of the scattered electrons enter the central detector, while most of them follow a trajectory which departs from the main beam orbit after several meters. A tagging system should therefore consist of one or more detectors located in specific regions along the beam line, where the electron yields would be most effective.

A design of the tagging system can be conceived only when a reasonable scheme of the machine layout is available. Independently from its final design, the desired features of the tagging system can be summarised as follows:

- it should be able to record the electrons from $\gamma\gamma$ reactions over as large as possible angular and energy ranges;
- it should be able to identify the nature of the hitting particle (i.e. separate electrons from muons and pions produced by the e^+e^- annihilation);
- it should possibly give informations about the energy and the scattering angle of the detected electrons;
- a high electron flux in the same angular region due to machine background (beam–gas bremsstrahlung) and radiative Bhabha events is expected. So fast detectors with relatively good radiation hardness are required. A photon detector could help vetoing the majority of these backgrounds.

To get an idea about the possibility to equip a low energy e^+e^- collider with a tagging system we can refer to the proposal submitted at the beginning of the DAFNE project [190, 191]. The system is composed of both small (SAT) and wide (WAT) angle tagging detectors. The SAT accepts electrons emitted forward at an angle lower than $20\,{\rm mrad}$. It is located at about $8.50\,{\rm m}$ from the interaction point (IP), following the split field magnet (SFM), that is the weak dipole which separates horizontally the beams in two independent rings. The electrons produced in $\gamma\gamma$ processes are affected by a larger bending inside the dipole with respect to the primary beam, because of their lower energies, so that they are sufficiently separated by the beam to be collected somewhere downward the SFM. Figure 17 shows a scheme of the SAT detector, taken from [190, 191]. The detector is located externally to the beam pipe and extends horizontally from a distance of 4 to $30\,{\rm cm}$ with respect to the beam line. The beam pipe should be shaped in order do not absorb the electrons that would cross it at small angles.

Figure 18 shows the energy of the collected electrons and the horizontal coordinate of their impact point on the SAT. The energy-position correlation provides an energy measurement with a few percent accuracy. The most energetic electrons follow an orbit close to the primary beam and cannot be collected by the SAT.

A cut is also observed on the minimum electron energy, mainly due to the correlation between the energy and the angle of the scattered electrons. That results in a limitation of the maximum invariant mass of the $\gamma\gamma \to \pi^0\pi^0$ system that can be tagged. As it is shown in Fig. 19, for $E_{\rm beam} = 510\,{\rm MeV}$, even in single tag mode, $W_{\gamma\gamma}$ is limited to $\sim 500\,{\rm MeV}/c^2$ at most. These results have been obtained with a Monte Carlo generator based on the Weizsacker–Williams approximation [226] and a ChPT two-loop cross section for $\gamma\gamma \to \pi^0\pi^0$ [203–205]. For $E_{\rm beam} = 1200\,{\rm MeV}$, the $W_{\gamma\gamma}$ has been limited to $1\,{\rm GeV}/c^2$ at generation level because of the poor reliability of the ChPT approximation above these energies.

The transport of the scattered $e^\pm$ is simulated according to the DAFNE magnet optics, with the intensity of the magnetic fields adjusted for the two different beam energies.

A WAT located in the interaction region, covering scattering angles larger than few degrees, would add about 10% of events in single tag mode. It is reasonable to conceive a detector in this region able to measure both the track angle and energy. This provides the quantity $Q^2 = 2E_{\rm beam}E'(1-\cos\theta_e)$, that is a measurement of the degree of virtuality of the photon. The Q^2 values expected in this region range between $10^{-4} - 10^{-1}\,{\rm GeV}^2$ (see also [227]). This is a very favourable situ-

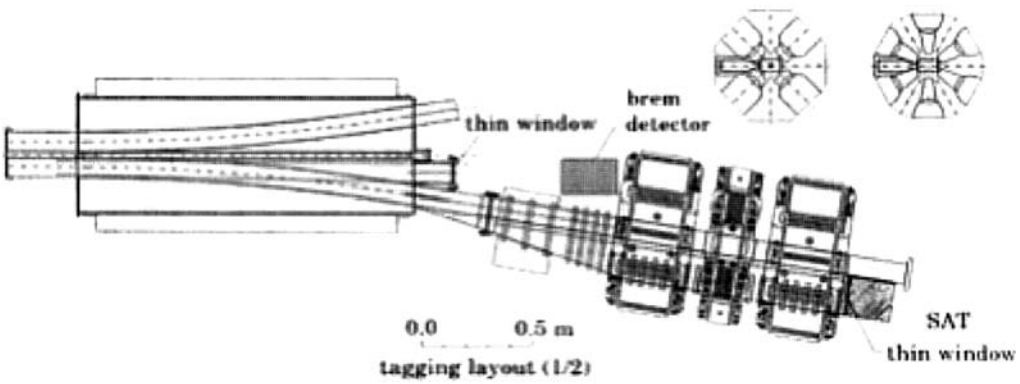

Fig. 17. A possible location for the small-angle tagger (SAT) in the present layout of DAFNE

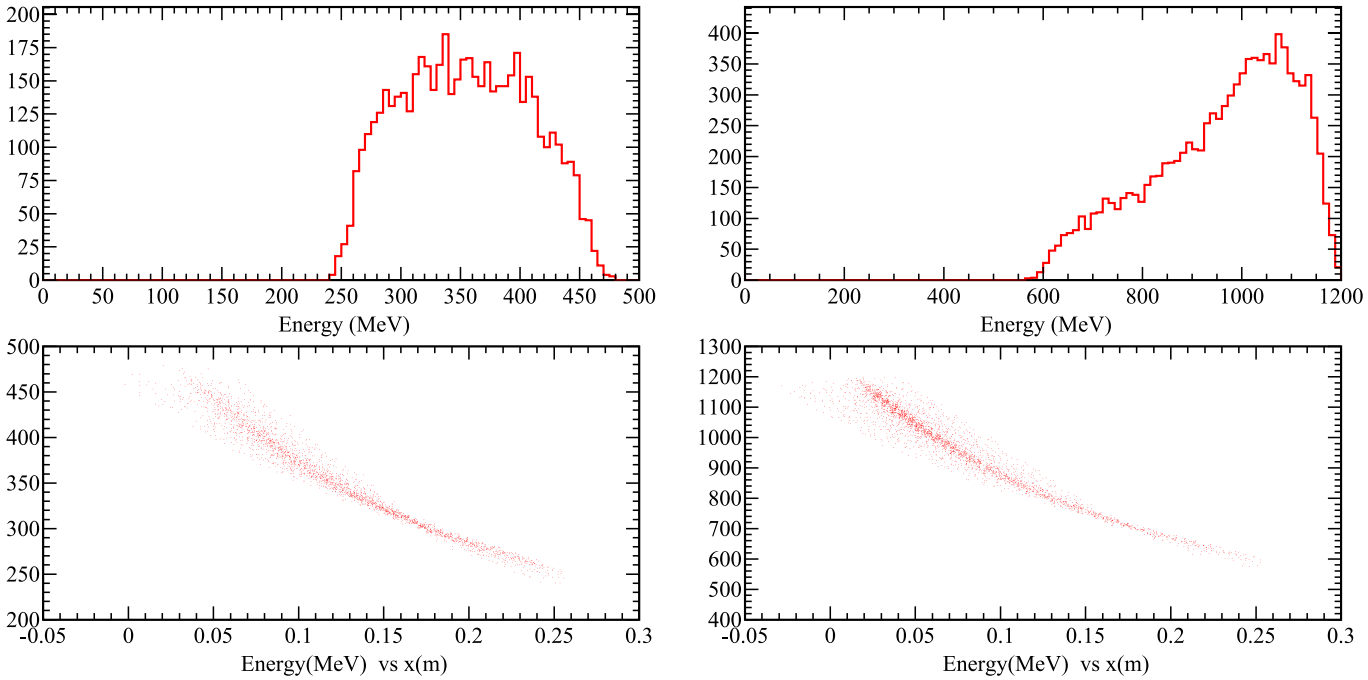

Fig. 18. Energy (*top*) and energy vs hit position on the SAT for scattered electrons. Electrons with an hit position $x < 0.04$ m are not yet escaped from the beam pipe and can not be detected. *Left plots* are for $\sqrt{s} = 1.02$ GeV, while *right plots* are for $\sqrt{s} = 2.4$ GeV

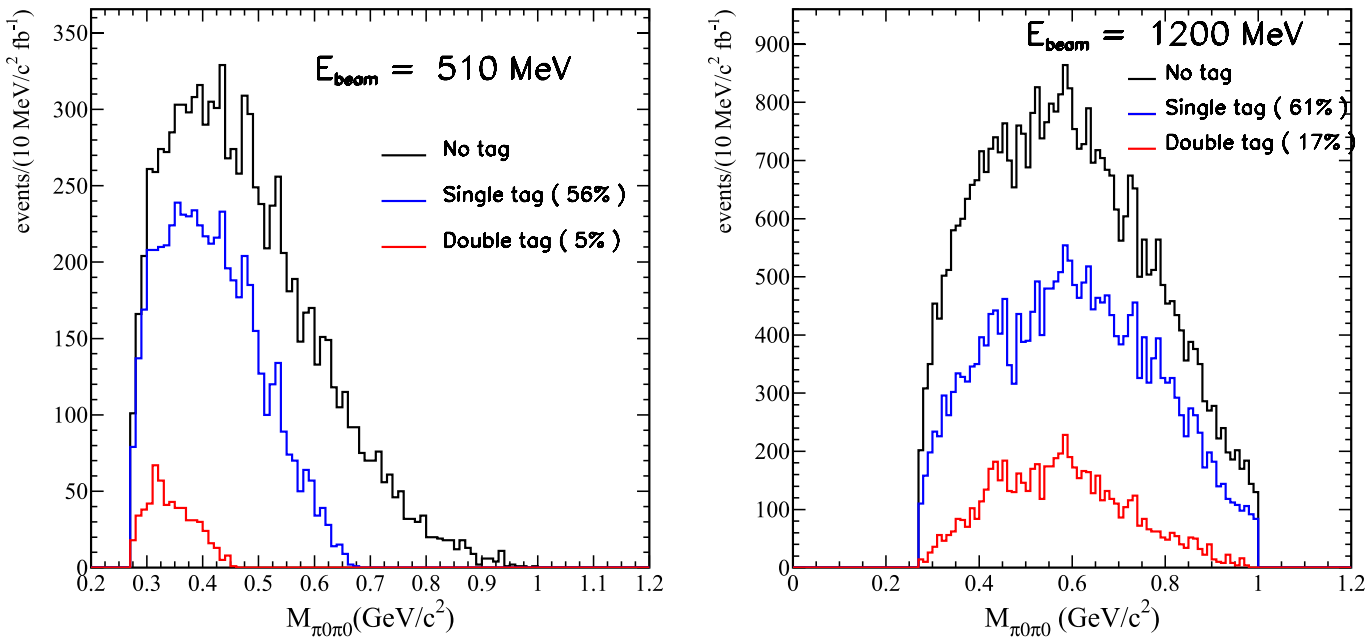

Fig. 19. Invariant mass of the $\gamma\gamma \to \pi^0\pi^0$ system in no-tag (*black line*), single-tag (*blue*) and double-tag (*red*) mode. Number of entries corresponds to the number of events expected for a 10 MeV$/c^2$ bin size and an integrated luminosity of 1 fb^{-1}. *Left plots* are for $\sqrt{s} = 1.02$ GeV while *right plots* are for $\sqrt{s} = 2.4$ GeV. The percentages in parenthesis are the overall reduction factors due to the single and double tagging

ation to measure the π^0 transition form factors (see Sect. 2.5.5) where the virtual photon is provided by the electron tagged at wide angle and the real photon is associated to an electron tagged in the SAT or even untagged, which can be assumed nearly on-shell.

2.5.7 Final Remarks

In the following we summarise the main results coming out from our studies. We considered two different working energies for the machine:

– $\sqrt{s} = 1.02\,\mathrm{GeV}$. The energy range accessible to $\gamma\gamma$ reactions is effectively limited to $W_{\gamma\gamma} \sim 600\,\mathrm{MeV}$. This energy range allows the measurement of the two-photon width and of the slope of the transition form factor for π^0 and η. As for the σ meson (assuming the resonance parameters quoted above) the resonance shape cannot be measured over its whole extension. From the experimental side, given the huge background associated to the ϕ-peak, this physics program cannot be exploited without a tagging system. As shown in the left panel of Fig. 19 tagging of electrons scattered at small angle results in a further limitation of the accessible $W_{\gamma\gamma}$ region.
– $\sqrt{s} = 2.5\,\mathrm{GeV}$. The $W_{\gamma\gamma}$ region accessible in this case extends over 1 GeV. Therefore the physics program outlined in the previous sections can be fully exploited. Even in this case a tagging system is needed to have a complete control of the hadronic backgrounds. This appears to be in any case a crucial condition in order to reach the required precision levels.

2.6 Hadron form factors in the time-like region

2.6.1 Introduction: The physics case

The form factors of hadrons, as obtained in electromagnetic processes, provide fundamental information on their internal structure, i.e. on the dynamics of quarks and gluons in the nonperturbative confined regime. A lot of data for nucleons have been accumulated in the space-like region using elastic electron scattering (for a review, see [228–231] and references therein). While the traditional Rosenbluth separation method suggests the well known scaling of the ratio $G_\mathrm{E}/G_\mathrm{M}$ between the electric and magnetic Sachs form factors, new measurements on the electron-to-proton polarization transfer in $e^- p \to e^- p$ scattering reveal strongly contradicting results, with a monotonically decreasing ratio for increasing momentum transfer $-q^2 = Q^2$ [232–235]. This in turn reflects in an approximate $1/Q$ trend of the ratio F_2/F_1 of the Pauli to Dirac form factors in the presently explored range $2 \le Q^2 \le 5.6\,\mathrm{GeV}^2$ [228–231], which is in contradiction with the $1/Q^2$ trend predicted by perturbative QCD and, more generally, by dimensional counting rules [236, 237]. This fact has stimulated a lot of theoretical work in order to test the reliability of the Born approximation underlying the Rosenbluth method (see [239, 240] and references therein).

In any case, the above scenario makes it critical to deepen our knowledge of G_E and G_M also in the time-like region by mapping the Q^2 dependence of their moduli and phases. In fact, while space-like form factors of stable hadrons are real because of the hermiticity of the electromagnetic Hamiltonian, time-like form factors, as they can be explored in $e^+e^- \to H\overline{H}$ or $p\overline{p} \to \ell^+\ell^-$ processes, are complex because of the residual interactions of the involved hadrons H (protons p). Their absolute values can be extracted by combining the measurement of total cross sections and center-of-mass (c.m.) angular distributions of the final products. The phases are related to the polarization of the involved hadrons. For example, in $e^+e^- \to B\overline{B}$ reactions with spin-$\frac{1}{2}$ baryons the normal polarization $\mathcal{P}_y$ to the scattering plane is proportional to the phase difference between G_E and G_M [241]. Such a polarization is present even if the electron and positron beams are not polarized. It is extremely sensitive to the theoretical input, as it is evident in Fig. 20, and it can discriminate among analytic continuations to the time-like region of models that successfully reproduce the proton $G_\mathrm{E}/G_\mathrm{M}$ data in the space-like region [242, 243].

Experimental knowledge of form factors in the time-like region is poor and it regards only pions and nucleons (for a review see [243]). As for the latter, there are no polarization measurements, hence the phases are unknown. The available unpolarized differential cross sections were integrated over a wide angular range, and data for $|G_\mathrm{M}|$ were extracted under the hypothesis that either $G_\mathrm{E} = 0$ or $|G_\mathrm{E}| = |G_\mathrm{M}|$. While the first hypothesis is arbitrary, the second one is true only at the physical threshold $q^2 \equiv s = 4M^2$, with M the nucleon mass; therefore, the relative weight of $|G_\mathrm{E}|$ and $|G_\mathrm{M}|$ in the cross section is yet unknown. As for the neutron, only one measurement is available by the FENICE collaboration [257] for $s \le 6\,\mathrm{GeV}^2$, which displays the same previous drawback.

Nevertheless, these few data reveal very interesting (and puzzling) properties. In fact, the form factors are analytic functions of q^2 in the whole domain. Therefore, the analytic properties and phases in the time-like region are connected to the space-like region by dispersion relations [258, 259]. In particular, $|G_\mathrm{M}|$ should asymptotically become real and scale as in the space-like region. However, a fit to the existing proton $|G_\mathrm{M}|$ data for $s \le 20\,\mathrm{GeV}^2$ is compatible with a size twice as larger as the space-like result [260]. Moreover, the very recent data from the BABAR collaboration on $|G_\mathrm{E}|/|G_\mathrm{M}|$ [261] show that the ratio is surprisingly larger than 1, contradicting the space-like results with the polarization transfer method [232–235] and the previous time-like data from LEAR [262]. Also the few neutron $|G_\mathrm{M}|$ data are unexpectedly larger than the proton ones in the corresponding s range [257]. Finally, all the available data show a steep rise of $|G_\mathrm{M}|$ for $s \sim 4M^2$, suggesting the

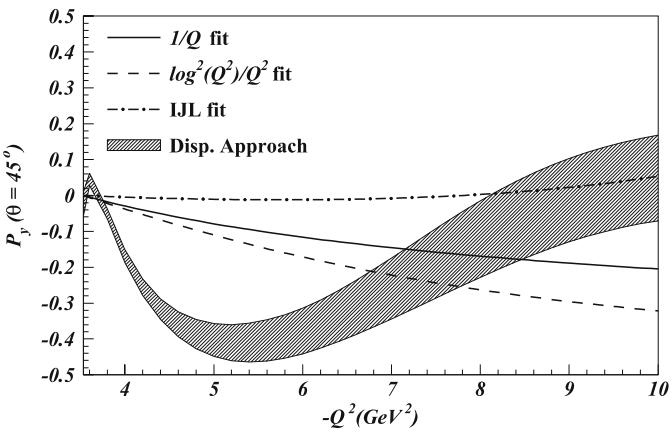

Fig. 20. Predicted proton polarization P_y for the $e^+e^- \to p\bar{p}$ process at scattering angle $\theta = 45^\circ$. *Solid line* for the analytic continuation of the $F_2/F_1 \propto 1/Q$ fit in the space-like region [244–251]; *dashed line* for the $\log^2(Q^2)/Q^2$ fit [252]; *dot-dashed* for a fit from Iachello, Jackson and Lande [253, 254]. The *lined band* is obtained by means of dispersive analysis of the ratio $G_\mathrm{E}/G_\mathrm{M}$, based on space-like and time-like data [255, 256]

possibility of interesting (resonant) structures in the unphysical region (for more details, see [263]).

The possible upgrade of the existing DAFNE facility [264] to enlarge the c.m. energy range from the ϕ mass to 2.5 GeV, would allow to explore the production of baryons from the nucleon up to the Δ. Therefore, in the following we will review the formalism necessary to extract absolute values and phases of baryon form factors from cross section data (Sect. 2.6.2). We will also make numerical simulations of the experimental observables (Sect. 2.6.3), in order to explore under which conditions DAFNE-2 could give leading contributions in this field (Sect. 2.6.4).

2.6.2 Survey of the formalism

The matrix element for the reaction $e^+e^- \to B\overline{B}$, where an electron and a positron with momenta k_1, k_2, annihilate into a spin-$\frac{1}{2}$ baryon and an antibaryon with momenta p_1, p_2, can be obtained by crossing of the corresponding matrix element for elastic e^-B scattering. There are several equivalent representations; here, we use the one involving the axial current [265]. The matrix element can be fully parametrized in terms of three complex form factors $G_{\rm E}(s,t), G_{\rm M}(s,t), A(s,t)$, which are functions of $s=(p_1+p_2)^2$ and $t=(k_2-p_1)^2$. In the Born approximation, $G_{\rm E}, G_{\rm M}$, reduce to the usual Sachs form factors and depend on s only, while $A=0$. We also define $\Delta G_{\rm E}(s,t)$ and $\Delta G_{\rm M}(s,t)$ the non-Born contributions to $G_{\rm E}(s)$ and $G_{\rm M}(s)$.

By replacing the t dependence in the form factors with $\cos\theta$, where θ is the scattering angle between the incoming positron and the produced baryon, charge conjugation invariance imposes general symmetry properties of the Born and non-Born amplitudes with respect to the $\cos\theta \to -\cos\theta$ transformation [240]. In particular, $\Delta G_{\rm E,M}$ are antisymmetric, while A is symmetric. If we neglect bilinear combinations of the non-Born terms $\Delta G_{\rm E,M}, A$, the unpolarized cross section contains the pure Born term and the interference between Born and non-Born contributions. Its general angular dependence is given by [266, 267]

$$\begin{aligned}\frac{{\rm d}\sigma^o}{{\rm d}\cos\theta} &= \frac{{\rm d}\sigma^{\rm Born}}{{\rm d}\cos\theta} + \frac{{\rm d}\sigma^{\rm int}}{{\rm d}\cos\theta} \\ &= a_0(s) + a_1(s)\cos^2\theta + \\ &\quad + \cos\theta[c_0(s) + c_1(s)\cos^2\theta + c_2(s)\cos^4\theta + \dots]\,, \end{aligned} \tag{12}$$

where a_0, a_1, are real combinations of $|G_{\rm E}|$ and $|G_{\rm M}|$, while c_i $(i=0,1,\dots)$ are coefficients incorporating effects from the s dependence of $\Delta G_{\rm E}, \Delta G_{\rm M}$, and A. In our analysis, we will take $\Delta G_{\rm E,M}=0$ and $c_i(s)=0$ for $i=1,2,\dots$. The result should represent somewhat a lower bound to the actual absolute strength of non-Born contributions.

In this framework, the unpolarized cross section in the c.m. frame of the annihilation becomes

$$\begin{aligned}\frac{{\rm d}\sigma^o}{{\rm d}\cos\theta} &\approx a(s)[1+R(s)\cos^2\theta] \\ &\quad - b(s)\,{\rm Re}\,[G_{\rm M}(s)A^*(s,t)]\cos\theta\,, \end{aligned} \tag{13}$$

$$a(s) = \frac{\alpha^2\pi}{2s}\frac{1}{\tau}\sqrt{1-\frac{1}{\tau}}\left(\tau|G_{\rm M}|^2+|G_{\rm E}|^2\right)\,, \tag{14}$$

$$b(s) = \frac{2\pi\alpha^2}{s}\frac{\tau-1}{\tau}\,, \tag{15}$$

$$R(s) = \frac{\tau|G_{\rm M}|^2-|G_{\rm E}|^2}{\tau|G_{\rm M}|^2+|G_{\rm E}|^2}\,, \tag{16}$$

where α is the fine structure constant and $\tau = s/4M^2$. If we neglect for the moment the non-Born contribution, measurements of ${\rm d}\sigma^o$ at fixed s for different θ allow to extract the angular asymmetry R, which can be combined with a measurement of the total cross section σ^o to separate $|G_{\rm E}|$ from $|G_{\rm M}|$. This procedure is the time-like equivalent of the Rosenbluth separation in the space-like region, but with the advantage that the time-like $s=q^2$ is automatically fixed: only the scattering angle needs to be changed, while keeping a space-like $Q^2=-q^2$ constant requires also to simultaneously vary the beam energy. In this framework, any deviation from the Born $(1+R\cos^2\theta)$ behaviour can be attributed to non-Born contributions. In general, the latter can come from the $\cos\theta$ dependence of each one of $\Delta G_{\rm E}, \Delta G_{\rm M}$, or A. Several independent observables are needed to better constrain and disentangle two-photon exchange mechanisms, including the polarization of the recoil proton and/or of the electron beam.

For spin-$\frac{1}{2}$ baryons with polarization $\mathbf{S}_{\rm B}$, the cross section is linear in the spin variables, i.e. ${\rm d}\sigma = {\rm d}\sigma^o(1+\mathcal{P}\mathcal{A})$, with ${\rm d}\sigma^o$ from (13) and $\mathcal{A}$ the analyzing power. In the c.m. frame, three polarization states are observable [241, 242]: the longitudinal $\mathcal{P}_z$, the sideways $\mathcal{P}_x$, and the normal $\mathcal{P}_y$. The first two ones lie in the scattering plane, while the normal points in the $\mathbf{p}_1\times\mathbf{k}_2$ direction, the x, y, z, forming a right-handed coordinate system with the longitudinal z direction along the momentum of the outgoing baryon. Here, we will concentrate on $\mathcal{P}_y$, because it is the only observable that does not require a polarization in the initial state [241, 242]. With the above approximations, it can be deduced by the following spin asymmetry

$$\begin{aligned}\mathcal{P}_y &= \frac{1}{\mathcal{A}_y}\frac{{\rm d}\sigma^\uparrow - {\rm d}\sigma^\downarrow}{{\rm d}\sigma^\uparrow + {\rm d}\sigma^\downarrow} \\ &\approx \frac{b(s)}{2\sqrt{\tau-1}{\rm d}\sigma^o}\sin\theta \\ &\quad \times \left\{ \cos\theta\,{\rm Im}\,[G_{\rm M}(s)G_{\rm E}^*(s)] \right. \\ &\quad \left. - \sqrt{\frac{\tau-1}{\tau}}\,{\rm Im}\,[G_{\rm E}(s)A^*(s,t)] \right\}. \end{aligned} \tag{17}$$

The final state interactions (FSI) between the final baryons may produce the phase difference in the form factors which emerges through the imaginary part of their interference. The spin asymmetry (17) can be nonvanishing even without polarized lepton beams, because it is produced by the mechanism $\mathbf{p}_1\times\mathbf{k}_2\cdot\mathbf{S}_{\rm B}$, a time-reversal odd combination which is forbidden in absence of FSI and, in general, in the Born approximation for the space-like elastic scattering.

The normal $\mathcal{P}_y$ vanishes at the end-points $\theta=0,\pi$ and at the physical threshold $\tau=1$. The Born contribution has a typical $\sin 2\theta$ behaviour, any deviation being due to non-Born terms. Interestingly, at $\theta=\pi/2$ the Born contribution vanishes, and $\mathcal{P}_y$ gives direct insight to the amplitude for multiple pho-

ton exchanges [265]. The measurement of $\mathcal{P}_y$ alone does not completely determine the phase difference of the complex form factors. By defining with $\delta_{\rm E}$ and $\delta_{\rm M}$ the phases of the complex $G_{\rm E}$ and $G_{\rm M}$, respectively, the Born contribution is proportional to $\sin(\delta_{\rm M}-\delta_{\rm E})$, leaving the ambiguity between $(\delta_{\rm M}-\delta_{\rm E})$ and $\pi-(\delta_{\rm M}-\delta_{\rm E})$. Only the further measurement of $\mathcal{P}_x$ can solve the problem, because $\mathcal{P}_x \propto {\rm Re}(G_{\rm M}\,G_{\rm E}^*) \propto \cos(\delta_{\rm M}-\delta_{\rm E})$ [242]. But at the price of requiring a polarized electron beam.

2.6.3 Numerical simulations

A Monte Carlo simulation was performed for the unpolarized cross section $\mathrm{d}\sigma^o$ and the normal polarization $\mathcal{P}_y$ using the approximations described in the previous section. From the expression of $a(s)$ in (13) and the known $|G_{\rm M}(s)| \sim 1/s^2$ scaling [236, 237], events were randomly sorted in the $4 < s < 50\,{\rm GeV}^2$ range using the $1/s^5$ distribution. Then, only those ones in agreement with the Born term of $\mathrm{d}\sigma^o$ were accepted. An initial sample of 280 000 events has been considered with the cut $4 < s < 6\,{\rm GeV}^2$. Since the total cross section for $e^+e^- \to p\overline{p}$ is approximately 1 nb, at the foreseen luminosity of $10^{32}\,{\rm cm}^{-2}\,{\rm s}^{-1}$ this sample can be collected in one month with efficiency 1. The error bars in the following figures are purely statistical: they are obtained by making 10 independent repetitions of the simulation.

Several extensions to the time-like region of models for nucleon form factors in the space-like region can be considered [242, 243]. For practical reasons, here we have considered the parametrizations of [253, 254, 268], because they have been updated in [243] by including all the available space-like and time-like data in the fit. Moreover, these models release separate parametrizations for the real and imaginary parts of $G_{\rm E}$ and $G_{\rm M}$, as they are needed in (13) and (17). Being both based on the vector-meson dominance (VMD) hypothesis, nevertheless they give drastically different results for $\mathcal{P}_y$ as a function of s [243]. However, in the s range here explored the first one produces very small P_y, which are statistically distinguishable from the second one but often consistent with zero. Therefore, in the following we will consider only observables produced by the updated parametrization of [268].

In Fig. 21, the angular distribution of $e^+e^- \to p\overline{p}$ events is shown according to the unpolarized cross section (13). In the left panel, approximately 52 000 events are accumulated for the c.m. squared energy $4 < s < 4.1\,{\rm GeV}^2$; in the right panel, 3 500 events for $5.6 < s < 5.7\,{\rm GeV}^2$. Filled (red) circles represent the Born contribution. For the non-Born correction, we have assumed ${\rm Re}[A(s)] \approx C\,{\rm Re}[G_{\rm E}(s)]$, since asymptotically the dimensional counting rules give the same $1/s^n$ trend irrespective from the number of virtual photons exchanged. We choose $C = 0.2$ as a sort of upper limit corresponding to 6% of two-photon radiative corrections required to restore the agreement between space-like cross sections obtained with the Rosenbluth and the polarization transfer methods [239, 240]. Downward (black) triangles and (blue) stars correspond to take ${\rm Im}(A) = -\,{\rm Re}(A)$ and ${\rm Im}(A) = {\rm Re}(A)$, respectively, which reflects our ignorance about the behaviour of the two-photon amplitude. The effect seems clearly detectable with one choice or the other, while for intermediate s the result overlaps with the Born one. In [266, 267], the angular distribution was fitted with

$$N(\cos\theta) = n\left[1 - B\cos\theta + C\cos^2\theta\right]\,. \qquad (18)$$

The parameter C allows for reconstructing the ratio $|G_{\rm E}/G_{\rm M}|$ within 5%–10%, once model inputs are used from [253, 254, 268] or from a simple dipole form [266, 267]. The parameter B introduces a left-right asymmetry in the $\cos\theta$ distribution, which is related to two-photon exchange according to (13). This term can be identified and estimated provided that $|A|$ is larger than 5% of $|G_{\rm M}|$ and the relative phases of the form factors do not produce severe cancellations [266, 267]. We stress that the above statements depend on the approximations discussed in the previous section, in particular on the truncation of the expansion (12). Finally, the error bars are negligible; nevertheless, the angular coverage should be limited to $\cos\theta < 0.85$, i.e. $\theta > 30$ deg., because the number of counts drops fastly for smaller angles.

In Fig. 22, the spin asymmetry for the polarized $e^+e^- \to p\overline{p}$ process is shown in its component $\mathcal{P}_y$ normal to the scattering plane, according to (17) with $\mathcal{A}_y = 1$. Notations are as in the previous figure. In the left panel, approximately 52 000 events are accumulated for the c.m. squared energy $4 < s < 4.1\,{\rm GeV}^2$; in the right panel, 9 000 events for $4.7 < s < 4.8\,{\rm GeV}^2$. The ${\rm Im}(A) = {\rm Re}(A)$ non-Born correction can be separated at the

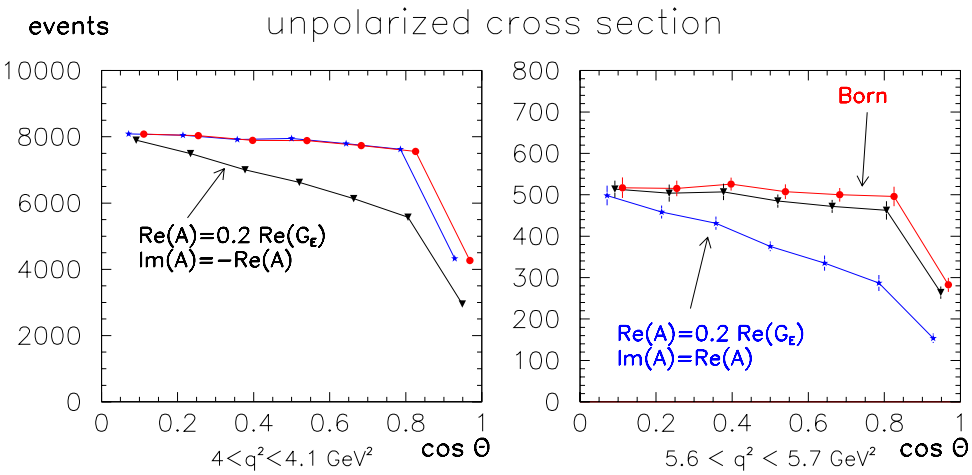

Fig. 21. Angular distribution of $e^+e^- \to p\bar{p}$ events according to (13). *Left panel*: 52 000 events at c.m. squared energy $4 < s < 4.1\,{\rm GeV}^2$. *Right panel*: 3500 events at $5.6 < s < 5.7\,{\rm GeV}^2$. *Filled* (*red*) *circles* for the Born contribution, *downward* (*black*) *triangles* and (*blue*) *stars* for two different choices of the non-Born axial form factor (see text). Statistical error bars only; lines are drawn to guide the eye

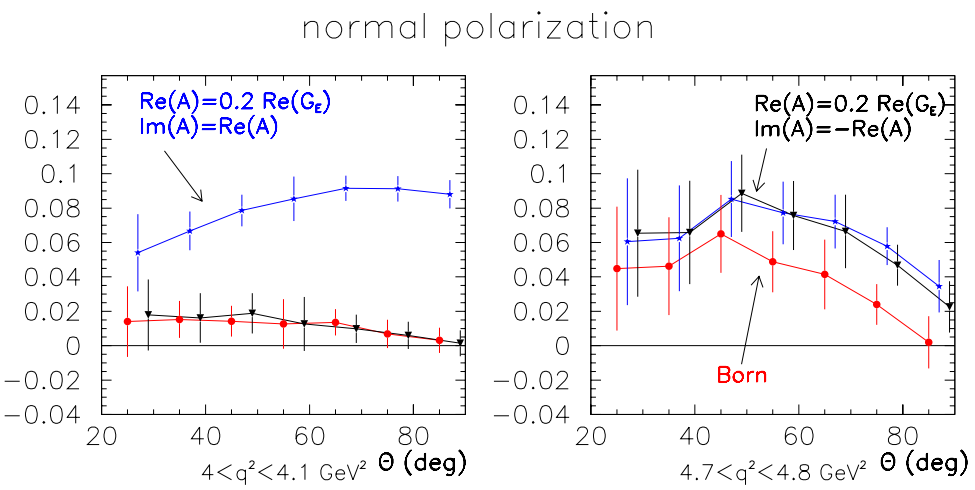

Fig. 22. Spin asymmetry of $e^+e^- \to p\bar{p}$ normal to the scattering plane, according to (17) with $\mathcal{A}_y = 1$. *Left panel*: 52 000 events at c.m. squared energy $4 < s < 4.1\,\mathrm{GeV}^2$. *Right panel*: 9 000 events at $4.7 < s < 4.8\,\mathrm{GeV}^2$. Same notations as in previous figure

lowest s, reaching an asymmetry of almost 10% at $\theta \sim 90$ deg. where the Born term vanishes, according to (17). This is not possible at higher s because of larger error bars. Nevertheless, the $\sin 2\theta$ tail of the Born term becomes clearly visible, reaching its (statistically nonvanishing) maximum at $\theta \sim 45$ deg, again according to (17).

2.6.4 Final remarks

At the foreseen luminosity of $10^{32}\,\mathrm{cm}^{-2}\,\mathrm{s}^{-1}$ DAFNE-2 can collect $e^+e^- \to B\overline{B}$ events at the considerable rate of 0.1 Hz. Moreover, extension of the available c.m. energy $\sqrt{s}$ up to ~ 2.5 GeV would allow to study the production of several baryons $B = p, n, \Lambda, \Sigma^0, \Sigma^\pm$. From the point of view of the detector, the experimental program outlined here is characterised by two peculiar aspects typically not satisfied by conventional general purpose detectors (like KLOE, see Sect. 4): the first is related to the measurement of the baryon polarisation, and the second to the detection of neutrons with kinetic energies between few and few hundred MeV. In fact, while the polarization of the Λ can be easily studied by looking at the angular distribution of its decay products, insertion of a polarimeter around the interaction region is required to measure the polarisation of nucleons (proton and neutron). Moreover, special care has to be devoted to the problem of detecting the n other than the $\overline{n}$ to have $n\overline{n}$ coincidences. This issue has been analysed, together with all the others concerning the measurement, in the letter of intent expressed in 2005 [264]. Before 2011, which can be a reasonable estimate of the time schedule for the DAFNE-2 update, three competitors will be active: VEPP-2000 [8–10], operating with the same luminosity but limited to nucleon detection only; BABAR [261], that will finish its data taking in 2008, exploring larger $\sqrt{s}$ but for unpolarized protons only; BES-III [269], starting in 2007, with a higher luminosity but detecting only unpolarized protons. Few years later, the PANDA collaboration [270] should start taking data at the same luminosity for Drell–Yan events with unpolarized $p\overline{p}$ pairs at $2M < \sqrt{s} < 5$ GeV. It should be followed, in few more years, by the PAX [271] collaboration that will consider polarized collisions.

In summary, we have shown that a sample of about 300 000 events, which is a factor $\sim 50\varepsilon$ larger than the present BABAR one [261] (with ε the efficiency), can be collected at DAFNE-2 in approximately one month of dedicated run. Since the event distribution falls approximately like $1/s^5$, a good angular coverage of $p\overline{p}$ is needed. In particular, selection of a specific angle to separate the s dependence of different theoretical contributions does not help.

Moreover, unpolarized cross section $\mathrm{d}\sigma^o$ and spin asymmetry $\mathcal{P}_y$ normal to the scattering plane, have been simulated by introducing crude simplifications in the non-Born term, which reflect the present theoretical ignorance about this contribution. In this context, from the angular tail of the results it seems that the proton detector should be best positioned in the range 30–70 deg. with respect to the beam direction (or 110–150 deg. because of the symmetry of the formulae). In fact, in this range Born and non-Born contributions to $\mathrm{d}\sigma^o$ can be separated to extract information on the absolute values of the proton form factors with a 5%–10% uncertainty (and, indirectly, also on the phase of G_M via its interference with the non-Born term, provided the latter is at least larger than 5% of $|G_\mathrm{M}|$) [266, 267]. The separation is possible also for $\mathcal{P}_y$ at the lowest s. For higher s, error bars are larger but in the same angular range the absolute size of $\mathcal{P}_y$ is maximum and the relative phases of the complex form factors might be extracted from the Born term, the non-Born correction being small.

Finally we mention that, as pointed out in [272–274], the $B\overline{B}$ final state opens the possibility to study the spin correlations predicted by quantum mechanics, or, assuming quantum mechanics, to test the CP invariance in the Λ decay. Particularly promising appears the case of $\Lambda\overline{\Lambda}$. In fact the $\Lambda \to p\pi^-$ decay plane is related to the spin direction, and represents a natural polarimeter. By calling κ_Λ and $\kappa_{\overline{\Lambda}}$ the unit vectors orthogonal to the decay planes of Λ and $\overline{\Lambda}$, the distribution of the scalar product $\kappa_\Lambda \cdot \kappa_{\overline{\Lambda}}$ is sensitive to deviations from quantum mechanics. An analysis based on about 700 events $J/\psi \to \Lambda\overline{\Lambda}$ has been done by DM2 [275].

2.7 Low energy kaon–nucleus interactions

The interest in the field covered here is of a systematic rather than exploratory nature: information on low-energy KN inter-

actions is scarce and of a poor statistical quality when compared to the corresponding πN ones [12, 276]. The low quality of these data reflects in turn on our knowledge of the parameters of the KN interaction, remarkably worse than in the SU(3)$_f$-related πN case [277–279]. On top of this situation, one must add the problem of understanding kaonic hydrogen (and deuterium) level-shifts and widths [280, 281], whose recent experimental determinations, despite having finally come out with the expected sign [282–284], are still awaiting an adequate explanation for their magnitude [285–288].

Data at very low momenta and at rest are essential to clarify many of the above-mentioned problems [276]: the two interaction regions of DAFNE are small-sized sources of low-momentum, tagged $K^{\pm}$'s and $K_{\rm L}$'s, with negligible contaminations (after suitable cuts on angles and momenta of the particles are applied event by event), in an environment of very low background radioactivity. This situation is simply unattainable with conventional technologies at fixed–target experiments. It is therefore of interest to consider the feasibility of low–energy, $K^{\pm}N$ and $K_{\rm L}N$ experiments at DAFNE.

Rates to be expected in a simple apparatus at DAFNE (similar in geometry to KLOE), filled by an almost ideal gas at room temperature (such as ^{4}He/^{3}He or H_2/D_2), are (for a luminosity of $8\times10^{32}\,{\rm cm}^{-2}\,{\rm s}^{-1}$) of the order of about 10^7 two-body events per year (in H_2 gas at atmospheric pressure, taken as yardstick because of the better known interactions), of which about 6.1×10^6 elastic scattering events, $3.8\times10^6\pi^+\Sigma^-$ and about 1.6×10^6 for each of the remaining four two-body channels $\pi^0\Sigma^0$, $\pi^0\Lambda$, $\overline{K}^0 n$, and $\pi^-\Sigma^+$. The above rates are enough to measure angular distributions in all channels, and also the polarisations for the self-analysing final-hyperon states, particularly for the decays $\Lambda\to\pi^-p$, π^0n and $\Sigma^+\to\pi^0p$. One could also expect a total of about 10^5 three-body final-state and 10^4 radiative-capture events, which should allow a good measurement on the absolute rates for these processes as well.

Such an apparatus will need: tracking for incoming and outgoing charged particles, time-of-flight measurements (for charged-particle identification), a moderate magnetic field (due to the low momenta involved) for momentum measurements, and a system of converters plus scintillators for photon detection and subsequent geometrical reconstruction of π^0 and Σ^0 decays.

The above figures for $K^{\pm}$ rates do not include particle losses in the beam-pipe wall and in the internal tracking system, which were assumed sufficiently thin (e. g. of a few hundred μm of low-Z material), nor rescattering effects in a nuclear target such as ^{4}He. We have indeed checked that, due to the shape of the angular distribution of the kaons, particle losses are contained (mostly at small angles, where K-production is negligible and events would be hard to be reconstructed), and momentum losses flat around $\theta=\pi/2$ (where most of the $K^{\pm}$'s are produced): even for a total thickness of the above–mentioned materials of 1 mm, kaon momenta do not decrease below $100\,{\rm MeV}/c$ and losses do not grow beyond a few percents. Rather, one could exploit such a thickness as a low–momentum, thin moderator, to span the interesting region just above the charge–exchange threshold at $p_{\rm L}(K^-)\simeq90\,{\rm MeV}/c$, measurements which would add precious, additional constraints on low-energy amplitude analyses [289].

Acceptable rates can thus be achieved, orders of magnitude above those of the existing data at about the same momentum, i.e. to the lowest-energy points of the British–Polish Track–Sensitive Target (TST) Collaboration, taken in the mid and late 70's at the NIMROD accelerator.

Since losses do not affect $K_{\rm L}$'s, a detector of the kind sketched above, could be used without any problem to study low-energy $K_{\rm L}\to K_{\rm S}$ regeneration and charge-exchange in gaseous targets, providing essential information for this kind of phenomena. Also, a DAFNE detector dedicated to kaon experiments on gaseous H_2 and D_2 can continue its active life to measure K^+-, K^--, and $K^0_{\rm L}$-interactions on heavier gases as well (He, N_2, O_2, Ne, Ar, Kr, Xe), exploring not only the properly nuclear aspects of these interactions, such as nucleon swelling in nuclei [290], but also producing $\pi\Sigma$, $\pi\Lambda$ and $\pi\pi\Lambda$ systems at invariant masses below the elastic $\overline{K}N$ threshold in the so-called unphysical region, with statistics substantially higher than those now available [291, 292], due to the $\simeq4\pi$ geometry allowed by a colliding-beam-machine detector.

For interactions in hydrogen, the c.m. energy of the pion–hyperon states is limited by momentum conservation to the initial one, equal (neglecting energy losses) to $w=(m_p^2+m_K^2+m_pM_\phi)^{1/2}$, or $1442.4\,{\rm MeV}$ for incident $K^{\pm}$'s and $1443.8\,{\rm MeV}$ for incident $K_{\rm L}$'s. As already mentioned, energy losses for charged kaons can be exploited to explore K^-p interactions down to the charge-exchange threshold at $w=1437.2\,{\rm MeV}$, corresponding to a K^- laboratory momentum of about $90\,{\rm MeV}/c$. For interactions in nuclei, momentum can instead be carried away by spectator nucleons, and the inelastic channels explored down to threshold. The possibility of reaching energies below the $\overline{K}N$ threshold allows exploration of the unphysical region, containing two resonances, the $I=0$, S-wave $\Lambda(1405)$ and the $I=1$, $J^P=\frac{3}{2}^+$ P-wave $\Sigma(1385)$, observed mostly in production experiments (and, in the first case, with limited statistics [291, 292]): the information on their couplings to the $\overline{K}N$ channel relies entirely on extrapolations of the low-energy $\overline{K}N$ data. The coupling of the $\Sigma(1385)$ to the $\overline{K}N$ channel, for instance, determined via dispersion relations involving the total sum of data collected at $t\simeq0$, still carries uncertainties which at their best are of the order of 50% of the SU(3)$_f$ prediction [293]. As for the $\Lambda(1405)$, even its spectroscopic classification is an open problem, given the paucity of the best available data. We could add that recently the presence of a second state has been claimed [294, 295], and to test such a claim would of course be important, for the role the state has both for kaonic atoms and the determination of the low-energy parameters of the KN interactions.

A formation experiment on bound nucleons, in an (almost) 4π apparatus with good efficiency and resolution for low–momentum γ's (such as KLOE), can measure a channel such as $K^-p\to\pi^0\Sigma^0$ (above threshold), or $K^-d\to\pi^0\Sigma^0n_s$ (both above and below threshold), which is pure $I=0$: up to now all analyses on the $\Lambda(1405)$ have been limited to charged channels, and assumed the $I=1$ contamination to be either negligible or smooth and non-interfering with the resonance signal. Since models for the $\Lambda(1405)$ differ mostly in the details of the resonance shape, and it is precisely the shape which could be changed even by a moderate interference with an $I=1$ background, such measurements would be decisive. Having in the same apparatus and at almost the same

energy tagged K^- and K_L produced at the same point, one can further separate $I = 0$ and $I = 1$ channels with a minimum of systematic uncertainties, by measuring all channels $K_L p \to \pi^0 \Sigma^+$, $\pi^+ \Sigma^0$ and $K^- p \to \pi^- \Sigma^+$, $\pi^+ \Sigma^-$, besides, of course, the above–mentioned, pure $I = 0$, $K^- p \to \pi^0 \Sigma^0$ one. It must be noted that the recent claim for two states [294, 295] is based on a low–statistics measurement [296] of the reaction $K^- p \to \pi^0 \pi^0 \Sigma^0$: an analysis of all $\pi\pi Y$ ($Y = \Lambda, \Sigma$) channels, possible with much higher statistics at DAFNE, would be therefore highly desirable.

Another class of interesting processes which are expected, at a much smaller rate, from DAFNE's kaons are the radiative capture ones $K^- p \to \gamma\Lambda$, $\gamma\Sigma^0$ and $K_L p \to \gamma\Sigma^+$ (both in hydrogen and nuclei), and $K^- n \to \gamma\Sigma^-$ and $K_L n \to \gamma\Lambda$, $\gamma\Sigma^0$ (only in nuclei). Up to now only searches for photons emitted after stops of K^-'s in liquid hydrogen and deuterium have been performed with some success: spectra are dominated by photons from unreconstructed π^0 and Σ^0 decays, and separating signals from this background poses serious difficulties. Indeed these experiments were able to produce only an estimate of the respective branching ratios [297]. The 4π geometry at DAFNE, combined with the "transparency" of a KLOE-like apparatus, its high efficiency for photon detection and its good resolution for spatial reconstruction of the events, should make possible (in an H_2/D_2 experiment) the full identification of the final states and therefore the measurement of the absolute cross sections for these processes, although in flight and not at rest.

A first proposal would be the following: before building a dedicated apparatus for low-energy experiments on gaseous targets, one could equip KLOE with a less restrictive trigger, that could select the interactions of anti-kaons (tagged by the particles on the opposite side, be they either K^+'s or K^0_S's) with the gas filling the chamber and reconstruct off-line the pion–hyperon, pion–pion–hyperon and single-γ–hyperon spectra for all charge combinations. Such data would contain both the $\Lambda(1405)$ and the $\Sigma(1385)$, including their interference, plus the effects of rescattering inside the remainder of the ^{4}He target. The latter will further feed – via charge–exchange processes – also such "exotic" combinations as $\Sigma^\pm\pi^\pm$, allowing a better understanding of the nuclear–medium distortions on the "elementary" processes $\overline{K}N \to \pi Y$, $\overline{K}N \to \pi\pi Y$ and $\overline{K}N \to \gamma Y$. KLOE (or a similar, scaled down apparatus) is unique for such a scope: the need for a good efficiency and high resolution for low-energy γ's (motivated for KLOE by decays such as $\phi \to \gamma(a_0, f_0)$ and the reconstruction of very low–momentum π^0's) allows also the identification and reconstruction of Σ^0's through their decay to $\Lambda\gamma$, virtually impossible in any other detector with an almost 100% efficiency. On the other hand, the very high efficiency for γ detection, combined with the high intensity of the source and the ease with which one can discriminate between kaons and pions (not to mention leptons) from the ϕ decays, allows an unprecedently clean determination of radiative capture events (even if in a slightly more complex target than hydrogen or deuterium).

As a closing remark one can add that contaminations due to the presence of a small admixture of other gases in helium, or to the tungsten wires running across the chamber, are not that important for the mass spectra (they amount to – small – distortions in the nucleon distribution functions, which the "elementary" amplitudes have to be convoluted with, with respect to those for pure ^{4}He), and even less for the ratio of γY (or $\pi\pi Y$) to πY spectra.

2.8 Conclusions

We have seen that DAFNE-2 offers the possibility to carry on a wide physics program, mainly based on the possibility to increase the center of mass energy up to 2.5 GeV but also by profiting of a high luminosity run at the ϕ resonance energy. This program includes important measurements that are essential for the most precise tests of the standard model, and a large number of relevant measurements in the field of hadronic physics. Some of these measurements can be done only in the DAFNE-2 environment. We remark that such a program considerably broadens the physics potential of the entire project being complementary to the kaon decays program. In Sect. 4 we will discuss the main requirements of this program to the foreseen detectors.

3 A higher energy option: The τ-charm factory

3.1 The physics case for a τ-charm factory at LNF

3.1.1 Overview

In this section we discuss the physics that could be addressed with a τ-charm factory at Frascati, the impact and competitiveness of such a research program with respect to the existing and planned ones. When the LHC will possibly have directly probed the existence of new physics at the TeV scale, further progress may be achieved with low energy experiments in high precision flavour physics. A dedicated τ-charm factory with unprecedented luminosity and much better systematics, to be ready in 2013 (we assume at least 5 years of construction after the end of DAFNE) , could be essential to constrain the new physics with intensive flavour studies.

Within flavour physics, the charm quark occupies a peculiar place. It is the lightest among the heavy quarks, i.e., the quarks with mass larger than the QCD scale Λ_{QCD}. Besides, it is the only up-type heavy quark that hadronises, which favours searches for Beyond the standard model (BSM) physics, since due to GIM mechanism the box diagram processes are suppressed in the standard model (SM). Therefore, the charm quark is a good testing ground for problems still open in the B sector. The charm quark is also a probe for BSM physics in the LHC era. For both statements, an obvious caveat has to be formulated, that is, the charm quark mass sits right in the middle of a range heavily populated of light quark resonances, the 2 GeV region. Final state interactions are particularly important, and should be carefully taken into account. Final state interactions, on the other hand, are useful for finding CP violation effects: they are an essential ingredient to find direct CPV through partial width asymmetries and, while in T-odd moments they can fake CP violation, nonetheless they can be disentangled at a τ-charm factory. Finally, the charm quark mass can be extracted both from hidden charm and open charm decays, which provides a valuable validation check.

Charm physics has been the driving force for modern detector development, and it is now investigated by B-factories and τ-charm factories [298–300]. A τ-charm factory is an e^+e^- collider running at center of mass energy from $c\bar{c}$ charmonium (J/ψ), to the $\psi(2S)$ (the $\tau\overline{\tau}$ threshold), the $\psi(3770)$ (the $D\bar{D}$ threshold) and above to the $D_s\overline{D}_s$ threshold. A collider attaining a center of mass energy of 3.8 GeV investigates a very broad spectrum of very important topics, such as charmonium spectroscopy, τ lepton decays, and D meson decays.

Studying charm decays produced at threshold in e^+e^- annihilation offers several special advantages. Most of the charmonium spectroscopy results have come from e^+e^- storage rings, where $J^{PC} = 1^{--}$ states are formed directly to lowest order. The non-vector states such as ^3P_J are observed in two-step processes like $e^+e^- \to \psi(2S) \to c\bar{c} + \gamma$. Threshold production of charmed hadrons leads to very clean low multiplicity final states with very low backgrounds. Clean events also imply favourable conditions for neutrino reconstruction via missing mass techniques. One can employ tagged events to obtain the *absolute* values of charm hadron branching ratios in a model independent way. The widths for $D^+ \to \mu^+\nu$ and $D_s^+ \to \mu^+\nu$ can be measured with unrivalled control over systematics. Finally, with the charm hadrons being produced basically at rest the time evolution of D^0 decays cannot be measured directly. Yet by comparing EPR correlations in D decays produced in $e^+e^- \to D^0\overline{D}^0$, $e^+e^- \to D^0\overline{D}^0\gamma$ and $e^+e^- \to D^0\overline{D}^0\pi^0$ one can deduce whether oscillations are taking place or not, as explained in detail in [298].

Several proposals have been discussed over the last 15 years for τ-charm factories with the ambitious goal of achieving luminosities up to the 10^{33}–$10^{34}\,\mathrm{cm}^{-2}\,\mathrm{s}^{-1}$ range for the c.m. energy interval of 3–5 GeV. A τ-charm factory project was proposed at CERN [301] (1987), at SLAC [302] (1989), in Spain [303] (1990), at JINR [304] (1992) and Argonne [305] (1994). It became reality with the CESR-c/CLEO-c and BEPC-II/BES-III projects, described in Sect. 3.2.

Exploring all the possibilities for the future of the LNF in the panorama of high energy physics during and after the LHC era includes also τ-charm physics. Expertise for both machine and detector does exist for (although the infrastructures of the LNF are probably not compatible with) a τ-charm project, a collider with an energy in the center of mass of 3.8 GeV, and maximum luminosity of $10^{34}\,\mathrm{cm}^{-2}\,\mathrm{s}^{-1}$, i.e. an order of magnitude above the BEPC-II design value. Such a machine could be based on a double symmetric ring collider, flat beams in multi-bunch operation, normal conducting magnets, one interaction region, and on-energy injection system [306, 307]. In the following, we shall assume an integrated $100\,\mathrm{fb}^{-1}$ integrated Luminosity per 10^7s year.

The detector is ambitious, but working examples already exist and operate. CLEO-III/CLEO-c [308, 309], for instance, is a solenoidal 4π hermetic detector with tracker, RICH, ECAL, potent DAQ and open trigger. No vertex detector is necessary in principle if the symmetric beam option is used, since $D\bar{D}$ pairs are produced at rest in the lab reference system.

In this section we shall review the τ-charm relevant physics topics in hidden and open charm physics, both SM- and BSM-related. In particular we shall underline the items functional to BSM characterisation in the LHC era, and discuss the relative merits of a τ-charm factory with respect to competition.

3.1.2 Hidden charm physics

Heavy quarkonium, being a multi-scale system, offers a precious window into the transition region between high energy and low energy QCD and thus a way to study the behaviour of the perturbative series and the nontrivial vacuum structure. The existence of energy levels below, close and above threshold, as well as the several production mechanisms, allows one to test the population of the QCD Fock space in different regimes and eventually to search for novel states with nontrivial glue content (hybrids, glueballs). Besides, a study of the final state in charmonium decays will open a novel tool for studying low energy spectroscopy and hadronization.

The diversity, quantity and accuracy of the data collected at several accelerator experiments (BES, KEDR, CLEO-III, CDF, D0, B-factories, Zeus, H1, RHIC) makes quarkonium an extremely relevant and timely system to study. In the near future, even larger data samples are expected from the CLEO-c and BES-III upgraded experiments, and in perspective at the LHC and at Panda at GSI.

From the theory point of view, the recent progress in the formulation of non-relativistic effective field theories (EFT) for heavy quarkonium (NRQCD, pNRQCD) [310] and the related lattice implementation, makes it possible to go beyond phenomenological models and, for the first time, provide a unified and systematic description of all aspects of heavy-quarkonium physics. This, together with the huge flow of experimental data, allows to use quarkonium as a benchmark for our understanding of QCD, for the precise determination of relevant SM parameters and for search of physics BSM.

A τ-charm machine with the characteristics discussed above would allow for record samples of J/ψ, $\psi(2S)$, $\psi(3770)$ with unmatched systematics and with very rich and interesting physics, complementary to the LHC program, that includes the following topics.

Precise extraction of SM parameters from quarkonium. Ground state observables may be studied in the framework of perturbative QCD [310–315]. These studies are relevant because they may allow, in principle, the precise extraction of some of the fundamental parameters of the SM, like the heavy quark masses and the strong coupling constant. A recent analysis performed by the Quarkonium Working Group [300], and based on all the previous determinations existing in the literature, indicates that the quark mass extraction from heavy quarkonium involves an error of about 50 MeV both in the bottom (1% error) and in the charm (4% error) case. Such error is already very competitive with extractions coming from other physical systems and in the future it should be reduced further up to 40% (30 MeV).

The present PDG [12] determination of α_s from heavy quarkonium pulls down the global α_s average quite noticeably, due to an error that has been largely underestimated. Using the latest development in the calculation of relativistic corrections and on the treatment of perturbative series [310], it is conceivable to use electromagnetic and hadronic decay widths, whose experimental accuracy is already sensitive to next-to-leading corrections, to provide a competitive sources of m_c and $\alpha_s(m_c)$.

Charmonium decays and transitions. The study of decay observables has witnessed in the last years a remarkable

progress. New experimental measurements, mainly coming from BELLE, BES, CLEO and E835 have improved existing data on inclusive, electromagnetic and several exclusive decay channels as well as on several electromagnetic and hadronic transition amplitudes [12, 300]. In some cases the new data have not only led to a reduction of the uncertainties but also to significant shifts in the central values. The error analysis of several correlated measurements has evolved and improved our determination of quarkonium branching fractions. New data have led to the discovery of new states. From a theoretical point of view several heavy quarkonium decay observables may be studied nowadays in the framework of effective field theories of QCD [310, 316–319].

By collecting huge statistical data samples one can open the era of precision measurements on several charmonium decays and transitions. In particular:

– *Electromagnetic transitions.* 1%–2% precision measurements on many radiative transitions will be possible, allowing access to the suppressed (M1, M2 and E2) amplitudes, which are mostly dependent on higher-order corrections and better test different theoretical approaches [300, 320, 321]. The transition $J/\psi \to \gamma\eta_c$ is a good example. Such transition is presently known with a 30% error (only one direct transition measurement [322], several measurements of the BRs $J/\psi \to \eta_c\gamma \to \phi\phi\gamma$ combined with one independent measurement [323] of $\eta_c \to \phi\phi$) and enters several charmonium BRs. Its uncertainty sets therefore the experimental error of several measurements. Runs at the $\psi(2S)$ energy will also provide a very large sample of tagged J/ψ decays (as more than half of these mesons decay to J/ψ), but are also an excellent source of χ_c's, and, as recently shown, of h_c's.
– *Radiative and hadronic decays.* Radiative and hadronic charmonium decays involve several open puzzles. For example in exclusive hadronic decays the $\rho\pi$ puzzle in J/ψ and $\psi(2S)$ decays is related to the anomalously small $\psi(2S) \to \rho\pi$ decay with respect to the $J/\psi \to \rho\pi$ decay, which is the largest two body hadronic decay mode of the J/ψ [298, 300]. New states can be discovered in charmonium decays. An example is the enhancement in the radiative J/ψ decay in proton-antiproton pair recently observed by BES [133] and identified also with a candidate for baryonium.
– *Hybrids and Glueballs.* The existence of gluonic excitations in the hadron spectrum is one of the most important unanswered questions in hadronic physics. Lattice QCD predicts a rich spectroscopy of charmonium hybrid mesons [300]. There are three important decay modes for charmonium hybrids [300]: (i) the decays to D mesons (ii) the cascade to conventional $c\overline{c}$ states (iii) decays to light hadrons via intermediate gluons, ψ_g hybrids with exotic J^{PC} quantum numbers offer the most unambiguous signal since they do not mix with conventional quarkonia. Gluonic excitations may be studied through radiative decay, i.e. $J/\psi \to \gamma X$ where X is a glueball [324]. Also $\psi(2S)$ radiative decays are expected to be a prime source for glue-rich final states. Although one expects the majority of this data to come from J/ψ running, $\psi(2S)$ decay would also allow flavour tagging through the hadronic decays where a low mass vector meson (i.e. ρ, ω, ϕ) replaces the radiative photon. The possibility of studying J/ψ decay using $\psi(2S)$ running and tagging the J/ψ from $\psi(2S) \to \pi\pi J/\psi$ is also promising.
– *Physics at* $\psi(3770)$. A run at $\psi(3770)$ energy, besides measuring f_D from $\overline{D}D$ decays, can also look for rare radiative and hadronic decays to lower $c\overline{c}$ states. This study can give a unique insight into the S–D mixing and coupling to decay channel effects. It may also give clues to the understanding of the ρ–π puzzle.

Search for new states. The new resonances recently observed at BELLE, BABAR, CLEO, BES and Fermilab [$X(3872)$, $Y(4260)$, $X(3940)$, $Y(3940)$, $Z(3939)$] [325], open a discovery potential for states of new type (molecular, multiquark, heavy hybrids) never seen before and of great impact for acquiring insight in the strong interaction dynamics. Studies of narrow resonances via the radiative return method will be feasible at the Frascati τ-charm factory and will greatly enhance such discovery potential. The observation of the $X(3872)$ [325] has been the start of challenging searches for non-vector states across the open flavour threshold. This is probably the richest experimental field of research on heavy quarkonia at present. The nature of this new, narrow state is not yet clear, and speculation ranges from a $D^0\overline{D^{0*}}$ molecule, a $^3D_2$ state to diquark–antidiquark state [326–329]. There are theoretical problems with all these interpretations, and further, more accurate measurements of its width and particularly of its decay modes are needed to shed light on this state. Studies on the nature of the $X(3872)$ can benefit from data taking at τ-charm factories. The study of the energy region above the $D\overline{D}$ threshold is one of the most interesting open problems in charmonium physics and will require high-statistics.

Investigation of low energy QCD. Theaccuracy with which the fundamental parameters can be measured is at present limited by nonperturbative contributions whose form is in many cases known [310], but whose size is not known with sufficient precision. Therefore, the main theoretical challenge is the precise determination of these nonperturbative contributions. We may use the lower quarkonium states as a theoretically clean environment to study the interplay of perturbative and nonperturbative effects in QCD and extract nonperturbative contributions by comparison with data. Therefore, precise quarkonium data are important today more than ever. They may check factorisation, and severely constrain theoretical determinations and predictions.

Searches for new physics with charmonium. Heavyquarkonium offers an interesting place where probing new physics which would manifest experimentally as slight but observable modifications of decay rates and branching fractions; unexpected topologies in decays; CP and lepton flavour violation [300].

CP tests with J/ψ decays. By using the decay mode $J/\psi \to \gamma\phi\phi$, the electric- and chromo-dipole moment can be probed at order of $10^{-13}\mathrm{e\,cm} \sim 10^{-14}\mathrm{e\,cm}$. A nonzero electrical dipole moment (EDM) of a quark or a lepton implies that CP symmetry is violated, since EDM's of quarks and leptons are very small in the SM, and, more importantly, that a signal exists for the intervention of BSM physics.

Lepton flavour violation. Lepton flavour is violated in many extensions of the SM, such as grand unified theories, supersymmetric models, left–right symmetric models, and models

where the electroweak symmetry is dynamically broken. Recent results indicate that neutrinos have nonzero masses and can mix with each other pointing to the fact that lepton flavour may be a broken symmetry in nature. Lepton flavour violation (LFV) can be tested via the two-body J/ψ decay (which conserves total lepton number): $J/\psi \to \ell\ell'$ with ℓ and ℓ' denoting charged leptons of different species. This process could occur at tree-level induced by leptoquarks, sleptons (both in the t-channel) or mediated by Z' bosons (in the s-channel). The large sample (5.8×10^7 events) collected in leptonic decays of J/ψ resonances at BEPC and analysed by BES up to now makes this search especially interesting; in fact, upper limits for different lepton combinations have already been set at 90% C.L. [330, 331]. In the future, larger samples collected at a τ-charm factory at LNF could allow to test LFV at a higher precision, severely constraining new physics models.

3.1.3 Open charm physics

Studying charm decays at the threshold process $e^+e^- \to \psi(3770) \to D\overline{D}$ offers many advantages. Threshold production of charm hadrons leads to extremely clean events, with optimum signal/background ratios; the background due to not-$D\overline{D}$ processes can be directly measured running below the production threshold. It is possible to tag the events to obtain absolute branching fraction measurements; the $D\overline{D}$ pairs are produced in a coherent quantum state providing information on D mixing and CP violation. In the SM, CP-violating amplitudes arise from penguin or box diagrams with b-quarks; however they are strongly suppressed by the small $V_{cb}V_{ub}^*$ combination of the CKM matrix elements. The SM does predict CPV in singly-Cabibbo suppressed modes at the level of 0.001 or so. No CP violation is allowed in the SM for Cabibbo-favoured nor doubly-Cabibbo suppressed modes. SM does direct CP in partial widths and in final state distributions (Dalitz plots, T-odd moments) and CP violation involving oscillations. The question is whether close to threshold one has systematic advantages, when the CP asymmetries are very small, i.e 0.001 or less. The $D\overline{D}$ pairs are produced in a $C = -1$ initial state so that final states containing two CP eigenstates of the same parity are a manifestation of CP violation. With integrated luminosities of the order of $100\,\mathrm{fb}^{-1}$ the discovery window in the analysis of these final states could be extended to the 10^{-4} level.

Moreover, it is possible to put stringent limits on the oscillations in the charm sector running above the $\psi(3770)$ and comparing the correlations in D decays produced in $e^+e^- \to D^0\overline{D}^0$, $e^+e^- \to D^0\overline{D}^0\gamma$ and $e^+e^- \to D^0\overline{D}^0\pi^0$ [298]. Although $D^0\overline{D}^0$ oscillations are not the most suitable tool to look for new physics, their study at the τ-charm factory is unique because of the absence of concurrent doubly-Cabibbo Suppressed decays in most of final states. At a τ-charm factory is also possible the measurement of the strong phase shift by comparing oscillations in hadronic and semileptonic final states. Other channels of interest are the FCNC decays, in particular the $D \to \pi\ l^+l^-$ and $D \to \rho l^+l^-$ which in the SM are expected to have a BR of the order of 10^{-6}: effects of new physics could show up in the region of low di-lepton masses [299].

Integrated luminosities of the order of $100\,\mathrm{fb}^{-1}$ would provide statistics for many important studies of the SM, summarised in Table 7

- Precision measurement of the $D^+ \to \mu^+\nu$ branching ratio, allowing the extraction of the charm decay constant f_D, can be carried out with unrivalled control over systematics. Extracting precise numbers for the decay constant f_D represents an important test for lattice QCD calculations [332] and will thus indirectly support the lattice calculations done in the beauty sector where direct precision measurements are not available. If the τ-charm factory could run at the D_s production threshold, one would be allowed to study also $D_s^+ \to \mu^+\nu$ and $D_s^+ \to \tau^+\nu$.

Table 7. Physics reach for outstanding SM studies at τ-charm factory. Estimates are extrapolated from CLEO-c, the factory presently operating at the Cornell storage ring, and projected to $100\,\mathrm{fb}^{-1}$ luminosity

Charmed meson	Produced	Detected
D^0	400×10^6	160×10^6
D^+	160×10^6	63×10^6
D_S^+	30×10^6	9×10^6
mode	decay constant	$\Delta f_{D_q}/f_{D_q}$
$D^+ \to \mu^+\nu$	f_D	0.5%
$D_S^+ \to \mu^+\nu$	f_{D_S}	0.4%
$D_S^+ \to \tau^+\nu$	f_{D_S}	0.3%
$\Delta(V_{cd})$	$\Delta(V_{cs})$	$\Delta R/R; R \equiv \lvert V_{cd}\rvert/\lvert V_{cs}\rvert$
0.3%	0.3%	0.2%
abs. hadronic BRs	num. double tags ($\times 10^3$)	stat. error
D^0	1500	0.1%
D^+	1800	0.1%
D_S^+	180	0.3%

– Significant improvements in the measurements of $|V(cd)|$ and $|V(cs)|$ from $D \to \ell\nu\pi$ and $D \to \ell\nu K$ modes could be obtained, providing also another sensitive test for the attainable precision with lattice QCD. Accurate charm data are very useful to understand the reliability of the description of non-perturbative dynamics.
– The absolute branching ratios for non-leptonic decays like $D^0 \to K\pi$ and $D^+ \to K\pi\pi$ could be measured with uncertainties of the order of per mil. Absolute measurements of hadronic charm meson branching fractions are relevant in the study of the weak interactions because they are needed to normalise several branching fractions, from which CKM matrix elements are extracted. Better results on modes like $D^0 \to K^-\pi^+$ or $D^+ \to K^-\pi^+\pi^+$ have already been obtained by the CLEO-c collaboration, and more data will be provided soon by BES-III. These data will help to get further insight into the scalar meson sector and a better determination of the parameters of the already well established resonances.
– Accurate studies of low mas hadronic spectroscopy in charm decays would be possible.

There is a deep interplay between precision measurements in the charm sector and the present/future physics programs in the beauty sector. Absolute charm branching ratios and decay chains represent important inputs for B decays, and the present uncertainties are becoming a bottleneck in the analysis of the beauty decays.

3.1.4 τ physics

The τ lepton is an ideal laboratory [333] for precise studies of the electroweak and strong sector of the SM. In addition, searches for physics beyond the SM can be performed, with precision measurements or direct searches for non-SM processes. τ-data can also be exploited to reconsider the contribution of the hadronic vacuum polarisation to $\alpha_{\rm QED}$ and the anomalous magnetic moment of the muon.

An e^+e^- collider reaching $\mathcal{L} \sim 10^{34}\,\mathrm{cm}^{-2}\,\mathrm{s}^{-1}$ at $\sqrt{s}$ just above 3.7 GeV could deliver $100\,\mathrm{fb}^{-1}$ per year ($1y = 10^7$ s), thus allowing for the study, with ~ 3 years of data taking, of the lepton-number violating channel $\tau \to \mu\gamma$ on the basis of a sample of 10^9 events, i.e. in the region of interest for the SUSY theories [334].

τ spectral functions, hadronic cross sections and τ decays. Hadronic τ decays provide one of the most powerful testing ground of QCD [333]. This is due both to the high statistics and high precision obtainable in the data and to the fact that the theoretical description is found to be dominated by perturbative QCD. Because of its large mass the τ can decay into hadrons while it has the QCD vacuum as the initial state and thus can provide a particularly clean tool to investigate strong interactions and charged weak hadronic currents. τ decays reveal a rich structure of resonances, while the leptonic environment provides a way to isolate clean hadronic systems and measure their parameters. Observables based on the spectral functions of hadronic τ decays can be used to obtain precise determinations of α_s, m_s, V_{us} and parameters of the chiral Lagrangian. τ decay results are complementary to the e^+e^- data to perform detailed studies at the fundamental level through the determination of the spectral functions. The non-strange vector spectral function is related, vis isospin symmetry, to the corresponding e^+e^- spectral function. The precision reached makes it necessary to correct for isospin-symmetry breaking. As discussed in Sect. 2.2 these vector spectral functions are used to compute vacuum polarisations, which enter the evaluation of the running of α and the muon anomalous magnetic moment. At present, τ and e^+e^- data sets produce a discrepancy at the 2–3 σ level which has to be clarified.

New physics searches with τ. Tests of charged-current lepton universality, electro-weak dipole moments and lepton-flavour violating decays such as $\tau \to \mu\gamma$ and $\tau^- \to l^+l^-l^-$ will be possible with the future high-precision and high-statistics τ decay data. Data in the τ sector should reach levels below the permil level. The observation of non-zero weak dipole moments would signal CP-violation BSM. The highest cross section for $\tau\overline{\tau}$ production occurs at the $\psi\prime$ resonance (3.69 GeV) where visible cross section is approximately proportional to $1/\sigma(E)$ ($\sigma(E)$ is the machine beam energy spread) and it is $\sim 3\,\mathrm{nb}$ for machines adopting standard optics. The recent upper limit obtained by BABAR Collaboration for the $\tau \to \mu\gamma$ [335] is $\mathrm{BR}(\tau \to \mu\gamma) \leq 6.8 \times 10^{-8}$ at 90% C.L., based on the analysis of $\sim 2 \times 10^8$ produced τ pairs. Radiative τ decays such as $\tau \to \pi\nu\gamma$ and $\tau \to \mu\pi\nu\nu\gamma$ are for the same reason best studied immediately above τ threshold. Moreover, the τ physics program includes precise measurement of the τ mass, sensitive studies of weak couplings and lepton universality via purely leptonic and semileptonic decays, and the measurement of other rare processes as those involving kaons. As stated above, thanks to the kinematic constraints, the $\tau \to \pi\pi^0\nu$ channel can be well separated from the other decays giving the opportunity for a new test of the CVC rule via the comparison with the $e^+e^- \to \pi^+\pi^-$ data.

CPV asymmetries in $\tau \to K_{S,L}\pi\nu$. It has been pointed out recently [337] how threshold production and decay of $\tau^+\tau^-$ pairs, such as $\tau \to K_{\rm S,L}\pi\nu$ would provide information on known SM sources of CP violations, complementary to $K_{\rm S,L}$ semileptonic decays.

3.2 Comparison with present and future competitors

CESR at Cornell, Ithaca (US), after almost twenty years of successful operation as a B-factory, with a long lasting record in peak luminosity ($1.3 \times 10^{33}\,\mathrm{cm}^{-2}\,\mathrm{s}^{-1}$ at the $\Upsilon(4S)$ energy), has been recently modified in order to run at lower center-of-mass energies (CESR-c) [300, 309, 338, 339]. SC wigglers have been added to increase the radiation damping and improve luminosity. CESR-c will run until 2008 at the τ, $D\overline{D}$ and $D_s\overline{D}_s$ thresholds. The goal peak luminosity is $3 \times 10^{32}\,\mathrm{cm}^{-2}\,\mathrm{s}^{-1}$. During first quarter of 2004, CLEO-c has been running [339] at a peak luminosity of about $5 \times 10^{31}\,\mathrm{cm}^{-2}\,\mathrm{s}^{-1}$. Their plan from today to 2007 is to integrate $3\,\mathrm{fb}^{-1}$ at the $\psi(3700)$ (or $1.3 \times 10^9 J/\psi$), then switch to the D_sD_s threshold and accumulate another $3\,\mathrm{fb}^{-1}$ (or 3×10^7 events), and finally to switch to the J/ψ aiming to collect 10^9 events, i.e., twenty times the BES statistics [300].

BEPC [269], at Beijing (China), which reached a peak luminosity of $1.1 \times 10^{31}\,\mathrm{cm}^{-2}\,\mathrm{s}^{-1}$, has been dismounted and is being upgraded to become BEPC-II, the first completely dedicated τ-charm factory, still maintaining synchrotron radiation production. Its design is based on a double ring scheme, with energies ranging between 1.5 and 2.5 GeV/beam, optimised at 1.89 GeV, with a design luminosity of $10^{33}\,\mathrm{cm}^{-2}\,\mathrm{s}^{-1}$. A new inner ring will be installed inside the old one, so that each beam will travel in half outer and half inner ring. SC cavities will also be installed. A by-pass will allow the electron ring to be used as a synchrotron light source as well. Commissioning of the new rings is planned for summer 2007. Experiment BES-III, that is an upgraded version of BES which provided record samples of J/ψ's and ψ''s in the last years, will run a new intensive program at these energies from 2007 on [300].

CLEO-c and BES address topics in both open charm and quarkonium physics. The world scenario for quarkonium [300], however, is not limited to them but sees other competitors

- τ-charm factories: besides BES and CLEO-c, KEDR which, exploiting the polarimeter in the VEPP-4 collider, has recently provided high precision measurements of J/ψ and ψ' masses;
- B-factories: after CLEO, BABAR and BELLE, have proved their large physics potential also as charmonium factories, through a rich variety of reactions (B decays to charmonium, $\gamma\gamma$, ISR, double $c\overline{c}$);
- $\overline{p}p$ charmonium factory: the antiproton accumulator of the Tevatron, at Fermilab, was exploited by the E835 experiment, to scan all known narrow charmonium states in formation from $p\overline{p}$ annihilation.

In these last years, clean record samples of all the narrow vector resonances have been accumulated. Table 8 (taken from [300]) shows the record samples of charmonia produced (or formed) in one B-factory (via B decays, $\gamma\gamma$, radiative return) with $250\,\mathrm{fb}^{-1}$ (such quantity is continuously increasing at present); the highest statistics runs recently done by the τ-charm factory BES ($58MJ\psi$'s and $14M\psi(2S)$); and the data samples formed in the $p\overline{p}$ charmonium experiment E835. Another $p\overline{p}$ charmonium factory is going to start data taking at GSI in the next decade.

3.2.1 Systematic limits of the present generation of high statistics experiments

Running at $D\bar{D}$ threshold has obvious advantages in terms of number of charm events over background, ratio of events produced, systematics and rates. Similar considerations do apply for threshold production of τ leptons. As an example, the sensitivity of the BABAR experiment for the $\tau \to \mu\gamma$ [335] decay discussed above is limited by the background, mainly from $\mu\mu(\gamma)$ and $\tau\tau(\gamma)$ events. Running near threshold, the radiative $\tau\tau\gamma$ component is suppressed, and the kinematics of the 2-body τ decays is quasi-monochromatic [306], giving further elements besides statistics to definitively improve the results from the B-factories. Radiative τ decays such as $\tau \to \pi\nu\gamma$ and $\tau \to \mu\pi\nu\nu\gamma$ are for the same reason best studied immediately above τ threshold. Finally, results from all e^+e^- experiments crucially depend on the subtraction of radiative corrections on the initial state [300].

3.3 Conclusions

When the LHC will have directly probed the physics at the TeV scale, precision studies of flavour physics will be necessary. Within flavour physics, the charm quark plays an important role [298, 299]. The physics program at a τ-charm factory is very broad and robust [300, 340] with a very strong list of SM issues such as charmonium spectroscopy and decays, absolute branching ratios, decay constants and CKM matrix elements from semileptonic decays. Besides, relevant BSM topics contribute to the understanding of the LHC scenario: CP violation, mixing, charm rare decays, tau rare decays.

Some of these topics are unique to τ-charm factories with respect to their direct competitors, the super-B-factories [341]: absolute branching ratios, purely leptonic decays. Other topics, both BSM- and SM-related, benefit from threshold running at τ-charm factories, such as mixing, semileptonic decays for meson decay constants, τ rare decays, searches for CP violation in the charm system, charmonium spectroscopy.

The interplay, compatibility, complementarity and overlap of the physics programs of future τ-charm factory and super-B-factory were subject recently of very detailed and specific discussion at DIF06 Workshop [342]. Main conclusions of the workshop were

- Flavour physics is crucial in the LHC era to constrain the flavour structure of the BSM physics found;
- If no BSM physics is found, flavour physics may be the only tool we shall have to acquire clues on the features of BSM physics;
- A super-B-factory is also a powerful τ-factory – in the τ sector, very few measurements are performed with great advantage running at threshold rather than at the $\Upsilon(4S)$;

Table 8. Charmonium states produced in the B-factories and τ-charm factories, or formed in $p\bar{p}$ (from [300])

Particle	$\psi(2S)$	$\eta_c(2S)$	χ_{c2}	χ_{c1}	χ_{c0}	J/ψ	$\eta_c(1s)$
B decays	$0.8M$	$0.4M$	$0.3M$	$0.9M$	$0.75M$	$2.5M$	$0.75M$
$\gamma\gamma$	–	$1.6M$	$1M$	–	$1.2M$	–	$8.0\ M$
ISR	$4M$	–	–	–	–	$9M$	–
$\psi(2S)$ decays	$14M$	?	$0.9M$	$1.2M$	$1.2M$	$8.1M$	$39K$
J/ψ decays	–	–	–	–	–	$58M$	$0.14\ M$
$p\bar{p}$	$2.8M$	?	$1M$	$1M$	$1.2M$	$0.8M$	$7M$

– A super-B-factory is also a charm-factory, although in this case running at charm threshold preserves a few uniqueness, such as charm mixing and absolute branching ratios;
– A super-flavour factory (i.e., a collider running at the $\Upsilon(4S)$ at $10^{36}\,\mathrm{cm}^{-2}\,\mathrm{s}^{-1}$ which retains the capability of lowering energy down to the J/ψ with peak luminosity there of $10^{34}\,\mathrm{cm}^{-2}\,\mathrm{s}^{-1}$) is a very attractive concept of a machine able to fulfil the need of a thorough investigation of the flavour sector;
– A super-flavour factory machine design could be based on new ideas [342], which heavily exploit the ongoing R&D for the ILC;
– Technical feasibility, cost and schedules for both machine and detector at a super-flavour factory need very careful insights.

Even if one restricts the scope to a τ-charm factory, machine [5, 307] and detector are expected to be challenging. Expertise on both machine and detector does exist in Frascati, but it is clear that such an enterprise must be an international joint venture. The new τ-charm factory rings would not fit the existing building, and it is likely that a new site close to Frascati should be selected, possibly in synergy with facilities compatible in energy and luminosity, such as medical therapy, FEL, material science and synchrotron radiation.

Finally, very strong competition does exist from the Beijing machine, which is scheduled to start commissioning in 2007. A τ-charm factory in Frascati with $10^{34}\,\mathrm{cm}^{-2}\,\mathrm{s}^{-1}$ would provide a 10-fold event sample with respect to the Beijing collider starting from 2013, its first planned year of operation. A Frascati τ-charm factory project indeed requires to meet a very tight schedule to be a winner.

4 Detector considerations

We discuss here the requirements posed by the DAFNE-2 physics program outlined in Sect. 2, on the possible detectors that can be used. This section complements the considerations done on each single section.

The variety of physics items described above puts forward a number of detector requirements well met by a general purpose detector, apart few special cases, namely the small angle tagger for the $\gamma\gamma$ physics, the neutron detector and the polarimeter for the nucleon form factor measurement. The small angle tagger for $\gamma\gamma$ physics has been partially discussed in the section dedicated to such final states (see Sect. 2.5). Its design, which is in principle very simple, depends very much on the accelerator choices and would be impossible here to discuss it in more details. However it can be realized with a moderate investment.

All the other requirements are easily summarised as follows:

1. full angular coverage;
2. efficient tracking, providing good momentum resolution down to low momentum values;
3. hermetic calorimetry with excellent photon detection capability;
4. good particle identification performances.

The first design of DAFNE-2 foresees one interaction region only. This implies that either one single detector is used, or that the possibility to move in and out different detectors in the same experimental region has to be considered.

In any case, for the sake of minimising the cost it is wise to consider the possibility of re-using large parts of the presently operating detectors at the DAFNE machine, namely KLOE [2] and Finuda [3]. Out of the two, only KLOE has been designed to be a general purpose detector, and thus matches broadly the requirements just stated. In fact, the KLOE detector provides full angular coverage, and consists of a large Helium drift chamber [343] immersed in a $5\,\mathrm{kG}$ solenoidal magnetic field, providing a momentum resolution of 0.4% for track with polar angle above 45°, surrounded by a lead-scintillating fibers calorimeter [344] able to detect photons down to few MeV with good efficiency and providing an energy resolution of $5.7\%/\sqrt{E}$ and a time resolution of $54\,\mathrm{ps}/\sqrt{E}\oplus 50\,\mathrm{ps}$. The excellent time of flight measurement provides also good particle identification.

The Finuda detector [3], designed and optimised for hypernuclear physics, has been shown recently well-suited for the determination of the nucleon form factors (both in the proton and in the neutron final state). With the implementation of a polarimeter in the upgraded detector, it is also able to measure the normal polarisation of the outgoing baryon and hence the phases of the form factors. We refer the interested reader to the Letter of Intent recently submitted [264].

In the following we will make the assumption that the KLOE detector can be used as a starting point to realize a detector for DAFNE-2. We will consider first the issues related to operating KLOE as it is, and secondly we will discuss the possible detector upgrades.

4.1 Operating the KLOE detector at DAFNE-2

To run at DAFNE-2 without major modifications, the KLOE detector must face essentially 3 challenges:

1. the aging of the electronics and the obsolescence of all the computing systems, both online and off-line;
2. the increase in event rate, by a factor of ~ 10, due to the increased luminosity of the machine at the ϕ peak;
3. the increase in center of mass energy, by a factor of ~ 2, needed for some of the measurements described in the previous sections.

The first point is of key importance, given the fact that the DAFNE-2 machine is not expected to start operating before year 2010, and will have to run for at least 5 years.

Front-end electronics. Aging is a common issue both for calorimeter and chamber electronics, and the only reasonable solution can be to redo (and probably redesign) a sizeable part of it. On the other hand, the increased rate should not be a big problem, provided the on-board data buffers are replaced with deeper ones. The energy increase instead will require to extend the dynamic range of the calorimeter ADCs.

Trigger. Apart from the common aging problem, the KLOE trigger system [345] would not have problems to run at an increased energy, while the rate increase would certainly be an issue, particularly if we consider a possible increase also of the machine background, at least in the first 1–2 years of

operation. In more detail, it has been designed as "minimum bias" trigger, made of two independent systems: one based on the calorimeter multiplicity and the other on the drift chamber multiplicity. The system results in a rate of 2–3 kHz with the present DAFNE luminosity and background conditions.

At DAFNE-2 minimum bias trigger with the same philosophy would produce a rate around 20 kHz, putting severe constraints both on data acquisition and on the data processing and storage. However a different philosophy (selective triggers) seems really unaffordable given the variety of the physics channels to be studied and the precision required for some of the measurements (for example the hadronic cross section), where even small trigger bias could be very important. But at least the minimum bias trigger could be fruitfully completed by an effective third level stage, based on online event reconstruction, able to reduce the machine background, the cosmic and noise events stored on tape.

Data acquisition. Here again the aging issue is critical for the entire KLOE data acquisition system [346], and applies not only to custom boards but also to commercial CPUs, operating systems and data transmission protocols. The construction of a brand new system is highly advisable. However the architecture of the KLOE system can be safely extended to the DAFNE-2 environment, provided some modifications are implemented in order to increase the maximum sustainable rate. In fact the system was designed to sustain 50 Mbyte/s and has been tested up to 80 Mbyte/s, while the usual bandwidth during the present KLOE run does not exceed 10 Mbytes/s. If the minimum bias philosophy is kept for the trigger at DAFNE-2, and if the event size will increase (in case the KLOE detector is upgraded in some parts), it is necessary to foresee a much higher data throughput.

4.2 Possible upgrades to the KLOE detector

The KLOE detector was optimised to efficiently detect in-flight decays of the $K_{\rm L}$, thus leaving some important weak points from the point of view of DAFNE-2 physics. In fact all the channels discussed in this document include prompt particles, with momentum spectra often extended to very low values, whose detection could be inefficient in KLOE due to the absence of any tracking device in a radius of 25 cm from the interaction point. Also, the value of the magnetic field is such that many low momentum tracks may escape detection by spiralising before entering any detector.

On the other hand, a number of the final states we are considering contains many photons, for which the readout granularity of the KLOE calorimeter has proven to be too coarse, thus inducing accidental cluster splitting or merging. A refinement of the calorimeter readout granularity would be also of great help in $e/\mu/\pi$ separation, which is required to reject background in various channels.

Magnetic field. The magnetic field value used in KLOE ($\simeq 0.52\,T$) was chosen to maximise the kinematical separation between the $K_{\rm L} \to \pi^+\pi^-$ and the $K_{\rm L} \to \pi\mu\nu$ decays in the drift chamber volume. Due to such high B field a sizeable fraction of the low momentum tracks coming from the interaction point falls out of the detector acceptance. Furthermore, the smaller the track curvature radius, the higher the probability that the pattern recognition splits it in two or more segments. An example of this effect is shown in Fig. 23 for simulated $K_{\rm S} \to \pi^0\pi^+\pi^-$ decays, which are kinematically very similar to $\eta \to \pi^0\pi^+\pi^-$. The momentum distribution of the two charged pions at the generation level and after the reconstruction is shown in the right plot, where it is clear the acceptance drop at low momenta.

However it must be kept into account that lowering the magnetic field would have an effect on momentum resolution and vertex efficiency, which would be further worsened in the DAFNE-2 high energy run. The prediction of such effects and their convolution as a function of the B field value is not trivial and depends very much on the specific final states. A careful simulation is necessary, selecting a subset of benchmark channels. However, it is clear that the run at the ϕ and the high energy run may use a different magnetic field value.

Inner tracker. There is no doubt that a tracking device as close as possible to the interaction point, providing 3-dimensional spatial measurements with moderate hit resolution (few hundreds μm), would greatly improve the KLOE tracking and vertexing performances, and would allow to safely afford all the measurements discussed in this document. However the choice of the detector to be used and its design must be carefully tuned according to the following considerations:

1. compatibility with the kaon physics program at DAFNE-2;
2. amount of material required (for the detector, its supporting structure, electronics and cables) and its effects on multiple scattering and photon conversions;
3. sustainable rate and occupancy, mainly with respect to Bhabha events rate and machine background.

The first point is due because it is clear that during the run at the ϕ peak a kaon physics program will be also pursued, using exactly the same detector we are considering here. Up to now we have not considered the (more stringent) detector requirements coming from kaon physics, but in this case we cannot avoid it, because an inner tracker too close to the interaction region would definitely spoil any study of kaon interferometry. The minimal distance required amounts to $20K_{\rm S}$ lifetimes, i.e. about 12 cm. This essentially means that the spherical beam pipe structure used by KLOE will have to be kept at DAFNE-2, and that a possible cylindrical inner tracker must have inner radius ≥ 12 cm and outer radius ≤ 25 cm (which is the KLOE chamber inner wall radius).

For low momentum tracks the multiple scattering contribution to the momentum and vertex resolution is dominant. Vertex resolution is not crucial for most of the measurements we are considering here, but the momentum resolution must be kept very good to allow the kinematic closure of events and reduce selection systematics. Moreover, when searching for rare decays, small non Gaussian tails in the measured distributions should be avoided in order to keep the background under control. A first study of the multiple scattering influence on the momentum resolution has been performed, and is shown in Fig. 24, where the effect of KLOE drift chamber inner wall is compared with what would happen adding 1 mm or 1.5 mm of equivalent silicon thickness. The reference line of $\frac{\delta p}{p} = 1\%$ is

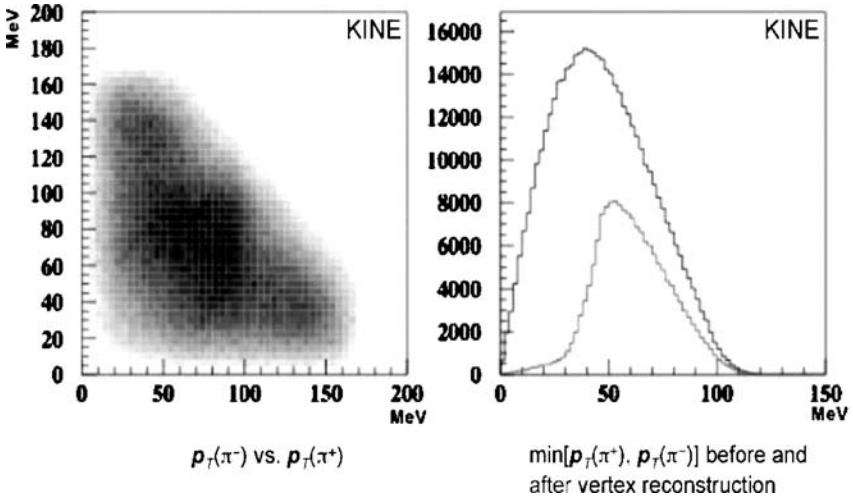

Fig. 23. (*Left*) momentum distribution of the charged pions from $K_S \to \pi^0\pi^+\pi^-$. (*Right*) Momentum distribution of the same charged pions at generation level and after the reconstruction

also drawn: it is clear that below 100 MeV the resolution worsens very rapidly, and it would be a good choice not to exceed 1 mm of silicon equivalent thickness ($\sim 1\%X_0$) for the whole inner tracker.

The event rate coming from ϕ events at DAFNE-2 is expected to be of the order of 10 kHz, with low particle multiplicity, and then should be easily tolerable for any type of inner tracker. Bhabha events may be a problem instead, but they are peaked in the forward region: the event rate can be kept under control by simply limiting the inner tracker acceptance at polar angles above 30°. On the other hand it is very difficult to estimate the machine background contribution, because its rate, composition (electron vs. photons), and spatial and momentum distribution are highly dependent on the machine optics and operation conditions. However if we scale the single counting rate observed on the KLOE drift chamber wires closer to the IP (at a radius of $\simeq 28$ cm), we obtain that a cilyndrical active layer at a radius 12–20 cm from IP would see a rate of the order of 10–20 MHz. Such rough estimate is consistent with the one based on the counting rate of the Finuda vertex detector: at a radius of 6 cm from IP the silicon detector collected $7/8$ hits/planes in 2 μs of integration time at a luminosity near 10^{32} cm^{-2}s^{-1}, which scaled to DAFNE-2 expected luminosity yields a rate around 30 MHz. To cope with such environment, the tracker should be designed as fast as possible, with a short integration time to minimise the pile-up of machine background.

Obviously a detailed simulation study is needed before the choice of a specific technical solution, however, bearing in mind the considerations reported above, we suggest to discuss 3 possible choices:

1. Light drift chamber: designed as an extrapolation toward IP of the KLOE drift chamber.The longitudinal coordinate can be given both by stereo geometry wires and by charge division. It would have the advantage to be very light and to require a limited number of channels (of the order of few hundreds), but the disadvantage of being slow due to the drift. However a suitable choice of the cell size (for example 0.5×0.5 cm^2) could solve the problem.
2. Silicon detector: organised in 4 or 5 cylindrical planes of the well established double sided strip readout, which would provide 3-dimensional space measurements with very good hit resolution, and maybe also $\mathrm{d}E/\mathrm{d}x$ measurement. If the strip pitch is not chosen too small (also 1 mm could be enough for many measurements) the number of channels could be limited around 10^4, depending on the number of layers. However the big disadvantage of this solution if the material thickness required, not only for the detector but also for the electronics and support structure.

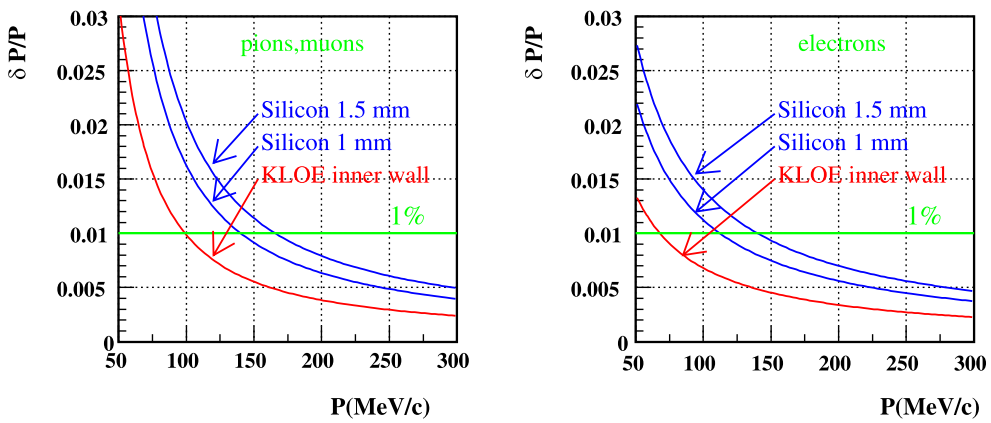

Fig. 24. Relative uncertainty on the momentum measurement as a function of the particle momentum for different thickness of silicon equivalent compared to the uncertainty due to the KLOE drift chamber inner wall

3. Cylindrical GEM: this very promising new technology has been widely developed and tested at LNF [347], where a valuable expertise is present. Three dimensional spatial measurement is easily implemented, and the overall material thickness can be kept very low. However if $1\,\mathrm{cm}^2$ readout pads are implemented, around 3×10^4 channels are required.

Calorimeter. The KLOE calorimeter read-out cell size is $4.4 \times 4.4\,\mathrm{cm}^2$, for a total of 5000 read-out cells, equally divided between barrel and endcaps. Such a segmentation has to be compared with a Moliere radius of the order of $1.5\,\mathrm{cm}$. A finer granularity is then suggested by the natural transverse size of the showers in the calorimeter, and could be of great help to minimise cluster splitting and/or merging, and would allow a better cluster shape analysis for particle identification.

The effect of cluster splitting/merging affects any analysis with cluster counting, and in particular the search for rare decays into neutrals. In Fig. 25 is shown a striking example of cluster merging in the search for $\eta \to \pi^0\gamma\gamma$ events, where a huge background survives the kinematical fit coming from $\eta \to 3\pi^0$ decays with double merged clusters. Due to the merging of two couple of photons the topology of the background becomes equal to the signal, since the invariant mass of the four photons peaks anyway at the η mass.

The best readout granularity choice can be studied by a detailed simulation of the calorimeter, using a package, like FLUKA or GEANT4, which implements an accurate description of low energy processes. Such simulations should however be verified by test beams, where also the technical solution to refine granularity could be tested.

The read-out device to be used with the new granularity must not spoil the excellent energy and time resolution of the calorimeter, i.e. it should have high quantum efficiency and fast timing performances. At the moment the most interesting solutions on the market are the multi-anode photomultipliers (R760000 M4 or M16 or M64 by Hamamatsu) which have rise-time and quantum efficiency similar to the KLOE photomultipliers.

The increase in the number of channels can be really sizeable: a simple reduction by a factor of 2 in the cell linear size results in a factor of 4 increase of the number of channels. However it is also possible to implement the granularity refinement only on the first 2 planes of the calorimeter, provided the simulation and the tests show this is sufficient to reduce clusterization errors. To cope with a high number of channels, it would be advisable to process the signal as near as possible to the detector, and send out only the digitised information.

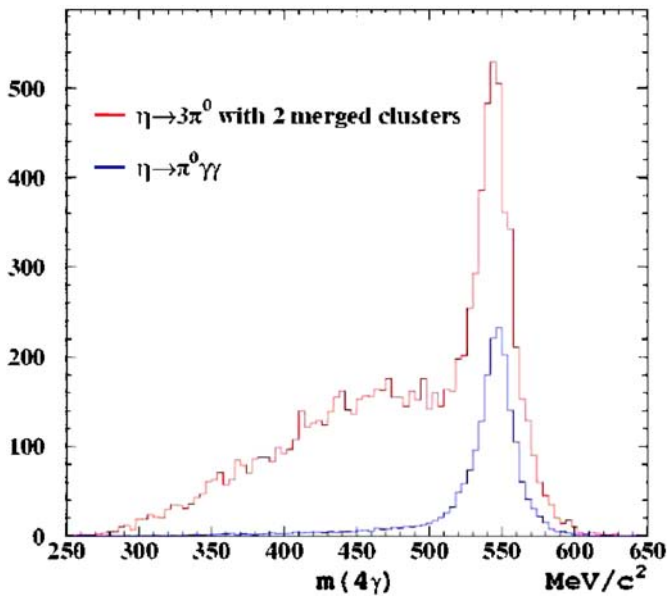

Fig. 25. Invariant mass of the four photons for the $\eta \to \pi^0\gamma\gamma$ events and for the $\eta \to 3\pi^0$ background with two cluster merging

4.3 Detector requirements for nucleon form factor measurements

The KLOE detector is in principle well-suited for the measurement of the proton form factor, apart from the proton polarisation and also for Λ and Σ form factors, through the measurement of their decay products. On the other hand, concerning the neutron form factor, the key point is to understand the efficiency for neutron detection. We discuss here the two items of neutron detection efficiency and of proton polarisation measurement.

The neutron detection capability of the KLOE detector is not known up to now. Although neutron detection with bulk organic scintillators is known to have roughly an efficiency of 1% per each cm of scintillator thickness, it is not clear how this figure can be applied to the peculiar lead-scintillator structure of the KLOE calorimeter, where an equivalent thickness of about $11\,\mathrm{cm}$ is embedded in a fine grain sampling structure. Studies on this subject are in progress.

A proton polarimeter is also required for the form factor measurement. Such a device normally consists of a layer of carbon placed between two precise tracking devices, typically silicon detectors. This object cannot be easily incorporated in the KLOE structure and would spoil the tracking resolution of the detector. It should then be inserted only for a dedicated run, maybe replacing part of the beam pipe or of the inner tracker.

Finally the wide program of measurements of the KN interactions in the $p_K \sim 100\,\mathrm{MeV}/c$ momentum region, requires in principle several different gaseous targets around the interaction region. On this respect, as pointed out in Sect. 2.7, the present KLOE drift chamber, filled with a helium based gas mixture provides a good starting point for a complete measurement of kaon interactions on ^{4}He nuclei.

5 Summary

The DAFNE-2 project, starting around the year 2011, will have a relevant impact on a wide variety of physics topics, ranging from precision tests of the standard model to several controversial subjects in the field of hadronic physics. For each single item, we have compared the physics potential of the project with the possible present and future competitors. In Table 9 we summarise the most relevant competitors that we have considered.

Table 9. List of the competitors for the DAFNE-2 project. For each experiment we indicate which measurement among those of the DAFNE-2 program can be done. Moreover we indicate the time scale of the project. With the symbol (?) we indicate those measurements that in principle can be done by the experiment but have not yet been done. For discussions and comparisons we refer to the single paragraphs of Sect. 2

Experiment	Measurements	Time scale
VEPP-2000	hadronic cross section 0.4–2.0 GeV proton and neutron FF at threshold	start in 2007
BES-III	hadronic cross section ≥ 2.4 GeV proton FF for $q^2 \geq 6\,\mathrm{GeV}^2$	start in 2007
BABAR	hadronic cross section 0.3–5 GeV proton FF for q^2 up to $\sim 10\,\mathrm{GeV}^2$ $\gamma\gamma$ physics (?)	data taking up to 2008
BELLE	hadronic cross section 0.3–5 GeV (?) proton FF for q^2 up to $\sim 10\,\mathrm{GeV}^2$ (?) $\gamma\gamma$ physics: $(\gamma\gamma \to \pi^+\pi^-)$ $W_{\gamma\gamma} \geq 700$ MeV	data taking
PANDA	proton FF up to high q^2	start in 2013
PAX	proton FF (including polarisation) up to high q^2	beyond 2015
CrystalBall at MAMI	η and η' physics	data taking
WASA at COSY	η and η' physics	start in 2007

The present KLOE detector with some upgrades appears well-suited for the measurements discussed here. Among the upgrades we remark the relevance of the inner tracker, of the small angle tagger for the $\gamma\gamma$ physics, and of the proton polarimeter to access the phases of the nucleon form factors. For the latter subject, the possibility to use the Finuda detector should also be considered.

We remark that a large part of the DAFNE-2 program is based on the assumption that the center of mass energy will be increased up to at least 2.5 GeV, and will not be possible in case DAFNE-2 will work at the ϕ only. Moreover we stress that, since many of the measurements discussed here are precision refinements of measurements already done, the project will be significant only if it will provide "ultimate" and complete measurements. This has to be taken into account in the design of the experiments.

We have also considered the physics potential of a higher energy e^+e^- collider, a τ-charm factory with a luminosity of order $10^{34}\,\mathrm{cm}^{-2}\,\mathrm{s}^{-1}$. It offers interesting possibilities for flavour physics. Among the relevant topics we mention charmonium spectroscopy, the study of charmed mesons decays and τ physics. It should be considered as an option in the framework of the super-flavour factory.

Acknowledgements. We warmly acknowledge the colleagues who contributed to the analyses presented here: A. Bianconi, S. Eidelman, R. Escribano, F. Jegerlehner, B. Pasquini, E. Tomasi-Gustafsson, N. Tornqvist, L.Trentadue. We thank the Frascati Laboratories and the INFN units of Milano and Roma, for hospitality during the preparation of the document. We thank the Director of the Frascati Laboratories M. Calvetti and the President of the INFN CSN-1 F. Ferroni, who supported this work. Finally we express our gratitude to L. Maiani for many discussions especially on the subject of low mass scalar spectroscopy, to I. Bigi for his suggestions concerning the τ-charm physics, and to R. Baldini for his support on all the topics discussed in this report.

References

1. L. Maiani, G. Pancheri, N. Paver (Eds.), The Second DAFNE Physics Handbook (1995)
2. See http://www.lnf.infn.it/kloe
3. See http://www.lnf.infn.it/esperimenti/finuda/finuda.html
4. See http://www.lnf.infn.it/esperimenti/dear/
5. M. Zobov et al., DAFNE operations and plans for DAFNE-2, proc. of PAC2005 (Knoxville-USA) SLAC-PUB-11655
6. This possibility has been widely discussed at the super-B-factory meeting, Frascati, Nov. 11–12 2005, see http://www.lnf.infn.it/conference/supbf05
7. See http://www.infn.it/csn1/Roadmap/Gruppok/index.html
8. I.A. Koop et al., Frascati Phys. Ser. **16**, 393 (1999)
9. I.A. Koop et al., AIP Conf. Proc. **588**, 319 (2001)
10. B. Khazin, S. Eidelman, contributions to the International Workshop "e^+e^- collisions from ϕ to ψ", February 27th – March 2nd 2006, Novosibirsk, Russia
11. P.J. Mohr, B.N. Taylor, Rev. Mod. Phys. **77**, 1 (2005)
12. Particle Data Group, S. Eidelman et al., Phys. Lett. B **592**, 1 (2004)
13. F. Jegerlehner, Nucl. Phys. Proc. Suppl. **131**, 213 (2004)
14. A. Sirlin, Phys. Rev. D **22**, 971 (1980)
15. A. Sirlin, Phys. Lett. B **232**, 123 (1989)
16. W.J. Marciano, A. Sirlin, Phys. Rev. D **22**, 2695 (1980)
17. W.J. Marciano, A. Sirlin, Phys. Rev. D **31**, 213(E) (1985)
18. G. Degrassi, S. Fanchiotti, A. Sirlin, Nucl. Phys. B **351**, 49 (1991)
19. A. Ferroglia, G. Ossola, A. Sirlin, Phys. Lett. B **507**, 147 (2001)
20. M.J.G. Veltman, Nucl. Phys. B **123**, 89 (1977)
21. CDF Collaboration, F. Abe et al., Phys. Rev. Lett. **74**, 2626 (1995)
22. D0 Collaboration, S. Abachi et al., Phys. Rev. Lett. **74**, 2632 (1995)
23. G. Degrassi, P. Gambino, M. Passera, A. Sirlin, Phys. Lett. B **418**, 209 (1998)
24. G. Degrassi, P. Gambino, Nucl. Phys. B **567**, 3 (2000)

25. A. Ferroglia, G. Ossola, M. Passera, A. Sirlin, Phys. Rev. D **65**, 113 002 (2002)
26. M. Awramik, M. Czakon, A. Freitas, G. Weiglein, Phys. Rev. D **69**, 053 006 (2004)
27. M. Awramik, M. Czakon, A. Freitas, G. Weiglein, Phys. Rev. Lett. **93**, 201 805 (2004)
28. H. Burkhardt, B. Pietrzyk, Phys. Rev. D **72**, 057 501 (2005)
29. LEP Electroweak Working Group, SLD Electroweak Group and SLD Heavy Flavour Group, hep-ex/0509008
30. LEP Electroweak Working Group, SLD Electroweak Group and SLD Heavy Flavour Group, hep-ex/0511027
31. LHC/LC Study Group, G. Weiglein et al., hep-ph/0410364
32. M. Steinhauser, Phys. Lett. B **429**, 158 (1998)
33. N. Cabibbo, R. Gatto, Phys. Rev. **124**, 1577 (1961)
34. S. Eidelman, F. Jegerlehner, Z. Phys. C **67**, 585 (1995)
35. H. Burkhardt, B. Pietrzyk, Phys. Lett. B **356**, 398 (1995)
36. A.D. Martin, D. Zeppenfeld, Phys. Lett. B **345**, 558 (1995)
37. M.L. Swartz, Phys. Rev. D **53**, 5268 (1996)
38. M. Davier, A. Höcker, Phys. Lett. B **419**, 419 (1998)
39. M. Davier, A. Höcker, Phys. Lett. B **435**, 427 (1998)
40. J.H. Kuhn, M. Steinhauser, Phys. Lett. B **437**, 425 (1998)
41. S. Groote et al., Phys. Lett. B **440**, 375 (1998)
42. J. Erler, Phys. Rev. D **59**, 054 008 (1999)
43. A.D. Martin, J. Outhwaite, M.G. Ryskin, Phys. Lett. B **492**, 69 (2000)
44. R. Alemany, M. Davier, A. Höcker, Eur. Phys. J. C **2**, 123 (1998)
45. R.R. Akhmetshin et al., Phys. Lett. B **578**, 285 (2004)
46. J.Z. Bai et al., Phys. Rev. Lett. **88**, 101 802 (2002)
47. H. Burkhardt, B. Pietrzyk, Phys. Lett. B **513**, 46 (2001)
48. F. Jegerlehner, J. Phys. G **29**, 101 (2003)
49. K. Hagiwara, A.D. Martin, D. Nomura, T. Teubner, Phys. Rev. D **69**, 093 003 (2004)
50. J.F. de Trocóniz, F.J. Ynduráin, Phys. Rev. D **71**, 073 008 (2005)
51. A. Aloisio et al., Phys. Lett. B **606**, 12 (2005)
52. H.N. Brown et al., Phys. Rev. D **62**, 91101 (2000)
53. H.N. Brown et al., Phys. Rev. Lett. **86**, 2227 (2001)
54. G.W. Bennett et al., Phys. Rev. Lett. **89**, 101 804 (2002)
55. G.W. Bennett et al., Phys. Rev. D **89**, 129 903(E) (2002)
56. G.W. Bennett et al., Phys. Rev. Lett. **92**, 161 802 (2004)
57. G.W. Bennet et al., Phys. Rev. D **73**, 072 003 (2006)
58. A. Czarnecki, W.J. Marciano, Phys. Rev. D **64**, 013 014 (2001)
59. R.M. Carey et al., Proposal of the BNL Experiment E969 (2004)
60. B.L. Roberts, hep-ex/0501012
61. J-PARC Letter of Intent L17, contact person B.L. Roberts
62. M. Passera, J. Phys. G **31**, R75 (2005)
63. M. Passera, Nucl. Phys. Proc. Suppl. **155**, 365 (2006)
64. M. Davier, W.J. Marciano, Ann. Rev. Nucl. Part. Sci. **54**, 115 (2004)
65. M. Knecht, hep-ph/0307239
66. A. Czarnecki, W.J. Marciano, Nucl. Phys. Proc. Suppl. **76**, 245 (1999)
67. V.W. Hughes, T. Kinoshita, Rev. Mod. Phys. **71**, S133 (1999)
68. J.S. Schwinger, Phys. Rev. **73**, 416 (1948)
69. T. Kinoshita, M. Nio, Phys. Rev. D **73**, 053 007 (2006)
70. A. Czarnecki, W.J. Marciano, A. Vainshtein, Phys. Rev. D **67**, 073 006 (2003)
71. G. Degrassi, G.F. Giudice, Phys. Rev. D **58**, 53007 (1998)
72. C. Bouchiat, L. Michel, J. Phys. Radium **22**, 121 (1961)
73. M. Gourdin, E. de Rafael, Nucl. Phys. B **10**, 667 (1969)
74. CMD-2 Collaboration, V.M. Aulchenko, JETP Lett. **82**, 743 (2005)
75. I. Logashenko, contribution to the HEP2005 International Europhysics Conference on High Energy Physics EPS, Lisboa, Portugal, July 21–27 2005, Proc. Sci. HEP2005 (2005)
76. M.N. Achasov et al., J. Exp. Theor. Phys. **101**, 1053 (2005)
77. M.N. Achasov, contribution to the International Workshop "e^+e^- collisions from ϕ to ψ", February 27th – March 2nd 2006, Novosibirsk, Russia, hep-ex/0604052
78. M. Davier, Nucl. Phys. Proc. Suppl. **144**, 238 (2005)
79. B.A. Shwartz, Nucl. Phys. Proc. Suppl. **144**, 245 (2005)
80. G. Colangelo, Nucl. Phys. Proc. Suppl. **131**, 185 (2004) and references therein
81. A. Höcker, hep-ph/0410081
82. M. Davier, A. Hocker, Z. Zhang, hep-ph/0507078 (to be published in Rev. Mod. Phys.)
83. M. Davier et al., Eur. Phys. J. C **31**, 503 (2003)
84. Belle Collaboration, K. Abe et al., hep-ex/0512071
85. M. Fujikawa, contribution to the International Workshop "e^+e^- collisions from ϕ to ψ", February 27th–March 2nd 2006, Novosibirsk, Russia
86. W.J. Marciano, A. Sirlin, Phys. Rev. Lett. **61**, 1815 (1988)
87. V. Cirigliano, G. Ecker, H. Neufeld, Phys. Lett. B **513**, 361 (2001)
88. V. Cirigliano, G. Ecker, H. Neufeld, JHEP **0208**, 002 (2002)
89. S. Ghozzi, F. Jegerlehner, Phys. Lett. B **583**, 222 (2004)
90. M. Davier, Nucl. Phys. Proc. Suppl. **131**, 123 (2004)
91. K. Maltman, Phys. Lett. B **633**, 512 (2006)
92. K. Maltman, C.E. Wolfe, Phys. Rev. D **73**, 013 004 (2006)
93. B. Krause, Phys. Lett. B **390**, 392 (1997)
94. M. Knecht, A. Nyffeler, Phys. Rev. D **65**, 73 034 (2002)
95. M. Knecht, A. Nyffeler, M. Perrottet, E. de Rafael, Phys. Rev. Lett. **88**, 71802 (2002)
96. A. Nyffeler, Acta Phys. Pol. B **34**, 5197 (2003)
97. M. Hayakawa, T. Kinoshita, Phys. Rev. D **57**, 465 (1998)
98. M. Hayakawa, T. Kinoshita, Phys. Rev. D **66**, 019 902(E) (2002)
99. J. Bijnens, E. Pallante, J. Prades, Nucl. Phys. B **474**, 379 (1996)
100. J. Bijnens, E. Pallante, J. Prades, Nucl. Phys. B **626**, 410 (2002)
101. K. Melnikov, A. Vainshtein, Phys. Rev. D **70**, 113006 (2004)
102. S. Binner, J.H. Kühn, K. Melnikov, Phys. Lett. B **459**, 279 (1999)
103. G. Rodrigo, A. Gehrmann-De Ridder, M. Guilleaume, J.H. Kühn, Eur. Phys. J. C **22**, 8 (2001) [hep-ph/0106132]
104. J.H. Kühn, G. Rodrigo, Eur. Phys. J. C **25**, 21 (2002) [hep-ph/0204283]
105. G. Rodrigo, H. Czyż, J.H. Kühn, M. Szopa, Eur. Phys. J. C **24**, 7 (2002) [hep-ph/0112184]
106. H. Czyż, A. Grzelińska, J.H. Kühn, G. Rodrigo, Eur. Phys. J. C **27**, 56 (2003) [hep-ph/0212225]
107. H. Czyż, A. Grzelińska, J.H. Kühn, G. Rodrigo, Eur. Phys. J. C **33**, 33 (2004) [hep-ph/0308312]
108. NA7 Collaboration, S.R. Amendolia et al., Nucl. Phys. B **277**, 168 (1986)
109. B. Aubert et al., Phys. Rev. D **70**, 072 004 (2004)
110. B. Aubert et al., Phys. Rev. D **71**, 052 001 (2005)
111. B. Aubert et al., Phys. Rev. D **73**, 052 003 (2006)
112. A. Antonelli et al., Z. Phys. C **56**, 15 (1992)
113. S. Godfrey, N. Isgur, Phys. Rev. D **32**, 189 (1985)
114. A. Donnachie, Y.S. Kalashnikova, Phys. Rev. D **60**, 114 011 (1999)
115. A. Donnachie, Y.S. Kalashnikova, Proc. of IXth Int. Conf. on Hadron Spectroscopy, Protvino (Russia), 2001, AIP Conf. Proc. **619**, 5 (2002)
116. G. Busetto, L. Oliver, Z. Phys. C **20**, 247 (1983)

117. P. Geiger, E.S. Swanson, Phys. Rev. D **50**, 6855 (1994)
118. H.G. Blundell, S. Godfrey, Phys. Rev. D **53**, 3700 (1997)
119. P.R. Page et al., Phys. Rev. D **59**, 034016 (1999)
120. F.E. Close et al., Phys. Rev. D **67**, 074031 (2003)
121. F.E. Close et al., Phys. Rev. D **65**, 092003 (2002)
122. D.R. Thompson et al., Phys. Rev. Lett. **79**, 1630 (1997)
123. A. Abele et al., Phys. Lett. B **423**, 175 (1998)
124. I.I. Ivanov et al., Phys. Rev. Lett. **86**, 3977 (2001)
125. C.J. Morningstar, M. Peardon, Phys. Rev. D **56**, 4043 (1997)
126. C.A. Meyer, hep-ex/0308010
127. R.L. Jaffe, Phys. Rev. D **17**, 1444 (1978)
128. J.M. Richard, Nucl. Phys. B Proc. Suppl. **86**, 361 (2000)
129. C.B. Dover et al., Phys. Rev. C **43**, 379 (1991)
130. A. Antonelli et al., Phys. Lett. B **365**, 427 (1996)
131. G. Bardin et al., Nucl. Phys. B **411**, 3 (1994)
132. B. Aubert et al., Phys. Rev. D **73**, 012005 (2006)
133. J.Z. Bai et al., Phys. Rev. Lett. **91**, 022001 (2003)
134. M. Ablikim et al., Phys. Rev. Lett. **95**, 262001 (2005)
135. M.Z. Wang et al., Phys. Lett. B **617**, 141 (2005)
136. Y.J. Lee et al., Phys. Rev. Lett. **93**, 211801 (2004)
137. M. Agnello et al., Phys. Lett. B **527**, 39 (2002)
138. D.M. Alde et al., Z. Phys. C **66**, 379 (1995)
139. T. Komada, Proc. of XI Int. Conf. on Hadron Spectroscopy, Rio de Janeiro (Brazil), 2005, AIP Conf. Proc. **814**, 458 (2006)
140. J.M. Link et al., Phys. Lett. B **545**, 50 (2002)
141. R.R. Akhmetshin et al., Phys. Lett. B **595**, 101 (2004)
142. R.R. Akhmetshin et al., Phys. Lett. B **466**, 392 (1999)
143. S. Pacetti, to be published in Eur. Phys. J. A
144. S.J. Brodsky, G.R. Farrar, Phys. Rev. D **11**, 1309 (1975)
145. S.J. Brodsky, G.P. Lepage, Phys. Rev. D **24**, 2848 (1981)
146. B.V. Geshkenbein, Yad. Fiz. **9**, 1232 (1969)
147. J.J. Sakurai, Phys. Lett. B **46**, 207 (1973)
148. B. Aubert et al., Phys. Rev. D **71**, 052001 (2005)
149. P.L. Frabetti at al., Phys. Lett. B **578**, 290 (2004)
150. P.L. Frabetti et al., Phys. Lett. B **514**, 240 (2001)
151. E. Solodov, Workshop on Nucleon Form Factors, LNF (Frascati) (2005)
152. H. Yang, Int. J. Mod. Phys. A **20**, 1985 (2005)
153. J.Z. Bai et al., Phys. Rev. Lett. **91**, 022001 (2003)
154. J. Gasser, H. Leutwyler, Ann. Phys. **158**, 142 (1984)
155. J. Gasser, H. Leutwyler, Nucl. Phys. B **250**, 465 (1985)
156. G. Grayer et al., Nucl. Phys. B **75**, 189 (1974)
157. S.M. Flatte, Phys. Lett. B **63**, 224 (1976)
158. N.A. Törnqvist, Phys. Rev. Lett. **49**, 624 (1982)
159. R.L. Jaffe, Phys. Rev. D **15**, 267 (1997)
160. J. Weinstein, N. Isgur, Phys. Rev. Lett. **48**, 659 (1982)
161. M.N. Achasov et al., Phys. Lett. B **440**, 442 (1998)
162. M.N. Achasov et al., Phys. Lett. B **485**, 349 (2000)
163. R.R. Akhmetshin et al., Phys. Lett. B **462**, 380 (1999)
164. M.N. Achasov et al., Phys. Lett. B **479**, 53 (2000)
165. A. Aloisio et al., Phys. Lett. B **536**, 209 (2002)
166. A. Aloisio et al., Phys. Lett. B **537**, 21 (2002)
167. F. Ambrosino et al., Phys. Lett. B **634**, 148 (2006)
168. N.N. Achasov, V.V. Gubin, Phys. Rev. D **64**, 094016 (2001)
169. S. Giovannella et al., Proc. of 40th Rencontres de Moriond on QCD and High Energy Hadronic Interactions, La Thuile (Italy), Mar. 12–19 2005, hep-ex/0505074
170. A. Aloisio et al., Phys. Lett. B **591**, 49 (2004)
171. F. Ambrosino et al., Phys. Lett. B **606**, 276 (2005)
172. C. Jarlskog, E. Shabalin, Phys. Rev. D **52**, 248 (1995)
173. A.H. Fariborz, J. Schechter, Phys. Rev. D **60**, 034002 (1999)
174. N. Beisert, B. Borasoy, Nucl. Phys. A **716**, 186 (2003)
175. D.M. Alde et al., Z. Phys. C **36**, 603 (1987)
176. V. Nikolaenko et al., Proc. of the Int. Conf. on Low Energy Antiproton Physics, Juelich (Germany), May 16–22 2005, AIP Conf. Proc. **796**, 154 (2005)
177. S.I. Bityukov et al., Z. Phys. C **50**, 451 (1991)
178. A. Abele et al., Phys. Lett. B **402**, 195 (1997)
179. M. Acciarri et al., Phys. Lett. B **418**, 399 (1998)
180. E. Kou, Phys. Rev. D **63**, 054027 (2001)
181. D.J. Gross, S.B. Treiman, F. Wilczek, Phys. Rev. D **19**, 2188 (1979)
182. T. Walcher, Prog. Part. Nucl. Phys. **24**, 189 (1990)
183. See http://www.fz-juelich.de/ikp/cosy/en/index.shtml
184. D. Watts et al., Proc. of 11th International Conference on Calorimetry in High-Energy Physics, Perugia (Italy), 28 Mar–2 Apr 2004
185. H.H. Adam et al., nucl-ex/0411038
186. F.E. Close, A. Donnachie, Y.S. Kalashnikova, Phys. Rev. D **67**, 074031 (2003)
187. F.E. Close, A. Donnachie, Y.S. Kalashnikova, Phys. Rev. D **65**, 092003 (2002)
188. A. Donnachie, Y.S. Kalashnikova, hep-ph/0110191
189. see the recent review by M. Pennington, hep-ph/0511146 and references therein
190. G. Alexander et al., Nuovo Cim. A **107**, 837 (1994)
191. F. Anulli et al., The Second DAFNE Physics Handbook, Vol. II, ed. by L. Maiani, G. Pancheri, N. Paver (1995) p. 607
192. M. Gell-Mann, M. Lévy, Nuovo Cim. **16**, 705 (1960)
193. see also J. Schwinger, Phys. Rev. **82**, 664 (1951)
194. I. Caprini, G. Colangelo, H. Leutwyler, hep-ph/0512364
195. E.M. Aitala et al., Phys. Rev. Lett. **86**, 770 (2001)
196. M. Ablikim et al., Phys. Lett. B **598**, 149 (2004)
197. A.H. Fariborz, R. Jora, J. Schechter, Int. J. Mod. Phys. A **20**, 6178 (2005)
198. G. Ecker, hep-ph/9501357
199. A. Deandrea, A.D. Polosa, Phys. Rev. Lett. **86**, 216 (2001)
200. S. Gardner, U. Meissner, Phys. Rev. D **65**, 094004 (2002)
201. I. Bigi, hep-ph/0601167
202. B. Aubert et al., Phys. Rev. Lett. **95**, 121802 (2005)
203. J. Gasser, M.A. Ivanov, M. Sainio, Nucl. Phys. B **728**, 31 (2005)
204. see also S. Bellucci, J. Gasser, M. Sainio, Nucl. Phys. B **423**, 80 (1994)
205. S. Bellucci, J. Gasser, M. Sainio, Nucl. Phys. B **431**, 413 (1994) [Erratum]
206. F. Nguyen, F. Piccinini, A.D. Polosa, Eur. Phys. J. C **47**, 65 (2006)
207. S. Brodsky, T. Kinoshita, H. Terazawa, Phys. Rev. D **4**, 1532 (1971)
208. L. Maiani, F. Piccinini, A.D. Polosa, V. Riquer, Phys. Rev. Lett. **93**, 212002 (2004)
209. H. Marsiskie et al., Phys. Rev. D **41**, 3324 (1990)
210. T. Oest et al., Z. Phys. C **47**, 343 (1990)
211. M.R. Pennington, in: The Second DAFNE Physics Handbook, ed. by L. Maiani, G. Pancheri, N. Paver (1995) p. 531
212. M.R. Pennington, Phys. Rev. Lett. **97**, 0011601 (2006)
213. T. Mori et al., Proc. of the Int. Symposium on Hadron Spectroscopy, Tokyo (KEK Proceedings 2003-7, 2003) p. 159
214. M. Sainio, private communications
215. M. Boglione, M.R. Pennington, Eur. Phys. J. C **9**, 11 (1999)
216. T. Feldmann, P. Kroll, Phys. Scripta T **99**, 13 (2002)
217. R. Kaiser, H. Leutwyler, Eur. Phys. J. C **17**, 623 (2000)
218. T. Feldmann, P. Kroll, Eur. Phys. J. C **5**, 327 (1998)
219. T. Feldmann, P. Kroll, B. Stech, Phys. Rev. D **58**, 114006 (1998)
220. R. Escribano, J.M. Frere, J. High Energ. Phys. **06**, 029 (2005)

221. K. Kampf, M. Knecht, J. Novotny, hep-ph/0510021
222. S.J. Brodsky, G.P. Lepage, Phys. Rev. D **24**, 1808 (1981)
223. H.J. Behrend et al., Z. Phys. C **49**, 401 (1991)
224. J. Gronberg et al., Phys. Rev. D **57**, 33 (1998)
225. A.P. Bakulev, hep-ph/0410134
226. A. Courau, The Frascati ϕ Factory, ed. by G. Pancheri (1991) p. 373
227. S. Ong, hep-ex/9902030
228. H. Gao, Int. J. Mod. Phys. E **12**, 1 (2003)
229. H. Gao, Int. J. Mod. Phys. E **12**, 567 (2003) [Erratum]
230. C.E. Hyde-Wright, K. De Jager, Ann. Rev. Nucl. Part. Sci. **54**, 217 (2004)
231. JLab Hall A Collaboration, I.A. Qattan et al., Phys. Rev. Lett. **94**, 142 301 (2005)
232. JLab Hall A Collaboration, V. Punjabi et al., Phys. Rev. C **71**, 055 202 (2005)
233. JLab Hall A Collaboration, V. Punjabi et al., Phys. Rev. C **71**, 069 902 (2005) [Erratum]
234. JLab Hall A Collaboration, O. Gayou et al., Phys. Rev. Lett. **88**, 092 301 (2002)
235. JLab Hall A Collaboration, M.K. Jones et al., Phys. Rev. Lett. **84**, 1398 (2000)
236. S.J. Brodsky, G.P. Lepage, Phys. Rev. D **24**, 2848 (1981)
237. S.J. Brodsky, G.R. Farrar, Phys. Rev. D **11**, 1309 (1975)
238. A.V. Afanasev et al., Phys. Rev. D **72**, 013 008 (2005)
239. P.G. Blunden, W. Melnitchouk, J.A. Tjon, Phys. Rev. C **72**, 034 612 (2005)
240. M.P. Rekalo, E. Tomasi-Gustafsson, Eur. Phys. J. A **22**, 331 (2004)
241. A.Z. Dubnickova, S. Dubnicka, M.P. Rekalo, Nuovo Cim. A **109**, 241 (1996)
242. S.J. Brodsky et al., Phys. Rev. D **69**, 054 022 (2004)
243. E. Tomasi-Gustafsson et al., Eur. Phys. J. A **24**, 419 (2005)
244. J.P. Ralston, P. Jain, Phys. Rev. D **69**, 053 008 (2004)
245. J.P. Ralston, P. Jain, R.V. Buniy, AIP Conf. Proc. **549**, 302 (2000)
246. G.A. Miller, M.R. Frank, Phys. Rev. C **65**, 065 205 (2002)
247. M.R. Frank, B.K. Jennings, G.A. Miller, Phys. Rev. C **54**, 920 (1996)
248. G. Holzwarth, Z. Phys. A **356**, 339 (1996)
249. F. Cardarelli, S. Simula, Phys. Rev. C **62**, 065 201 (2000)
250. R.F. Wagenbrunn et al., Phys. Lett. B **511**, 17 (2001)
251. S. Boffi et al., Eur. Phys. J. A **14**, 17 (2002)
252. A.V. Belitsky, X. Ji, F. Yuan, Phys. Rev. Lett. **91**, 092 003 (2003)
253. F. Iachello, A.D. Jackson, A. Lande, Phys. Lett. B **43**, 191 (1973)
254. F. Iachello, Q. Wan, Phys. Rev. C **69**, 055 204 (2004)
255. R. Baldini et al., Nucl. Phys. A **755**, 286 (2005)
256. R. Baldini et al., Eur. Phys. J. C **46**, 421 (2006)
257. FENICE Collaboaration, A. Antonelli et al., Nucl. Phys. B **517**, 3 (1998)
258. P. Mergell, U.-G. Meissner, D. Drechsel, Nucl. Phys. A **596**, 367 (1996)
259. H.-W. Hammer, U.-G. Meissner, D. Drechsel, Phys. Lett. B **385**, 343 (1996)
260. E685 Collaboration, M. Andreotti et al., Phys. Lett. B **559**, 20 (2003)
261. BABAR Collaboration, B. Aubert et al., Phys. Rev. D **73**, 012 005 (2006)
262. LEAR Collaboration, B. Bardin et al., Nucl. Phys. B **411**, 3 (1994)
263. R. Baldini et al., Eur. Phys. J. C **11**, 709 (1999)
264. N. Apokov et al., Measurement of the Nucleon Form Factors in the Time-Like region at DAFNE, Letter of Intent, October 2005, see http://www.lnf.infn.it/conference/nucleon05/loi06.pdf
265. G.I. Gakh, E. Tomasi-Gustafsson, Nucl. Phys. A **771**, 169 (2006)
266. A. Bianconi, B. Pasquini, M. Radici, Phys. Rev. D **74**, 034 009 (2006)
267. A. Bianconi, Phys. Rev. D **74**, 074 012 (2006)
268. E.L. Lomon, Phys. Rev. C **66**, 045 501 (2002)
269. Z.A. Liu, BESIII project – Quarkonium Working Group, Beijing (China), October 2004, see http://www.qwg.to.infn.it/WS-oct04/index.html
270. PANDA Collaboration, Letter of Intent for the Proton–Antiproton Darmstadt Experiment (2004), see http://www.gsi.de/documents/DOC-2004-Jan-115-1.pdf
271. P. Lenisa, F. Rathmann, hep-ex/0505054
272. N. Tornqvist, Found. Phys. **11**, 171 (1981)
273. N. Tornqvist, Phys. Lett. A **117**, 1 (1986)
274. N. Tornqvist, Europhys. Lett. **377**, 1 (1986)
275. M.H. Tixier et al., Phys. Lett. B **212**, 523 (1988)
276. P.M. Gensini, The Second DAFNE Physics Handbook, ed. by L. Maiani, G. Pancheri, N. Paver, Vol. II (Frascati, 1995) p. 739, and references therein
277. P.M. Gensini, G. Violini, Workshop on Science at the KAON Factory, ed. by D.R. Gill, Vol. II (TRIUMF, Vancouver, 1991) p. 193
278. P.M. Gensini, R. Hurtado, G. Violini, πN Newslett. **13**, 296 (1997)
279. P.M. Gensini, Genshikaku Kenkyu **48**, 51 (1998)
280. C.J. Batty, A. Gal, Nuovo Cim. A **102**, 255 (1989)
281. C.J. Batty, First Workshop on Intense Hadron Facilities and Antiproton Physics, ed. by T. Bressani, F. Iazzi, G. Pauli (S.I.F., Bologna, 1990) p. 117
282. M. Iwasaki et al., Phys. Rev. Lett. **78**, 2067 (1997)
283. T. Ito et al., Phys. Rev. C **58**, 2366 (1998)
284. G. Beer et al., Phys. Rev. Lett. **94**, 212 302 (2005)
285. J.A. Oller, J. Prades, M. Verbeni, Phys. Rev. Lett. **95**, 172 502 (2005)
286. J.A. Oller, J. Prades, M. Verbeni, Phys. Rev. Lett. **95**, 172 502 (2005)
287. J.A. Oller, J. Prades, M. Verbeni, Phys. Rev. Lett. **96**, 199 202 (2006)
288. B. Borasoy, R. Niß ler, W. Weise, Phys. Rev. Lett. **96**, 199 201 (2006)
289. See the discussion on this point by D.J. Miller, Proc. of the Int. Conf. on Hypernuclear and Kaon Physics, ed. by B. Povh (M.P.I., Heidelberg, 1982) p. 215
290. E. Piasetzky, Nuovo Cim. A **102**, 281 (1989)
291. R.J. Hemingway, Nucl. Phys. B **253**, 742 (1985)
292. see also, for formation on bound nucleons, B. Riley, I.T. Wang, J.G. Fetkovich, J.M. McKenzie, Phys. Rev. D **11**, 3065 (1975)
293. G.C. Oades, Nuovo Cim. A **102**, 237 (1989)
294. E. Oset, V.K. Magas, A. Ramos, nucl-th/0512090
295. E. Oset, V.K. Magas, A. Ramos, hep-ph/0512361
296. S. Prakhov et al., Phys. Rev. C **70**, 034 605 (2004)
297. See the review by J. Lowe, Nuovo Cim. A **102**, 167 (1989)
298. S. Bianco, F.L. Fabbri, D. Benson, I. Bigi, Riv. Nuovo Cimento **26N7**, 1 (2003)
299. G. Burdman, I. Shipsey, Ann. Rev. Nucl. Part. Sci. **53**, 431 (2003)
300. N. Brambilla et al., hep-ph/0412158, published as CERN Yellow Report, CERN-2005-005, CERN-Geneva (2005), see also http://www.qwg.to.infn.it

301. J. Kirkby, A Tau Charm Factory At Cern, CERN-EP/87-210 (1987)
302. M.L. Perl, The Tau Charm Factory And Tau Physics, Proc. of Rencontres de Moriond on QCD and High Energy Hadronic Interactions, La Thuile (Italy), SLAC-PUB-4971 (1989)
303. J. Kirkby, Physics and design of the tau charm factory in Spain, CERN-PPE-92-030 (1992)
304. E.A. Perelshtein et al., JINR tau-charm factory study, JINR-E9-92-259 (1992)
305. J. Norem, J. Repond, A tau-charm-factory at Argonne, ANL-HEP-CP-94-39 (1994)
306. A. Antonelli et al., Future Research Activities at LNF, Frascati preprint LNF-33-IR (2005)
307. P. Raimondi, Proc. of Rencontres de Moriond on QCD and High Energy Hadronic Interactions, La Thuile (Italy), to appear on Frascati Phys. Series (2005)
308. G. Viehhauser, Nucl. Instrum. Methods A **462**, 146 (2001)
309. R.A. Briere et al., CLEO-c and CESR-c: A New Frontier of Weak and Strong Interactions, CLNS 01/1742 (2001)
310. N. Brambilla, A. Pineda, J. Soto, A. Vairo, Rev. Mod. Phys. **77**, 1423 (2005)
311. A. Pineda, J. Soto, Nucl. Phys. Proc. Suppl. **64**, 428 (1998)
312. N. Brambilla, A. Pineda, J. Soto, A. Vairo, Nucl. Phys. B **566**, 275 (2000)
313. N. Brambilla, Y. Sumino, A. Vairo, Phys. Rev. D **65**, 034001 (2002)
314. B.A. Kniehl, A.A. Penin, A. Pineda, V.A. Smirnov, M. Steinhauser, Phys. Rev. Lett. **92**, 242001 (2004)
315. A.A. Penin, A. Pineda, V.A. Smirnov, M. Steinhauser, Nucl. Phys. B **699**, 183 (2004)
316. W.E. Caswell, G.P. Lepage, Phys. Lett. B **167**, 437 (1986)
317. G.T. Bodwin, E. Braaten, G.P. Lepage, Phys. Rev. D **51**, 1125 (1995)
318. G.T. Bodwin, E. Braaten, G.P. Lepage, Phys. Rev. D **55**, 5853 (1997) [Erratum]
319. N. Brambilla, D. Eiras, A. Pineda, J. Soto, A. Vairo, Phys. Rev. D **67**, 034018 (2003)
320. N. Brambilla, Y. Jia, A. Vairo, Phys. Rev. D **73**, 054005 (2006)
321. J.J. Dudek, R.G. Edwards, D.G. Richards, hep-ph/0601137
322. J. Gaiser et al., Phys. Rev. D **34**, 711 (1986)
323. BELLE Collaboration, H.C. Huang et al., Phys. Rev. Lett. **91**, 241802 (2003)
324. F.E. Close, G.R. Farrar, Z.P. Li, Phys. Rev. D **55**, 5749 (1997)
325. For a description of these states and the original references see http://www.qwg.to.infn.it/QWG-spectr/spectrnews.html
326. E. Braaten, M. Kusunoki, Phys. Rev. D **72**, 054022 (2005)
327. E. Braaten, M. Kusunoki, Phys. Rev. D **72**, 014012 (2005)
328. L. Maiani, F. Piccinini, A.D. Polosa, V. Riquer, Phys. Rev. D **71**, 014028 (2005)
329. E.S. Swanson, hep-ph/0601110
330. J.Z. Bai et al., Phys. Lett. B **561**, 49 (2003)
331. J.Z. Bai et al., hep-ex/0406018
332. C.T.H. Davies et al., Phys. Rev. Lett. **92**, 022001 (2004)
333. M. Davier, A. Hocker, Z. Zhang, hep-ph/0507078
334. X.G. He, G. Valencia, Y. Wang, Phys. Rev. D **70**, 113011 (2004)
335. BABAR Collaboration, B. Aubert et al., Phys. Rev. Lett. **95**, 041802 (2005)
336. A. Hocker, hep-ph/0410081 and references therein
337. I.I. Bigi, A.I. Sanda, Phys. Lett. B **625**, 47 (2005)
338. D.G. Cassel, hep-ex/0307038
339. B. Heltsley, CLEO-c program – Quarkonium Working Group, Beijing (China), October 2004, see http://www.qwg.to.infn.it/WS-oct04/index.html
340. Z. Zhao et al., hep-ex/0201047
341. See also conclusions of report of super-B factories – INFN roadmap working group (convener M. Giorgi)
342. Proc. of Int. Workshop on Discoveries in Flavor Physics at e^+e^- Colliders in the LHC Era, Frascati, Feb. 28 2006, to appear in Frascati Phys. Series (2006)
343. M. Adinolfi et al., Nucl. Instrum. Methods A **488**, 1 (2002)
344. M. Adinolfi et al., Nucl. Instrum. Methods A **482**, 364 (2002)
345. M. Adinolfi et al., Nucl. Instrum. Methods A **492**, 134 (2002)
346. A. Aloisio et al., Nucl. Instrum. Methods A **516**, 288 (2004)
347. G. Bencivenni et al., Nucl. Instrum. Methods A **488**, 493 (2002)